NEURAL NETWORK ANALYSIS OF SPARSE DATASETS – AN APPLICATION TO THE FRACTURE SYSTEM IN FOLDS OF THE LISBURNE FORMATION, NORTHEASTERN ALASKA

A Dissertation

by

THANG DINH BUI

Submitted to the Office of Graduate Studies of
Texas A&M University
in partial fulfillment of the requirements for the degree of

DOCTOR OF PHILOSOPHY

August 2004

Major Subject: Petroleum Engineering

NEURAL NETWORK ANALYSIS OF SPARSE DATASETS – AN APPLICATION TO THE FRACTURE SYSTEM IN FOLDS OF THE LISBURNE FORMATION, NORTHEASTERN ALASKA

A Dissertation

by

THANG DINH BUI

Submitted to the Office of Graduate Studies of
Texas A&M University
in partial fulfillment of the requirements for the degree of

DOCTOR OF PHILOSOPHY

Approved as to style and content by:

Jerry L. Jensen (Chair of Committee)	David S. Schechter (Member)
Catherine L. Hanks (Member)	Walter B. Ayers (Member)
Judith S. Chester (Member)	Stephen A. Holditch (Head of Department)

August 2004

Major Subject: Petroleum Engineering

ABSTRACT

Neural Network Analysis of Sparse Datasets – An Application to the Fracture System in Folds of the Lisburne Formation, Northeastern Alaska. (August 2004)
Thang Dinh Bui, B.S., Moscow Institute of Oil and Gas;
M.S., Texas A&M University
Chair of Advisory Committee: Dr. Jerry L. Jensen

Neural networks (NNs) are widely used to investigate the relationship among variables in complex multivariate problems. In cases of limited data, the network behavior strongly depends on factors such as the choice of network activation function and network initial weights. In this study, I investigated the use of neural networks for multivariate analysis in the case of limited data.

The analysis shows that special attention should be paid when building and using NNs in cases of limited data. The linear activation function at the output nodes outperforms the sigmoidal and Gaussian functions. I found that combining network predictions gives less biased predictions and allows for the assessment of the prediction variability.

The NN results, along with conventional statistical analysis, were used to examine the effects of folding, bed thickness, structural position, and lithology on the fracture properties distributions in the Lisburne Formation, folded and exposed in the northeastern Brooks Range of Alaska. Fracture data from five folds, representing different degrees of folding, were analyzed. In addition, I modeled the fracture system using the discrete fracture network approach and investigated the effects of fracture properties on the flow conductance of the system.

For the Lisburne data, two major fracture sets striking north/south and east/west were studied. Results of the NNs analysis suggest that fracture spacing in both sets is similar and weakly affected by folding and that stratigraphic position and lithology have

a strong effect on fracture spacing. Folding, however, has a significant effect on fracture length. In open folds, fracture lengths in both sets have similar averages and variances. As the folds tighten, both the east/west and north/south fracture lengths increase by a factor of 2 or 3 and become more variable. In tight folds, fracture length in the north/south direction is significantly larger than in the east/west direction. The difference in length between the two fracture sets creates a strong anisotropy in the reservoir. Given the same fracture density in both sets, the set with the greater length plays an important role for fluid flow, not only for flow along its principal direction but also in the orthogonal direction.

DEDICATION

To my wife, Tuyet, and my son, Viet, for their support and sacrifice,

and to my parents for their encouragement in my educational endeavors.

ACKNOWLEDGEMENTS

I wish to express my sincere thanks and appreciation to my research advisor, Dr. Jerry L. Jensen for his invaluable guidance and support throughout my education, research, and stay at Texas A&M University.

I would like to thank Dr. Catherine Hanks from the University of Alaska at Fairbanks for serving on my graduate advisory committee and for her valuable comments and helpful suggestions during the course of this research.

I would like to thank Dr. Walter Ayers, Dr. David Schechter, and Dr. Judith Chester for serving on my graduate advisory committee and their valuable comments and advice.

I would like to thank Dr. John Lee and Dr. Daulat Mamora for encouraging me and giving me the opportunity to come back to Texas A&M University after I finished my M.S. program.

I would like to thank Nestor Rivera for helpful discussions and many others at Petroleum Engineering Department at Texas A&M University for their help throughout my study at Texas A&M University.

I would also like to thank Joe Brinton at the University of Alaska Fairbanks for providing the data and Golder and Associates for making FracMan software available for this research.

TABLE OF CONTENTS

CHAPTER Page

CHAPTER Page

CHAPTER Page

LIST OF FIGURES

FIGURE Page

FIGURE Page

FIGURE Page

FIGURE Page

LIST OF TABLES

TABLE Page

CHAPTER I

INTRODUCTION

Naturally fractured reservoirs (NFRs) play an important role in oil and gas exploration and production because a large number of oil and gas reservoirs are naturally fractured (Aguilera, 1995; Nelson, 2001). Production from those reservoirs is usually affected by the presence of a system of connected fractures. This fracture network can contribute significant porosity and permeability to a reservoir. Also, it creates a greater degree of heterogeneity in the porous media than is present in unfractured reservoirs. Because of this heterogeneity, production from NFRs usually suffers from low recovery, early water breakthrough, and decreasing productivity index during production (Aguilera, 1995; Nelson, 2001). Understanding and quantifying the fracture distribution, such as identifying the location of highly fractured zones within the reservoir and determining the degree of reservoir anisotropy, can be critical for NFR exploration and development.

Geostatistical approaches such as kriging are commonly used to estimate the spatial distribution of the reservoir properties in a field. When used for NFRs, these approaches exploit the spatial relationships but not the factors that are causes for the fracture development. Studies indicate that the fracture density is affected by geological factors such as formation curvature (e.g., Harris et al., 1960; Lisle, 1994) that can be determined across the field. Thus, while geostatistical methods may help in modeling NFRs, another technique which accounts for the effect of geologic factors can greatly enhance fracture distribution prediction and hence improve the quality of the reservoir management.

This dissertation follows the style and format of American Association of Petroleum Geologists Bulletin.

The stratigraphic factors that could potentially affect fracture distribution include formation rheology, bed thickness, and the interactions between beds. Many studies of the effects of mechanical stratigraphy on fracture distribution have focused on 2 major parameters: bed thickness and lithology. The observations have been that the average fracture spacing is proportional to bed thickness, and lithology controls the difference in fracture spacing in beds of equal thickness (e.g., Huang and Angelier, 1989; Narr and Suppe, 1991; Hanks et al., 1997). In single-bedded folded strata, the fracture density is enhanced by the degree of folding and depends on the mechanism of the fold (e.g., Price and Cosgrove, 1990). For example, the fracture density is greater in the region with greater formation curvature (Murray, 1968; Lisle, 1994).

For a particular geological setting, the spatial distribution of fractures can be a very complex function of different geological factors. For example, the effect of a single geologic parameter on fracture distribution can be enhanced or masked, depending on the values of the remaining parameters. The question of how fracture properties change with an increase of folding, as a function of bed thickness and lithology, is of critical importance not only for the prediction of the fracture distribution within the reservoir but also for understanding the development of the fracture system within the geological setting. Conventional statistical analysis with linear relationships between variables is usually used to examine the relationships between these variables. However, in the case of complex nonlinear relationship among variables as found in NFRs, an alternative technique is needed.

During the last decade, the application of neural networks for identification of nonlinear and non-stationary systems has increased. Artificial neural networks have been used widely in finance, engineering, medicine, and management (Garson, 1998). Neural networks, which can extract relationships among multiple variables underlying observed data, seem to be an excellent tool for investigating the fracture density as a function of multiple geologic parameters. Properly designed and used, the neural network is attractive for analyzing the complex nonlinear system because it does not require *a-priori* knowledge about the functional structure among variables. Ouenes et al.

(1998) used neural networks to analyze the ultimate recovery distribution within the naturally fractured reservoir as a function of the bed thickness, formation resistivity, and formation curvature.

A challenge remains, however, when using neural networks to assess geological relationships. This is because neural networks will have to be applied to a situation with a limited number of observations. The behavior of the neural network in this case is strongly depends on how the model is built and used for analysis. For example, the typical use of a neural net is to divide available data into a training and a validating set but, in a case of limited data, this may create the sets which are not representative of the data. The network behavior also depends on other factors such as initial network weights and the network activation function. Thus, some special attention or modifications are needed.

It is commonly observed that fractures usually develop in sets, each having different orientation, density, and geometric parameters. The interaction of the fractures from different sets creates a highly heterogeneous system that can greatly affect the effective exploration and development of NFRs. The question of how the conductivity of the fracture system behaves as a function of the fracture properties of each fracture set is of critical importance in reservoir management. The flow characteristic of the fracture system can be assessed by using discrete fracture modeling (Chiles and de Marsily, 1993; Karpov, 2001). In this model, a fracture system with required statistical characteristics is statistically generated. The hydraulic isotropy of the system can be estimated by analyzing the flow conductance between specified source and sink within the system.

This research investigates the use of neural network in the cases of limited data. The results are used to investigate the effects of bed thickness, degree of folding, and lithology on the fracture density of the detachment folded Carboniferous Lisburne Group, exposed in northern Alaska. The results of the network analysis are compared to those obtained using conventional multivariate statistical analysis. The discrete fracture

network system is built to investigate the flow characteristics of the system as a function of fractures properties, their orientations and interactions.

This study is a part of a larger project, sponsored by the U.S. Department of Energy, to study the fracture patterns and geometries in folded regions of the Lisburne Group exposed in the northeastern Alaska and to investigate the role of folding and other geological factors in the potential development of a fractured reservoir. In my research, I hypothesize that the major parameters that affect fracture density are degree of folding, bed thickness, lithology, stratigraphic position, and position on folds. Fracture data and associated geologic parameters, collected and defined by geologists at University of Alaska at Fairbanks (UAF), are used for the analysis.

The main objectives of my research are to investigate how:

1. neural networks can be used in case of limited data;
2. statistical and neural network analyses compare for the characterization of fracture systems;
3. fracture density and size (height and length) change as a function of the bed thickness, the lithology, structural position on the fold, and degree of folding; and
4. fracture density, size, termination and filling pattern affect the connectivity of the fracture system;

The results of this research suggest that network behaviors strongly depend on the network initial weights and that the linear activation outperforms other functions in case of limited data. Using multiple realization of the cross validation network training allows uniquely selecting the optimal network configuration and assessing the network prediction variability. Applying these results to our fracture data suggest that lithology and stratigraphic position have strong effects on fracture spacing: in general, fracture density is higher in packstone than in grainstone and fracture density of the two major orientations observed in the field is closely related to the structural position on folds. The degree of folding does not have a strong effect on the fracture spacing, but does

appear to strongly affect fracture length. In tight folds, the fracture length is significantly larger than in open folds.

The difference in size and the actual termination pattern and cementation of the two fracture sets may create a strong degree of permeability anisotropy in the reservoir. Given two fracture sets with similar spacing characteristics, the set with the greater length and height controls not only flow along its principal direction, but also in the orthogonal direction.

The results of this study give insight into the relationships between mechanical stratigraphy and fracture distribution in the detachment-folded Lisburne Group. In addition, the use of neural networks for sparse data sets and the analysis of network prediction variance are discussed in detail and may benefit other applications involving analysis of geological systems. Neural networks are attractive tools for investigating complex, nonlinear systems. However, constructing, training, and interpreting the results of the network may be an arduous task that requires special attention and sufficient experience. Users of the neural network should be aware of the possible negative behavior of the network such as overfitting the training data and converging to local minimum. In cases of data scarcity, special attention should be paid to choosing the optimal network configuration, the activation function used in network, and assessing the prediction variability.

This dissertation consists of 8 chapters. This chapter (Chapter I) describes the problem, objectives, and outlines the dissertation. Chapter II reviews relevant studies. It focuses on the controlling parameters of the fracture distribution associated with folded formations, the application of neural networks, and discrete fracture modeling of fracture systems. Chapter III briefly describes the geological setting of the Carboniferous Lisburne Group, the fracture data, and the results of the analysis done by geologists at UAF. Chapter IV gives the results of conventional linear analysis of the fracture data to characterize the fracture data and to assess the relationships between fracture density and mechanical parameters. Chapter V presents results of testing the neural networks for the case of limited data where the relationship is known. Chapter VI presents the results of

neural network analysis to average fracture spacing as a function of degree of folding, bed thickness, structural position, lithology, and stratigraphic position. Chapter VII presents the results of the DFN study on the flow conductivity of the fracture system. Finally, Chapter VIII presents the conclusions and lists recommendations of this research.

CHAPTER II

LITERATURE REVIEW

This chapter reviews fracture characterization and fracture distribution as related to folding and mechanical stratigraphy. Also, it briefly presents the background of artificial neural networks and their applications in studying complex, nonlinear relationships among variables. Finally, it briefly introduces discrete fracture network modeling and its application to studying the flow characteristics of fracture systems.

II.1. Fractures and Folds

Fracturing is defined as the loss of cohesion of the material along some plane (Price and Cosgrove, 1990). This occurs when the difference between maximum principal stress direction and minimum principal stress direction is greater than the cohesive strength of the material. Fractures in rock can be classified as extension or shear fractures. Shear fractures involve the movement of the fracture wall parallel to the fracturing plane, whereas extensional fractures do not have such movement (Stearns and Friedman, 1972). For any triaxial stress state in the rock, there are two potential shear fracture orientations and one potential extension fracture orientation. The two shear-fracture planes form an angle of about 60º and the axis of the maximum principal stress bisects this acute angle. The extension fracture is parallel to the plane of the maximum (σ_1) and intermediate (σ_2) principle stress axes and normal to the minimum principle stress (σ_3) (Figure 2.1).

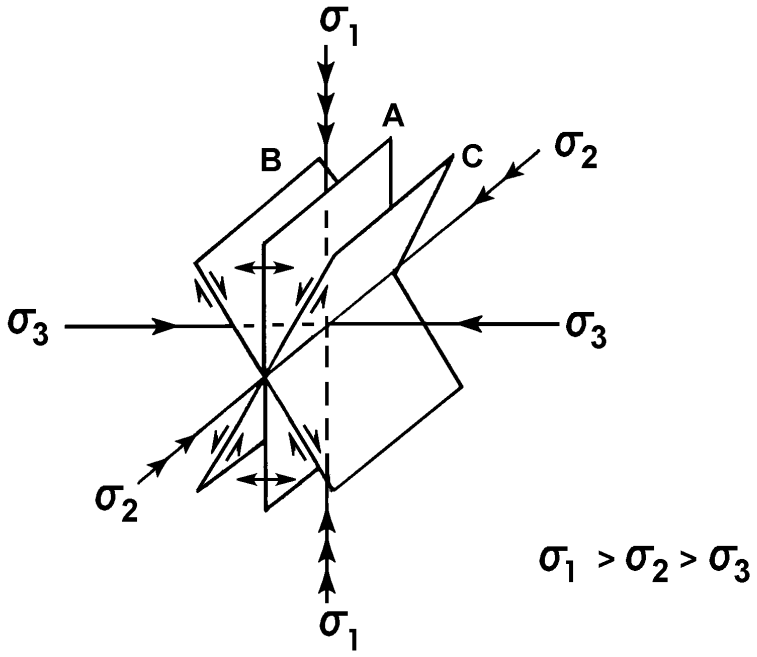

Figure 2.1 – Potential fracture planes developed in compression tests: extension fractures (A) and shear fractures (B and C). (After Nelson, 2001).

Fracture systems that are both pervasive and consistently oriented in a large volume of rock can be divided into two major classes: regional and structure-related fractures (Stearns and Friedman, 1972). The regional fractures form as a result of the structural development of a large region and are usually composed of two regular and continuous fracture sets that are normal to one another. The structure-related fractures are associated with specific local features such as faults or folds and are determined by the deformation mechanism within a specific structure. Fractures associated with faults are generally related to the same stress state that caused the fault. Fractures associated with folds are affected by the history and kinematics of the folds. The folded strata can undergo several different stress states through the folding history (Stearns and Friedman, 1972).

Stearns (1967) identified the two most common fracture patterns associated with a fold. Both patterns consist of two conjugate shear fractures and an extension fracture. The difference between two patterns is the fracture orientation with regard to the fold axis. The extensional fractures in first fracture pattern are oriented normal to the fold axis, whereas extensional fractures in the second pattern are oriented parallel to the fold axis (Figure 2.2A, C**)**. In both cases, the intermediate principal stress axes with respect to the fold axes are the same. In many cases, depending on the amount of overburden, other fracture patterns (Figure 2.2B, D) can occur.

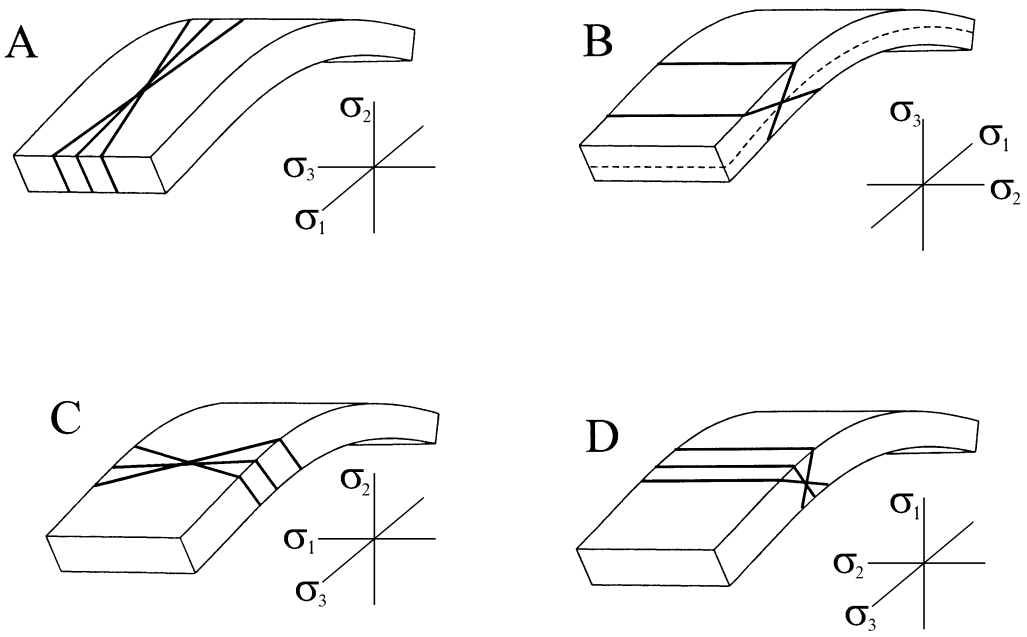

Figure 2.2 – Common fracture patterns associated with folding. (After Stearns, 1967).

More recent studies on fracture patterns associated with folds suggest that the fracture distribution is determined by the fold kinematics. Several models of folding have been proposed (Price and Cosgrove, 1990; Lisle, 2000) and have implications for explaining the fracture distribution.

One of the most common models relating folding to fracturing in a homogeneous single layer is the tangential longitudinal strain model (Figure 2.3A). This model of the fold for a single layer of homogeneous, isotropic material suggests that fracturing is concentrated around the fold hinge, with extensional fractures in the outer curve of the fold and compressional fractures in the inner curve of the fold (Price and Cosgrove, 1990; Cosgrove and Ameen, 2000). These two regions are separated by a neutral surface. In this model, one of the principal strains is always parallel to the layer boundary. The outer arc of the hinge area experiences extension and the maximum principal extension is parallel to the layer boundary. The inner arc is compressed and the minimum principal extension is parallel to the layer boundary (Price and Cosgrove, 1990). This model suggests that the fracture density relates to the degree of deformation of the strata.

Several researchers have investigated the effects of the degree of deformation on the fracture distribution. Harris et al. (1960), Lisle (1994), Jamison (1997), and Henning et al. (2000) suggest that fracture density increases with the increasing bed curvature: if the fracturing relates to the folding process, the higher the degree of folding, the greater the fracture density.

In multiple layers, folding can be modeled as developing via flexural slip folding (Figure 2.3B). In flexural slip folding, bedding planes slide past each other (Price and Cosgrove, 1990; Cosgrove and Ameen, 2000), resulting in a different strain distribution pattern compared to those in a tangential longitudinal strain model. Bedding-parallel shear and en echelon tension gashes are commonly occur in conjunction with flexural slip (Price and Cosgrove, 1990). These features generally die out towards the hinge of the fold, where the slip between beds is zero.

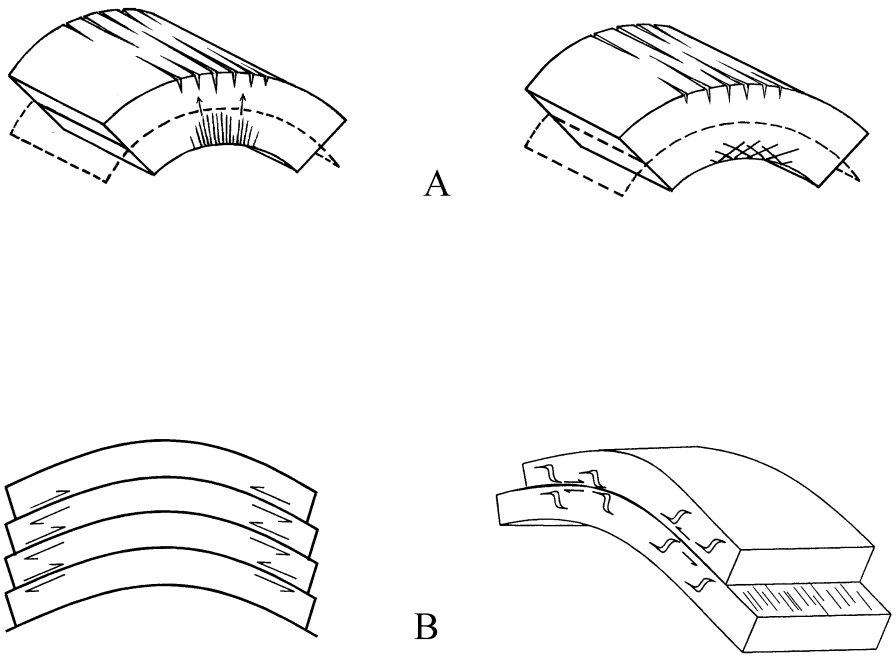

Figure 2.3 – Fracture patterns from tangential longitudinal strain model and multiple layer flexural slip folding. (After Price and Cosgrove, 1990).

A detachment fold forms when a layer of relatively competent rock deforms above a bedding-parallel thrust fault. Detachment folds are commonly found in layered strata, where a relatively competent layer overlies a relatively incompetent unit. Detachment folds have been modeled with fixed hinges and rotating limbs (e.g., Poblet and McClay, 1996; Homza and Wallace, 1997) or with a migrating hinge and non-rotating limbs (e.g., Poblet and McClay, 1996; Epard and Groshong, 1995; Homza and Wallace, 1997) Figure 2.4.

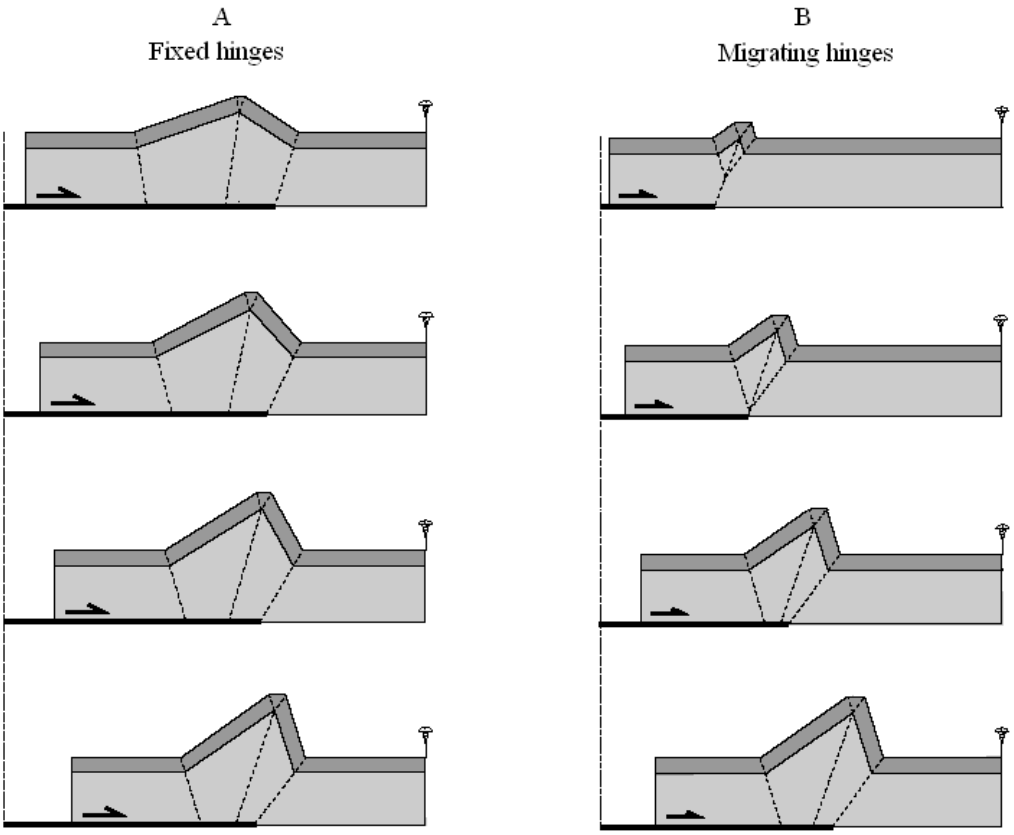

Figure 2.4 – Various detachment fold models. In model A, the position of hinge is fixed, but in model B the hinge migrates into limb position. (After Poblet and McClay, 1996).

In models where fold hinges are not fixed, the folded rocks migrate through the synclinal hinges, and thus, similar fracture pattern and fracture density would be found in both the limbs and the hinges. In fixed hinge models, the rocks are fixed with respect to all hinges. In this case, fracture density would be higher in the hinges than in the limbs and there would no overprinting of the hinge structure (intense cleavage, small-scale contractional folds and faults) found in the limb (Homza and Wallace, 1997; Jamison, 1997; Atkinson and Wallace, 2003). Thus, analysis of the fracture density as a function of structural position on a fold may help better understand the detachment folding process.

II.2. Fracture and Mechanical-Stratigraphy

Mechanical stratigraphy can be viewed as the rheological properties of the rock, the properties of the interfaces between layers, the bed thickness, and the overall scale of the multilayer packet being folded (Ramsay and Huber, 1987). Studies on the relationship between mechanical stratigraphy and fracture density have focused on the effects of several parameters including thickness of the fractured layer, lithology of the fractured layer, and the properties and relative thickness of the incompetent layer between the fractured layers.

The positive relationship between average fracture spacing and bed thickness has been observed in different geological settings. McQuillan (1973) investigated the Asmari limestone outcrops over an extensive area of the Zagros Mountains and proposed that fracture density has an inverse logarithmic relation to bed thickness, but is independent of the structural setting. Many authors, based on analysis of field data, suggest that the average fracture spacing is directly proportional to the formation bed thickness (e.g., Harris et al., 1960; Ladeira and Price, 1981; Huang and Angelier, 1989; Narr and Suppe, 1991). This fracture spacing – bed thickness relationship may depend on how well-developed the fracture system is (Narr and Suppe, 1991; Wu and Pollard, 1995). Wu and Pollard (1995) experimentally showed that, when the applied stress

reaches a certain value, the fracture spacing stops evolving and remains nearly constant. Spacing prior to saturation varies strongly with applied stress whereas, when saturated, spacing is a function of layer thickness. Ladeira and Price (1981) have shown that fracture spacing is a function of bed thickness for up to a 1.5 meter bed thickness. In beds thicker than 1.5 meters, thickness does not seem to correlate with fracture distribution. Hanks et al. (1997), studying the un-deformed section of the Lisburne formation in the northeastern Brooks Range, found no reliable relationship between fracture spacing and bed thickness.

Others have investigated the effect of the lithology on the fracture distribution, finding that the more brittle, competent rocks have more closely spaced fractures (Harris et al., 1960; Huang and Angelier, 1989). Hanks et al. (1997) showed that lithology is the primary controlling factor on fracture properties and characteristics in relatively undeformed sections of the upper Lisburne Group in the eastern Sadlerochit Mountains. In these undeformed carbonates, grainstones are the least fractured, with wider and more through-going individual fractures. Dolomitic mudstones are the most densely fractured, but have fractures of limited vertical extent that generally terminate at bed boundaries.

Ji and Saruwatari (1998) analytically show that the relationship between joint spacing and bed thickness is affected by the relationship between thickness of the competent and incompetent layers: the fracture density in the competent layers which adjoin thick, incompetent layers is smaller than when the adjacent layers are thin. Helgenson and Aydin (1991), studying fracture development in multilayer formations, concluded that the fracture distribution and orientation are affected by the relative thickness of the competent and incompetent layers. As the thickness of the incompetent layer increases, the degree of communication among fractures across shale decreases.

These studies of the effects of mechanical stratigraphy on fracturing have approached the properties of structure-related fractures as a function of a single lithology-mechanical stratigraphic parameter. In reality, the fractures are formed under the effects of a combination of all these and perhaps other parameters. The fracture density can be a complex function of bed thickness, lithology, degree of folding, and the

structural position on a fold. It is important to analyze and rank the effects of these parameters on fracture density. For this purpose, multivariate linear regression is often used. However, this method often fails in cases of complex and nonlinear relationship among variables. Artificial neural networks, however can provide a method to approach this problem.

II.3. Neural Network Analysis

II.3.1. Introduction

Multivariate linear analysis is usually used to study relationships between variables. In case of nonlinear relationships, some forms of nonlinear transformation of the variables can be used (Xue et al., 1997). The mathematical form of the nonlinearity is usually assumed to be known or empirically determined through trial and error. However, when the relationship among variables is complex and nonlinear, an alternative technique is often needed to solve the problem. One of the methods used for studying the complex relationship among variables is the artificial neural network (ANN). Compared to multivariate linear analysis, ANNs have several advantages. One of them is that the functional relationships between explanatory variables and dependent variables does not need to be known *a priori*. The network learns from examples and adjusts itself to generalize the underlying relationship among variables. Other advantages are that neural networks can have several outputs and also can use discrete variables as inputs or outputs.

There are many networks with different architectures specifically designed for solving different problems (Fausett, 1994; Ripley, 1996). All ANNs, however, consist of neurons (or processing units, or nodes) with an activation function associated with each of them and the connections between these neurons (Figure 2.5**)**.

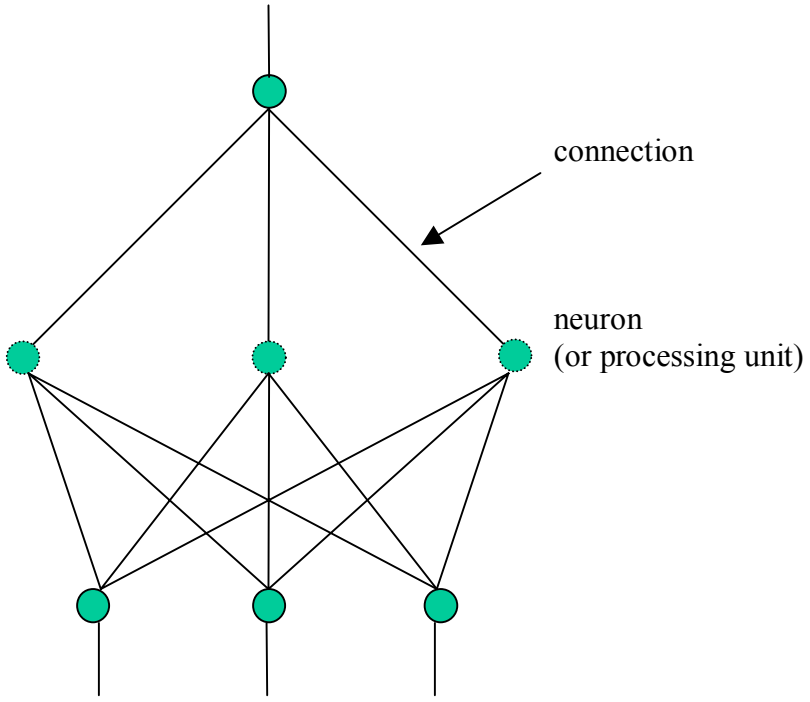

Figure 2.5 – Neural network elements: neurons and connections between neurons.

Neuron. Network neuron is the elemental processor of the neural network, where the data processing takes place. An ANN has input and output neurons. The input neurons represent explanatory variables and output neurons represent response variables. Each neuron of the network receives an input signal from other neurons or from external sources and uses it to compute an output signal (Figure 2.6). The mathematical function which relates the input to the output of a neuron is called an activation function.

Activation function. The activation function is the transform function *f* that is applied at each neuron on the input signal. It has this name from the analog of the neuron of the brain: upon receiving the signal, the neuron estimates the output and either remains

inactive or changes to active status. In an ANN, the activation function is also called the learning function. There are several learning functions that can be used. The choice of which function to use is arbitrary, problem dependent, and in most cases is determined by computational considerations of the training process. For the backpropagation training algorithm, the activation function should be differentiable (Fausett, 1994). It is also desirable that its derivative be easy to compute. The most frequently used functions are the linear, the sigmoidal, and the Gaussian functions. The mathematical forms of these functions are as follows.

Linear function: $f(x) = ax + b$

Sigmoidal function: $f(x) = \dfrac{1}{1+e^{-x}}$

Gaussian function: $f(x) = ae^{-x^2} + b$

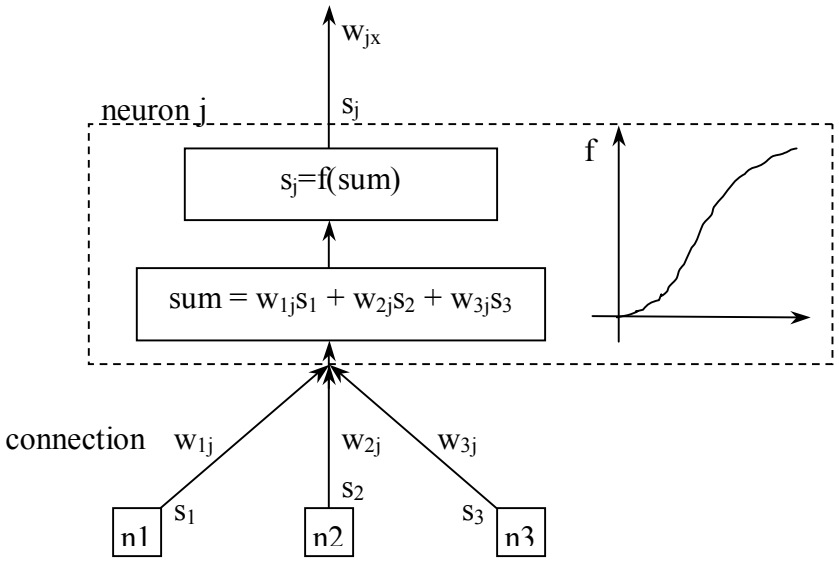

Figure 2.6 – Illustration of the data processing at a neuron.

Connection. Network connection represents the flow of data between neurons and has a weight. A connection between neurons A and B has a coefficient multiplying the signal from neuron A, before being fed to neuron B. Therefore, it represents the contribution of the neuron A in the input, and because of that, in the output of the neuron B. In Figure 2.6, at some moment the neuron j receives 3 signals s_1, s_2, and s_3 from neurons n_1, n_2, and n_3 respectively. This neuron j processes this information by first multiplying the input signals (s_1, s_2, and s_3) to the corresponding connection weights (w_{1j}, w_{2j}, and w_{3j}), then taking the summation and finally putting the result into its activation function. If the activation function *f* of this neuron is the sigmoidal function, then the output of the neuron j, which will be supplied to other neurons is:

$$s_j = f\left(\sum_{i=1}^{3} w_{ij} s_i\right) = \frac{1}{1+e^{-\left(w_{1j}s_1 + w_{2j}s_2 w_{3j}s_3\right)}} \tag{2.1}$$

The processing ability of neural networks rests on the system of weights of the network, which are iteratively adjusted so that, for a given value of the input variable, the output from the network matches the observed value of the response variable. Once this "training" phase is complete, the neural network can be used to predict and to investigate relationships between input and output variables.

Network training. Network training is the process of adjusting the network connection weights so that explanatory and response values match the data as closely as possible. In the case of nonlinear correlation, the most widely used criterion of match is the mean squared error (MSE) of the network output with regard to the observed values of response variable. Considering a neural network with one output node (accordingly to 1 response variables) and N_I input nodes (accordingly to N_I exploratory variable), the MSE of the network during training is calculated as:

$$E = MSE = \frac{1}{N_k}\sum_{k=1}^{N_k}\left[f(\mathbf{x}_k;\mathbf{w}) - Y_k\right]^2 \qquad (2.2)$$

where Y_k is the observed value of the response variable at given values of the exploratory variables $\mathbf{x}_k = (x_1, x_2, ..., x_{N_i})$, N_k is the number of data used in training, $f(\mathbf{x}_k;\mathbf{w})$ is the network estimate at $\mathbf{x}_k$, $\mathbf{w}$ is the vector of the network weights that specifies the model. Note that in places where a weight indicates a connection between two neurons, it is written in matrix notation such as w_{ij}.

The objective of the learning process is to find the weight vector **w*** which minimizes the objective function E. In neural networks, this is always done with iterative algorithms. The basic principle of these learning algorithms is that, given the current parameter vector $\mathbf{w}_k$, for each iteration, a direction $\mathbf{u}_k$ and a learning rate α_k are computed, and then a new set of **w**, $\mathbf{w}_{k+1}$, is calculated with the following rule:

$$\mathbf{w}_{k+1} = \mathbf{w}_k + \alpha_k \mathbf{u}_k \qquad (2.3)$$

Depending on how many terms of the Taylor's expansion of the objective function are used, learning algorithms can be classified in two broad categories: 1) first order and 2) second order methods (Wasserman, 1993). The first order learning algorithms are all varieties of gradient descent methods. The family of second order methods includes quasi-Newton and conjugate gradient methods (Wasserman, 1993; Hagan and Menhaj, 1994).

II.3.2. Feed Forward Neural Networks

There are several types of ANN, differing from each other by their architecture and learning process (Fausett, 1994). One of the most widely used ANNs for pattern recognition and multivariate correlation is the feed forward network with back propagation learning algorithm (Rumelhart and McClelland, 1986; Bishop, 1995;

Fausett, 1994; Garson, 1998). This study used this neural network for investigating the relationship between fracture density and geologic parameters.

A multilayer feed forward neural network (FFN) has neurons arranged in layers (Figure 2.7). The output of a neuron in one layer is directed as the input to each and every neuron in the immediately following layer. There are no lateral connections between neurons in the same layer and no feedback connection to the neurons in previous layers. For the network in Figure 2.7, there are three layers: the input layer, one hidden layer, and the output layer. Each neuron in the input layer represents one exploratory variable, while each neuron in the output layer represents one response variable. An additional neuron with constant value (usually 1) is often added to the input layer. This neuron is called a bias node and has a role similar to the constant term in the multiple linear regression, e.g. it allows shifting the origin defined by input variables for the network output. FFN can have one or more hidden layers between the input and output layers, depending on the complexity of the problem at hand. Hornik et al. (1990) showed that FFNs with one hidden layer are capable of approximating any continuous function. Networks with more hidden layers, however, can speed up the training process and can help avoid local minima during learning (Hirose et al., 1991; De Villiers and Barnard, 1993).

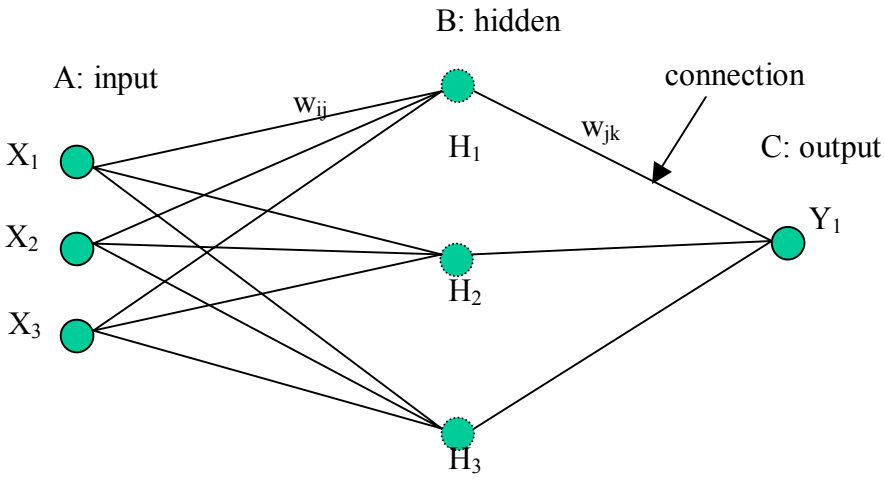

Figure 2.7 – Feed forward neural network with one hidden layer. The network has three input nodes (X_i, i=1 to 3), three hidden nodes (H_j, j=1 to 3), and two output nodes (Y_k, k=1 to 2).

At each neuron, a processing function is applied on the input signal. Often, the processing function at input neurons is the identity function, that is, $f(x)=x$. Supposed that at each neuron in hidden layer, function f_1 is applied and at each neuron in output layer, function f_2 is applied, then the network shown in Figure 2.7 can be mathematically expressed as:

$$f(\mathbf{x};\mathbf{w}) = f_2\left(\sum_{j=1}^{N_h} w_{j1} f_1\left(\sum_{i=1}^{N_i} w_{ij} X_i\right)\right) \tag{2.4}$$

where: X_i denotes the input value at input neuron i, w_{ij} is the connection weight between input neuron i and hidden neuron j, w_{j1} is the connection weight between hidden neuron j and output neuron 1, N_i=3 and N_h=3 are the number of input and hidden nodes. The notation $f(\mathbf{x};\mathbf{w})$ implies that the output of the network at output node is a function of given vector values **x** of exploratory variable and the weight vector **w**.

II.3.3. Back-Propagation Algorithm

Perhaps the most widely used training algorithm for FFNs is the back propagation method (Rumelhart and McClelland, 1986; Ripley, 1996; Bishop, 1995). This method propagates the error produced by the network for a given input backward through the layers to adjust the network weights. The training of a network by the back propagation algorithm involves three stages: the feed forward of the input training pattern, the calculation and back propagation of the associated error, and the adjustment of the connection weights. During feed forward, each input node receives an input signal (actual value of the explanatory variable) and feeds this value to each of the hidden nodes. Each hidden node then computes its activation function and sends the result to each output node. Each output node computes its activation to form the response of the net for the given input pattern. The output of the net is compared to the observed value to determine the associated error. This error is used to calculate the update of the connection weight.

A standard back propagation algorithm is the first order learning algorithm for FFNs. This algorithm is widely used because of its simplicity and small programming cost. In this algorithm, the gradient of the objective function E (Eq. 2.2) with respect to each of the weights $\mathbf{g}_k = \partial E / \partial w_k$ is computed at each iteration. This vector gives the direction of most rapid increase in E. Hence, the error can be reduced most rapidly in the direction of $-\partial E / \partial w_k$ and the weight vector is updated in the direction in which the error function decreases most rapidly.

The weight update at iteration k+1 for given learning rate α can be written as:

$$\mathbf{w}_{k+1} = \mathbf{w}_k - \alpha \mathbf{g}_k \tag{2.5}$$

The first values of the weight vector ($\mathbf{w}_0$) are randomly generated around zero and are called initial weights. Fausett (1994) gives a detailed derivation of the gradient with respect to each weight in FNNs and the algorithm for network training.

For large networks with large amounts of training data, a standard back propagation algorithm may be slow to converge to a solution. Several improvements to the algorithm have been proposed (Jacobs, 1988; Leonard and Kramer, 1990; Silva and Almeida, 1991). The adaptation of the learning rate (α_k) is used to speed up the training: the learning rate can be set at a higher value if the algorithm goes in the direction toward the minimum, otherwise, it is reduced. To avoid oscillation, accelerate the optimization, and reduce the problem of convergence to local minima, momentum, *m,* is often used to take into account the change in the previous iteration:

$$\mathbf{w}_{k+1} = \mathbf{w}_k - \alpha_k \mathbf{g}_k - m\mathbf{g}_{k-1} \tag{2.6}$$

The learning is stopped when the gradient of the objective function becomes small or $\mathbf{w}$ is said to be close to $\mathbf{w}^*$. After training, the neural net can be used for prediction just by applying the forward calculation, given any set of explanatory variable values.

II.3.4. Network Applications

The applications of ANNs show that it is a useful tool for modeling the complex relationship between variables where simple linear functions fail. Garson (1998) gave a summary of the wide applications of ANNs in finance, engineering, medicine, and management. Neural networks have been used for predicting permeability (e.g, Rogers et al., 1992 ; Huang et al., 1996). Ouenes et al. (1998) used a neural network to identify sweet spots for infill drilling and to prepare data for input into NFR fluid flow simulations. They used neural networks to establish the relationship between reservoir structure, bed thickness, and well performance to fracture density.

The use of the neural networks, however, has limitations:

- The behavior of the ANN output depends on several factors, such as network architecture, choice of activation function, and number of data used in training. Complex networks may lead to overfitting – a phenomenon which

occurs when the ANN "memorizes" the training data and fails to generalize the functional relationship between variables.

- The input variables relate to the outputs through a system of nonlinear connected weights. Hence, the analysis of causality between explanatory and response variables is not straightforward.
- Unlike multivariate linear regression, the variance of the network predictions is not easy to estimate. Thus, the assessing of the uncertainty related to the network prediction is not a straightforward task.

I elaborate on these issues below.

II.3.4.1. Network Generalization Ability

Similar to other parameter determination problems, the solution given by the neural network depends on the *degree of determination* of the system. The degree of determination of a system is defined as the ratio of available data points, N, to the number of unknown parameters, U:

$$D_1 = \frac{N}{U} \tag{2.7}$$

The system is called overdetermined if $D_1>1$. For a neural network, each connection weight is one unknown parameter. ANNs with $D_1<1$ have the potential to produce a solution that overfits the observed data. In this case, the training error is small but the neural network has failed to capture the general trend of the relationship between variables.

To reduce the probability of overfitting, a network should be as simple as it can be, yet still is able to produce good approximations of the true function. The requirement of a simplest model is called the parsimony requirement (Box and Jenkins, 1976). For a FFN with one hidden layer, the selection of the appropriate network leads to the choice of the number of hidden nodes in this layer. The performance criterion for

judging the neural network is the generalization ability, defined as the prediction accuracy of the neural network on data that were not used for determining the network weights. Several techniques have been proposed to select a simple network which gives better generalization ability for given data. One approach is to start with a large network and either iteratively simplify its architecture (LeCun et al., 1990), or include complexity terms in the objective function E to force as many weights as possible to zero (Chauvin, 1990). Others start with a simple network and iteratively add nodes to it (Ash, 1989).

For a given network architecture, one widely used approach to avoid over fitting is to use validation (Bishop, 1995; Ripley, 1996). The available data are divided into 2 sets: a training dataset and a validating dataset. The training dataset is used to train the network. The validating dataset is used to assess the generalization ability of the network. At any time during the training, two types of error are calculated: one is the usual training error and one is the error of the network on the validating data set. If both error terms are decreasing, the training continues. If the error on the validating data set starts increasing, the training is terminated.

Several authors (e.g., Wessels and Barnard, 1992; Bowden et al., 2002) have pointed out that the way data are divided into a training and a validating set can have a significant influence on the performance of an ANN. When the number of available data is small, division of data into datasets reduces the generalization ability of the network. Furthermore, it creates the subsets that may not represent the same population. As a result, this validating method tends to give widely variable estimates of prediction error which depend heavily on the partitioning of available data. Thus, in the case of small datasets, cross validation is used for selecting optimal network architecture (Moody and Utans, 1992; Zapranis and Refenes, 1999). This method uses incomplete datasets generated by bootstrapping and jackknifing for network training. The data that do not participate in the training are used to assess the prediction error of the network. Among different network architectures, the one that produces the smallest prediction error is the optimal configuration.

The main difference between bootstrapping and jackknifing is the way the subsets of data are created. Bootstrapping produces a large number of datasets by sampling from available data with replacement while jackknifing sequentially removes points from available data (Lewis and Orav, 1989). In ANN terminology, cross validation with jackknifed data is also called leave-v-out cross validation with v being the number of data points removed. If v=1, the method is called the leave one out cross validation method.

Empirical studies (e.g., Twomey and Smith, 1996) show that bootstrapping may need to generate a large number of subsets and gives similar results to the leave-one-out validation method. Because of this reason, the leave one out cross validation method is widely used for network configuration selection, especially when the data are of small or medium size. In cases where computational cost is a big consideration, the leave-v-out cross validation (with v>1) can be used at a price of less data used in training.

II.3.4.2. Network Interpretation

One major problem that prevents ANNs from wider use is the difficulty in analyzing the causal relationship between explanatory and response variable. The neural network is usually considered to be a "black box" for prediction (Bishop, 1995). Several researchers have tried to interpret the results from neural networks to answer the question: how does one input variable contribute to the output of the model. Ozesmi and Ozesmi (1999) proposed a neural interpretation diagram for providing a visual interpretation of the connection weights among neurons. The relative magnitude of each connection is represented on the diagram by line thickness (i.e. thicker lines representing greater weights) and line shading represents the direction of the weight (i.e. black lines representing positive and grey lines representing negative weights). Garson (1991) presented a simple method, later modified by Goh (1995), for partitioning the relative share of the output prediction associated with each input variable. This method, however, provides only the overall influence of each explanatory variable on the

network behavior. In cases where the input variables of the network are both continuous and categorical, the results of this weight partition method can be misleading (Goh, 1995).

A number of investigators have used sensitivity analysis to determine the spectrum of input variable contribution (e.g., Lek et al., 1996; Maier and Dandy, 1998). The method calculates the change in prediction if one of the inputs varies while the others are fixed at some value. This fixed value can be the mean of available input data or at several quantile values of the explanatory variables in the training dataset (Lek et al., 1996). This method provides detailed effects of each explanatory variable on the response variable and is a good choice for analyzing the causal relationship between variables in cases where some of the explanatory variables are discrete variables. Its drawback is that the resulting sensitivity matrix can be very big, especially for networks with many explanatory variables.

II.3.4.3. Network Prediction Variability

Another important issue in using neural networks is the ability to assess the uncertainty of the network prediction. Neural networks have been viewed as a black box for prediction. Recently, several authors have tried to relate the neural network to other statistical methods of inference (e.g., Chryssolouris et al. 1996; Zapranis and Refenes, 1999; Rivals and Personnaz, 2000). The methods of statistical inference fall into two categories: analytical and numerical. The analytical method assumes that the error of the network is distributed normally and the estimated weights represent the true parameters of the model. The numerical method uses resampling techniques to estimate the network prediction error. Those techniques include bootstrapping and jackknifing to build a prediction variance (Efron, 1993).

Chryssolouris et al. (1996) and Rivals and Personnaz (2000) proposed a method to calculate the ANN confidence interval based on the assumption of a normal distribution of the errors. If the model gives a good prediction of the actual system

behavior, then $\mathbf{w}$ is assumed to be close to the true value $\mathbf{w}^*$ of the model and a Taylor's expansion to the first order can be used to approximate network prediction $f(\mathbf{x};\mathbf{w})$ in term of $f(\mathbf{x};\mathbf{w}^*)$:

$$f(\mathbf{x};\mathbf{w}) \approx f(\mathbf{x};\mathbf{w}^*) + \mathrm{f}_0^T \cdot (\mathbf{w} - \mathbf{w}^*) \tag{2.8}$$

where f_0 is the gradient of the network prediction at a given input vector $\mathbf{x}$.

The assumption of the normality of the network prediction error leads to the following expression of the variance of error around the true value (Chryssolouris et al., 1996):

$$\mathrm{var}(y_0 - \hat{y}_0) \approx \sigma^2 + \sigma^2 \mathrm{f}_0^T (\mathbf{F}^T \cdot \mathbf{F} \cdot)^{-1} \mathrm{f}_0 \tag{2.9}$$

where y_0 is the true value of the system, $\hat{y}_0 = f(\mathbf{x};\mathbf{w})$ is the network predicted value at given $\mathbf{x}$, $\mathbf{F}$ is the Jacobian matrix of the network prediction with the dimensions N by p, N is the number of data points used to estimate the weight vector $\mathbf{w}$, p is the dimension of vector $\mathbf{w}$, σ^2 is the variance of the error associated with the function which models the system.

The unbiased estimator of σ is as follows:

$$s = \sqrt{\frac{\left\| y - f(\mathbf{x};\mathbf{w}) \right\|^2}{N - p}} \tag{2.10}$$

where N is the number of input data points, and p is the number of parameters in the model.

Thus, the 100(1-α) confidence interval for the predicted value $\hat{y}_0$ is:

$$\hat{y}_0 \pm t_{N-p}^{\alpha/2} s \left(1 + \mathrm{f}_0^T (\mathbf{F}^T \cdot \mathbf{F} \cdot)^{-1} \mathrm{f}_0 \right)^{\frac{1}{2}}, \ldots\ldots\ldots\ldots\ldots\ldots \tag{2.11}$$

where $t_{N-p}^{\alpha/2}$ is the two-tailed t statistic with N-p degrees of freedom.

Eq. 2.9 suggests that the analytical method can only work for the system where N>p, otherwise, the estimation of σ is undetermined. Furthermore, the confidence interval determined by this method is unreasonably large or unidentifiable in cases where **w** is not close to **w***, which is a common condition for networks with few degrees of determination. As it has been pointed out, FFNs can converge to the same criterion with different sets of weights (Bishop, 1995; Ripley, 1996). The analytical method for building confidence intervals therefore is applicable only for the cases where abundant data are available for network training.

The resampling approach for estimating prediction error of the neural networks consists of building a number of subsets from the available data for network training. The resulting network weights are used for assessing the prediction variance (Hwang and Ding, 1997). Researchers have used this resampling approach for model selection and for estimation of network prediction error (Moody and Utans, 1992; Twomey and Smith, 1996; Kalell et al., 2002).

Reviewing the applications of ANNs reported in literature, I found that ANNs are attractive and powerful tools for establishing the complex relationship among variables in high-dimension problems. A neural network has a number of attractive features compared to linear correlations. For example, it can model the data without the specification of the structural relationship between input and output data. However, this advantage can at the same time be a disadvantage: given enough complexity of the network, ANNs can fit almost any continuous function without giving a meaningful prediction. The results of the ANN analysis strongly depend on how the models are built, validated, and used. Strict rules governing the modeling process however are lacking and the effectiveness of using neural networks is highly problem dependent.

II.3.4.4. Sparse Dataset and Neural Networks

Neural networks are usually used in cases of abundant data. In cases of limited data, the selection of the optimum network configuration and the neural network

performance can be affected by the values of initial weights of the network. In this case, we have a system with sparse dataset.

The sparseness of the data is related to the number of parameters in the model and can be represented by the degree of determination (Eq. 2.7). A system with sparse datasets has a small degree of determination. Bishop (1995) suggested a degree of determination of at least 2 for using neural networks. Amari et al. (1997) suggests that the degree of determination must be 30 for the system to be independent of the initial weights. Neural networks with the degree of determination less than 1 can be considered as having been trained by a sparse dataset.

Since the network behavior strongly depends on the initial network weights, it is important to be sure that the prediction results are consistent and the variability of the prediction can be assessed in cases of data scarcity. In Chapter V, I will address the question of selecting the optimum network configuration using the leave one out cross validation method. I will also examine the use of the cross validation technique for assessing the FFNs' prediction variance.

II.4. Fracture Modeling

Fluid flow studies of fractured rocks require three-dimensional modeling of the fracture system, which consists of interconnected fractures. There are three approaches to simulate the fluid flow and transport in fractured rocks: discrete network simulation, continuum approximations based on either porous medium equivalent assumptions or statistical representation of mass transfer, and hybrid models that combine elements of both discrete fracture models and continuum approximations (Sahimi, 1995; Smith and Schwartz, 1993).

In continuous models, the flow behavior of the system is modeled by the classical continuum equations of transport. These represent the average behavior of the system, where the average is taken with respect to a representative volume. The representative volume must be large enough to encompass its variable influences on the

fluid flow within the network. This, however, is not always satisfied when several scales of fracturing occur within the rock mass: a small number of areally extensive fractures may have a predominant influence on the fluid flow behavior (Smith and Schwartz, 1993).

Discrete fracture models, in contrast to the continuum models, characterize the flow behavior of the fracture system on a fracture-by-fracture basis. Discrete fracture networks (DFNs) model a fracture system in space as a numbers of discrete fractures (Figure 2.8) with specified statistical distributions of the major characteristics and the rules governing the conditions of interaction with other fractures. Several models for generating the fracture system in the given rock volume have been proposed. The models differ from one another only with regard to the spatial distribution of the fractures, and the inter-relationship of fracture size and fracture location. Dershowitz and Einstein (1988) give a detailed description of DFN models.

A fracture system can be represented by a network of channels or pipes with given parameters or assigned hydraulic properties to the fracture intersections. Then, it is possible to calculate fluid flow through the network (Cacas et al., 1990; Billaux et al., 1989). Doe (1997) summarizes the principal steps in using a discrete fracture model:

1. Analysis of borehole and surface data to define the fracture geometry and properties of fractures. This includes identification of fracture sets and distributions of orientation, size and aperture.
2. Generation of fracture networks. This step builds the fracture network according to some spatial models and fracture properties obtained in step 1. Spatial models define fracture locations by any of several methods: random distributions, distributions with spatial correlation (geostatistical models), or distributions with power law variations of separation distance (fractal models).
3. Definition of boundary conditions for the model and preparing a numerical mesh for finite-element analysis.

4. Calculation of flow and solute transport through the network.

The following sections cover the issues related to data preparation for DFN as well as a few results of DFN applications for studying fracture systems.

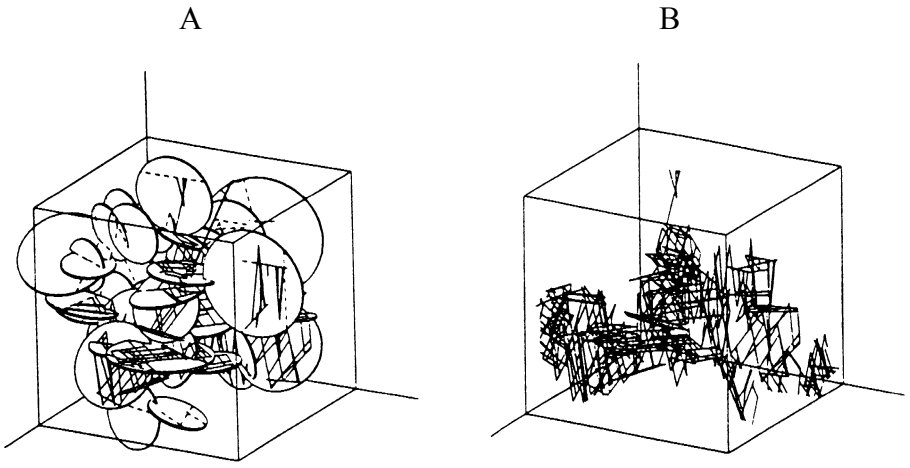

Figure 2.8 – Example of fracture networks. A) network of random disks; B) network of channels. (After Chiles and de Marsily, 1993).

II.4.1. Fracture Characterization

II.4.1.1. Fracture Survey

The first step in using DFNs is the collection of the fracture data. Fracture data are obtained through three main types of survey (Chiles and de Marsily, 1993):

1. Borehole surveys: the measurements are usually made on oriented cores or deduced from logs. Such surveys may provide information about fracture orientation, density, existence or possible fill, aperture, surface geometry, etc. But fracture size, one of the major parameters in the study of the hydraulic properties of the rock, is typically difficult to evaluate from borehole surveys.
2. Scanline surveys: fracture properties are sampled along a scanline drawn on an outcrop surface or a photograph. As an extension of the preceding technique to a 2D area, fracture trace size can be measured.
3. Areal surveys: all traces located within a specified area are collected.

In general, a complete description of a fracture system is often difficult due to limited exposure of fractures for sampling. It is typically inadequate to deterministically describe the actual system of fractures in the formation (Chiles and de Marsily, 1993). Instead, the fracture system is characterized by applying stochastic methods. The standard descriptive procedure is to represent each of the major fracture characteristics, including fracture orientation, fracture spacing, fracture size or trace length, and aperture by a statistical distribution (Dershowitz and Einstein, 1988).

II.4.1.2. Statistical Description of Fracture Properties

Substantial work has already been performed on the analysis and representation of fracture properties by using statistical distributions (Table 2.1). The most widely used distributions for fracture trace length include the exponential, lognormal, hyperbolic, and gamma distributions (e.g, Dershowitz and Einstein, 1988, Narr and Suppe, 1991; Wu and Pollard, 1995).

Rives et al. (1992) and Wu and Pollard (1995) suggest that the fracture spacing starts with an exponential distribution, changes to lognormal and then to normal as fracturing develops. Some authors (e.g. Barton and Zoback, 1992) argue that the

abundance of cases when the lognormal distribution is found for fracture length may be a result of inadequate sampling of small-scale features.

Stochastic modeling of fracture generation based on different processes leads to different distributions: random placement processes lead to exponential distributions; multiplicatory processes as they occur in breakage lead to lognormal distributions; and continuity of the process from smallest to largest sizes produces hyperbolic (fractal) distributions. In modeling fracture spacing, the most commonly used process is a Poison process. This process generates fracture location independently according to a uniform distribution and the spacing will be distributed according to an exponential distribution. If fracture location is generated by a Markov process, in which fracture location depends on the preceding one, the spacing will also be exponentially distributed (Dershowitz and Einstein, 1988).

Table 2.1 – Statistical distributions for fracture properties.

References	Distribution	
	Spacing	Extent
Rouleau and Gale (1985)	normal, exponential	lognormal
Dershowitz (1988)	exponential, lognormal	Gamma, exponential
Huang and Angelier (1989)	Gamma distribution	
Narr and Suppe (1991)	lognormal	
Rives et al. (1992)	exponential, lognormal	
Wu and Pollard (1995)	lognormal, normal	
Mathab et al. (1995)	lognormal	lognormal
Guo et al. (1999)	Pearson, extreme value	Pearson
Karpov (2001)	lognormal	lognormal

In choosing the distribution for fracture properties, however, a rigorous association of fracture size distribution with underlying geologic processes does not exist

at present (Dershowitz and Einstein, 1988). The standard distributions are often chosen to fit the shape of the distribution of fracture data. Researchers have used probability plots (Rouleau and Gale, 1985) for testing the candidate distributions that fit fracture data. Statistical goodness-of-fit tests such as the Kolmogorov - Smirnov test (Rouleau and Gale, 1985) or chi-squared goodness-of-fit statistics (Guo et al., 1999) have also been used to validate candidate distribution. Mathab et al. (1995) examined the goodness of fit of the normal, lognormal, exponential, Weibull, and gamma distributions to fracture spacing and length of 6 different fracture data sets. They concluded that the lognormal distribution provided the best fit in most cases. Karpov (2001) used the method of L-moments to identify suitable distributions for fracture spacing and height in a relatively undeformed section of the Lisburne formation. He found that fracture properties can be best represented by either the log-normal or gamma distributions.

Karpov (2001) pointed out that different distributions may give the best fit to the data at different intervals. For example, given the same mean and standard deviation, a change of models from the exponential to the lognormal and further to the gamma distribution will shift the mode towards a larger fracture size. Exponential and lognormal distributions will generate a greater number of smaller fractures as compared to the gamma model. However, the observed relative behavior of the distributions holds only over a certain range of the distribution parameters. Montroll and Schlesinger (1983) show analytically that the lognormal distribution can mimic a power-law distribution within a certain range of the variable.

II.4.2. DFN Modeling

II.4.2.1. Fracture Network

DFNs generate numerical fracture networks with the desired statistical properties. Several models for generating fracture systems in a given rock volume have been proposed (Dershowitz and Einstein, 1988; Chiles and de Marsily, 1993). The

models differ from one another only with regard to the special distribution of the fractures, and the interrelationship of fracture size and fracture location.

The simplest model generates fractures according to a Poisson process, in which fracture centers are located by a uniform distribution in space. With the assumption that fracture size and fracture orientation are independent of fracture location, fracture orientation and fracture size are drawn independently from given statistical distributions. The process continues until the fracture density satisfies the observed value. More complicated models such as the fractal or geostatistical model allow the inclusion of fracture density variations in space.

II.4.2.2. Flow Models

Once the fracture system has been generated, it is possible to calculate fluid flow through the network.

Early methods assumed that the flow in the fracture is 2D flow between two parallel plates with uniform equivalent conductivity. A semianalytical solution for the flow pattern inside each fracture has been proposed (Long et al., 1982), allowing the formulation and solution of the system of linear equations with as many unknowns as the number of nodes in the network. In this method of flow calculation, the nodes of the network are the intersections between the fractures. The conductivity of each fracture can be derived from the information about the fracture aperture.

In reality, the fracture aperture is difficult to describe accurately for several reasons (Chiles and de Marsily, 1993):

1- the aperture is not constant: there are voids and contact areas, and flow between two parallel plates separated by the mean aperture described in a model can be quite different from the actual flow; and

2- the aperture is stress dependent: the measured aperture may have little in common with an in-situ aperture.

Considering that flow within a fracture can consist of many flow channels, Cacas et al. (1990) proposed another approach for flow calculation. In this method of calculation, flow is assumed to occur through bonds joining the center of each fracture to the center of adjacent fractures, provided that the fractures are connected (Figure 2.9). The bonds are made up of two parts, one for each fracture, joining at the intersection of the two fractures. Each part of the connecting bond is assumed to be equivalent to the set of channels inside the fracture. The flow rate in a given bond between two fractures can be written as:

$$q = \frac{1}{L_1 / C_1 + L_2 / C_2} \Delta H \tag{2.11}$$

where ΔH is the head difference between the two nodes, C_1 and C_2 are the hydraulic conductivities of the two intersecting fractures, and L_1 and L_2 are the distances between the node and intersection in each fracture.

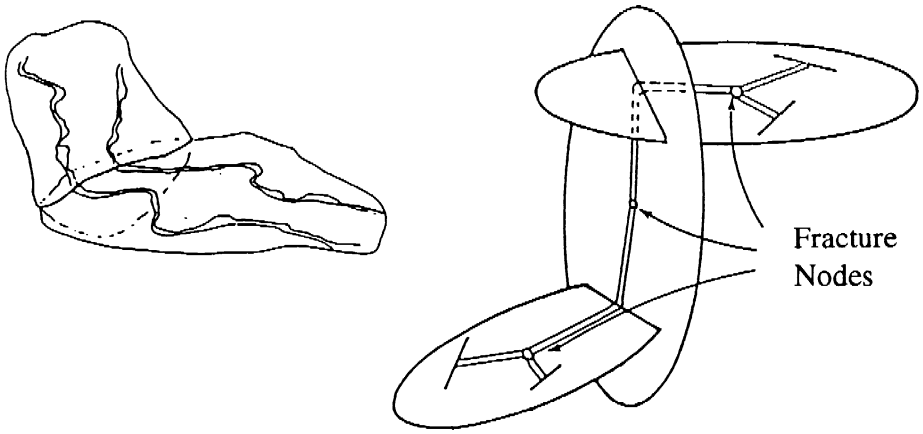

Figure 2.9 – Equivalent channel model for flow calculation. (After Cacas et al., 1990).

All methods of flow calculation in fracture network form a system of linear equations similar to the Kirchhoff problem in electricity or in pipeline network analysis. Solving the system of linear equations for the entire network allows calculation of flow anywhere in the system.

II.4.2.3. DFN Applications

In all methods of solving the flow in fracture networks, the hydraulic parameters of the model (aperture or fracture conductivity) are calibrated against the actual data (Dverstorp and Andersson, 1989). Cacas et al. (1990) provided an example of calibrating a model and interpreting the results for fracture data in Fanay, France. In their study, the lognormal distribution of the conductivity is assigned for the generated fracture set. The mean and standard deviation of the distribution is adjusted so that the distribution of the simulated result from the DFN is the same as the observed injection flow rate in the injection test.

DFNs, once calibrated, can be used to calculate large scale equivalent hydraulic conductivities of a continuum. Cacas et al. (1990) used a DFN to study the isotropy of the fracture system and to estimate the permeability of the system. Ouenes and Hartley (2000) used DFNs to upscale permeability fields to use in a reservoir continuum simulation and to estimate the relative equivalent size of the matrix block for use in a dual porosity reservoir simulation model.

The application of DFNs to actual field cases, however, is very computationally demanding. When the fracture density of the system is large, it can only be used for a small scale study. Since the flow is related to the connectivity and it is simpler to compute the connectivity than flow, the connectivity can be studied first to avoid flow calculations when they are not necessary (Chiles and de Marsily, 1993).

Karpov (2001), for example, studied the connectivity of a fracture system using a DFN model for optimization of well design, completion and operations based on an understanding of the inter-well scale connectivity. For a system with two fracture sets

orthogonal to the bedding planes, he found that the optimum horizontal wellbore orientation is at the bisection of the fracture strikes. His investigation on the sensitivity of the system to the progressive removal of small fractures showed that the flow characteristics of the fracture system were governed by a small portion of large, through-going fractures, and that the fracture termination has strong effects on the optimal wellbore orientation and fracture connectivity.

Karpov's (2001) study shows that by analyzing the characteristics of the system of fractures with the given statistical properties, one can investigate the general trend of isotropy and the possible effects of fracture properties on the flow characteristics of a fracture system.

In this study, I will use DFNs to investigate the fracture system isotropy and the effect of different parameters of the fracture properties on the conductance of the fracture system representing the data collected in the northestern Brooks Range, Alaska. I will use FracMan – a software package developed by Golder and Associates Inc., to investigate the effect of fracture size, fracture termination, and fracture filling on the system connectivity, and the effect of choosing different statistical distributions on the simulated conductivity of the fracture system.

CHAPTER III

GEOLOGICAL SETTING AND FRACTURE DATA

III.1. Geological Setting

III.1.1. Regional Setting

The Brooks Range is the northern extension of the Rocky Mountain fold-and-thrust belt and extends across northern Alaska and into northern Canada. The main axis of the Brooks Range is characterized by a Palezoic south-facing continental margin that was shortened by hundreds of kilometers during Middle Jurassic to Early Cretacious time (Wallace and Hanks, 1990; Moore et al., 1994). The northeastern Brooks Range is a prominent, northward-convex, topographic and structural salient with respect to the main Brooks Range axis. The northeastern Brooks Range is significantly younger than the remainder of the Brooks Range and has continued to shorten during Cenozoic time (Wallace and Hanks, 1990) (Figure 3.1).

III.1.2. The Northeastern Brooks Range

A partial stratigraphy of the northeastern Brooks Range is summarized in Figure 3.2. The Mississippian-Lower Cretaceous Ellesmerian sequence unconformably overlies the Precambrian to Devonian rocks. These older Paleozoic rocks are often referred to as "basement" or "Pre-Mississippian rocks" and consist of slightly metamorphosed sedimentary and volcanic rocks (Figure 3.2*)*. The Ellesmerian sequence is a northerly-derived Mississippian to Lower Cretaceous sequence of marine carbonate and clastic rocks. The boundary between the two sequences is an unconformity overlain by a basal conglomerate, the Mississippian Kekiktuk Conglomerate and an overlying shale, the Mississippian Kayak Shale.

The overall structure of the northeastern Brook Range is a north-vergent, regional duplex between a floor thrust at depth in the pre-Mississippian 'basement' rocks and a roof thrust in the Kayak Shale (Figures 3.2, 3.3). The structure of the overlying rocks is dominated by detachment folds in the dominant rigid element, the Lisburne Group (Figure 3.2) (Wallace and Hanks, 1990; Hanks et al., 1997).

The Lisburne Group is underlain by the Kayak shale, a thick black organic-rich shale with minor siltstone and limestone. The Kayak Shale fills the core of most of the detachment folds. The Lisburne Group in unconformably overlain by the Sadlerochit Group, (Figures 3.2, 3.3). The Sadlerochit Group is frequently detached from the underlying Lisburne, and develops tertiary scale folds.

The Lisburne Group is divided into two units: the upper Lisburne (Wahoo limestone) and the underlying lower Lisburne (Alapah limestone). The Wahoo Limestone is Mississippian and Pennsylvanian in age and typically consists of a massively bedded grainstones and packstones. The Alapah limestone is Mississippian in age and is relatively thinly bedded and consists of a variety of carbonate lithologies (Hanks et al., 1997). The detachment folded Lisburne Group exposed in northeastern Brooks Range (Figures 3.2, 3.3) is the target for the fracture investigation in this study.

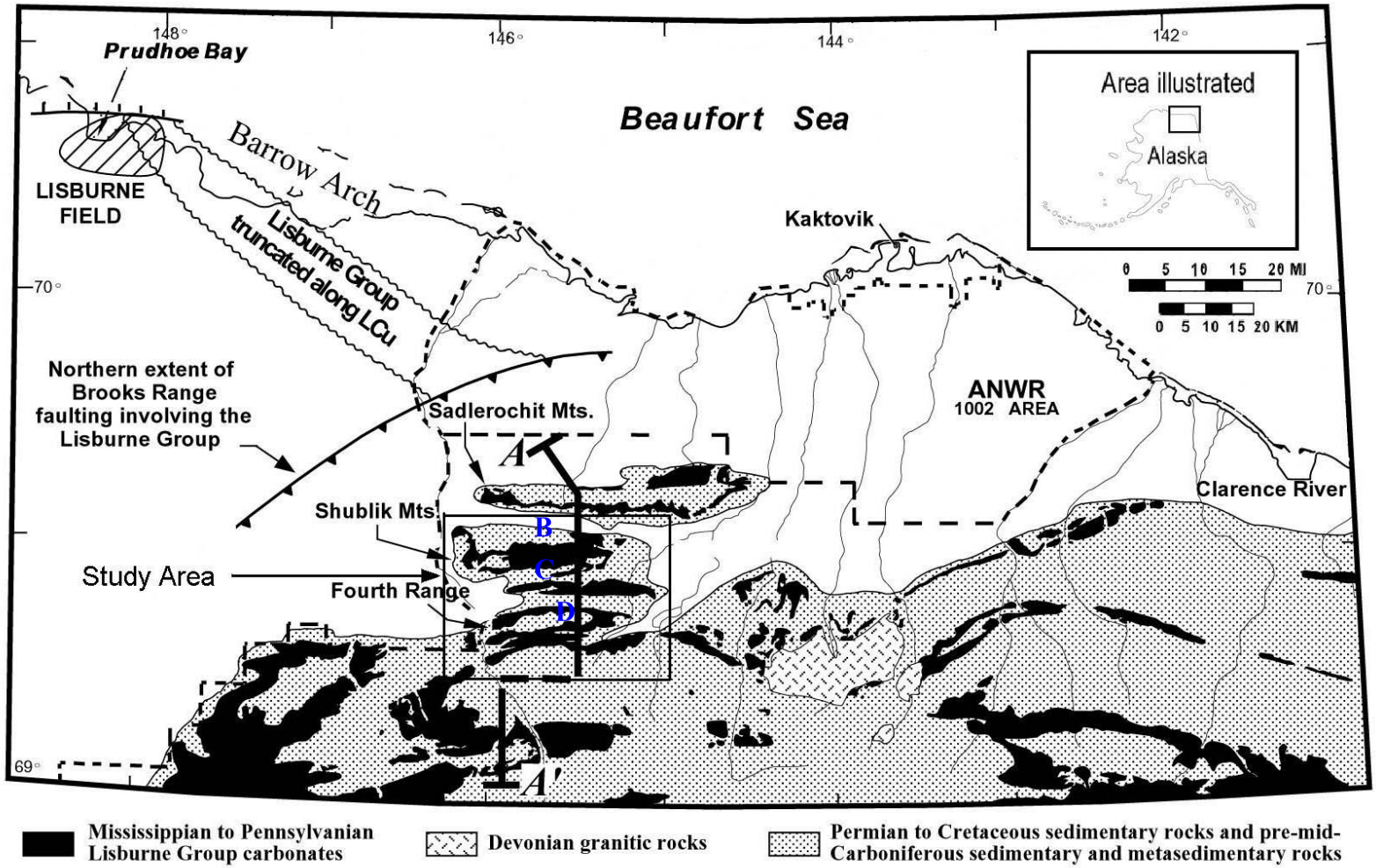

Figure 3.1 – Generalized geologic map of the northern part of the northeastern Brooks Range. (Modified from Hanks et al., 1997). B, C, D are the fracture study locations.

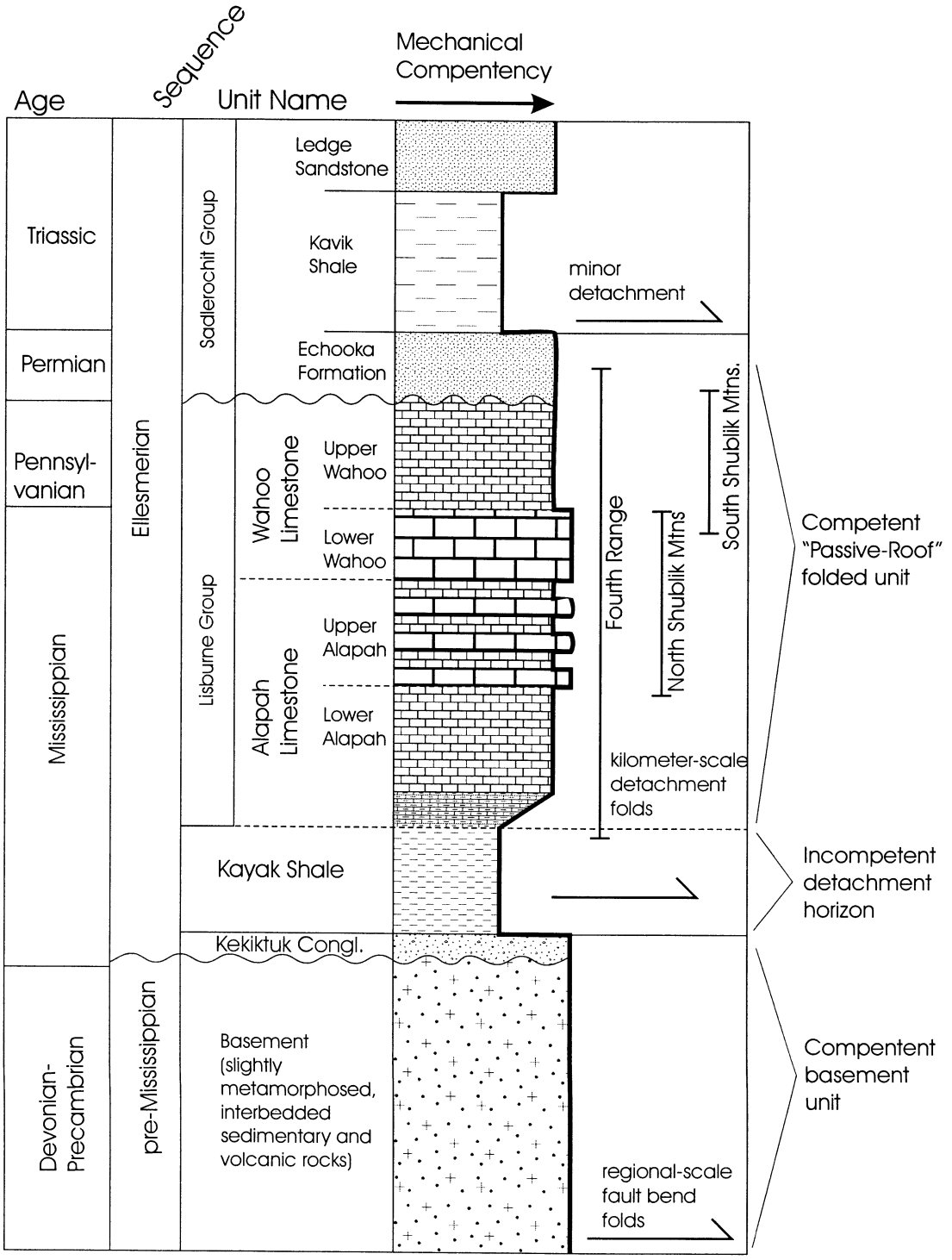

Figure 3.2 – Schematic lithostratigraphy and mechanical stratigraphy for the study areas. (After Brinton, 2002).

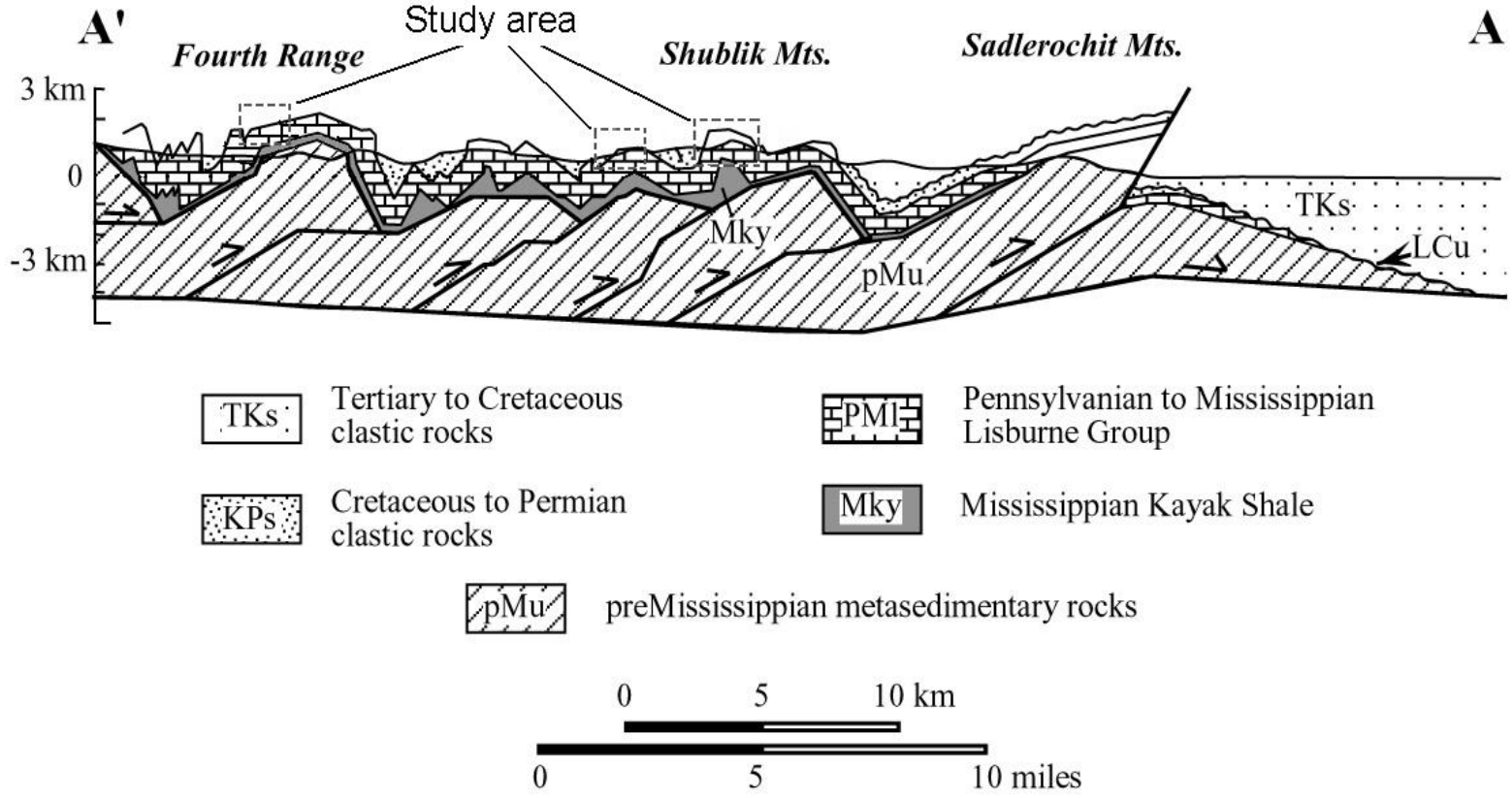

Figure 3.3 – Balanced cross section through the western part of the northeastern Brooks Range along section line A-A' in Figure 3.1. (Modified from Hanks et al., 1997).

III.2. Fracture Data

Fracture data used in this study were collected by UAF geologists during the summer of 1999 (Hanks et al., 2000). The fracture data were collected from the upper Alapah and lower Wahoo in the Fourth Range and North Shublik areas and the upper Wahoo in South Shublik area (Figure 3.2) (Brinton, 2002). Outcrops were chosen based on proximity to or location on a detachment fold as well as outcrop accessibility. The fracture properties and the geologic parameters such as lithology, bed thickness and degree of folding are defined and provided by UAF geologists as reported in Hanks et al., (2000) and Brinton, (2002).

At each location, bed thickness was measured normal to the bedding. The lithology of the formation was determined through examination of hand samples and was described according to the classification of Dunham (1962). Fractures were grouped into sets based on orientation and character. The fracture spacings were measured on the bedding plane or on cross-sectional exposures along the scan-lines perpendicular to the fracture set. Fracture height was measured along the fracture perpendicular to bedding. Fracture length was designated as the linear measurement along the fracture parallel to bedding. Detailed description of the data collection methodology is given in Brinton (2002).

Fracture data were collected from ten detachment folds (Figures 3.4-3.6). Five folds were chosen for detailed analysis because of the amount and quality of data obtainable and the accessibility to fractures in the hinge and both limbs of each fold. The data represented 25 outcrop locations, from which 19 are on limbs of folds and 6 are on hinges (Figures 3.4-3.5). All fractures are interpreted as extensional based upon the displacement across the fracture surface. Stratigraphic bed thicknesses ranged from 0.1m to 4m. The interlimb angle of the surveyed folds ranged from 90º to 160º. Detachment fold geometries in the studies areas varies and include open, boxy folds, and tight to isoclinal folds. Lithologies sampled range from carbonate mudstone to grainstone (Brinton, 2002).

Two major trends of the fracture orientation were observed: NS striking, which is perpendicular to the fold axes; and EW striking, parallel to the fold axes (Figure 3.7). In several locations, more than two fracture sets were identified on the basis of fracture orientation. For example, in hinge of fold II, four fracture sets were identified: the NS and EW fractures and north-dipping and south-dipping conjugate sets (Figure 3.8). The NS and EW fractures formed at high angles to bedding. The conjugate sets are nearly parallel in strike direction. Their dip directions are separated by an acute angle. Table 3.1 summarizes the main characteristics for all fracture sets.

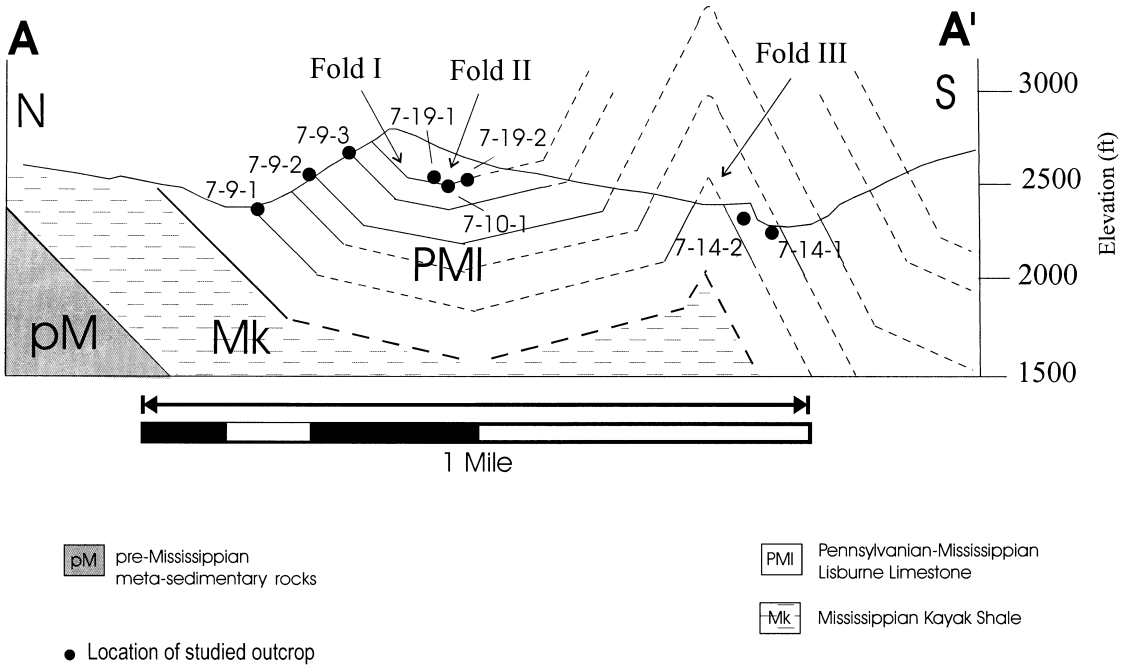

Figure 3.4 – Geologic cross section and sample location, Fourth Range study area (after Brinton, 2002).

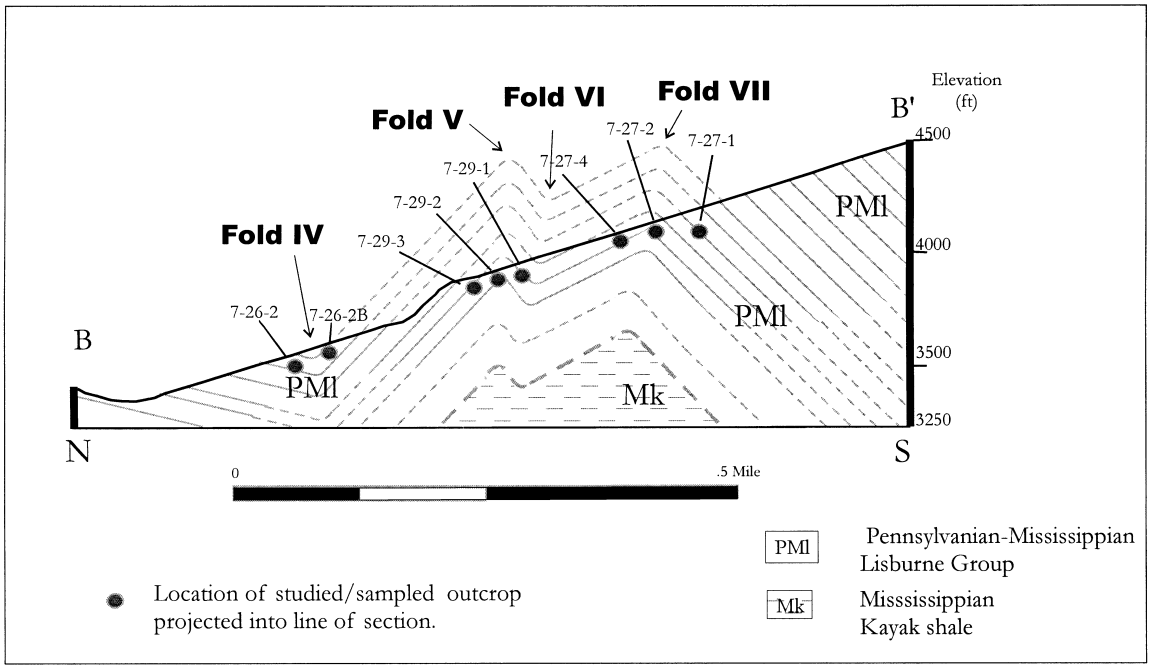

Figure 3.5 – Geologic cross section and sample location, North Shublik study area (after Brinton, 2002).

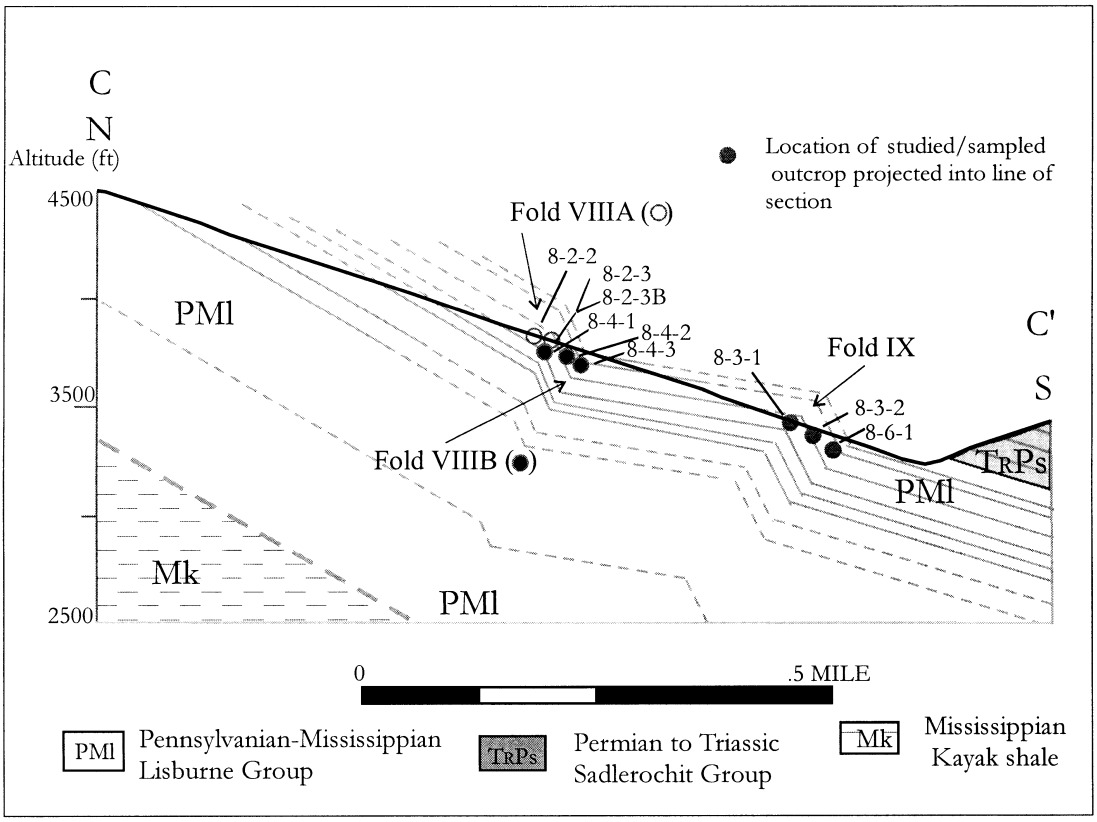

Figure 3.6 – Geologic cross section and sample location, South Shublik study area (after Brinton, 2002).

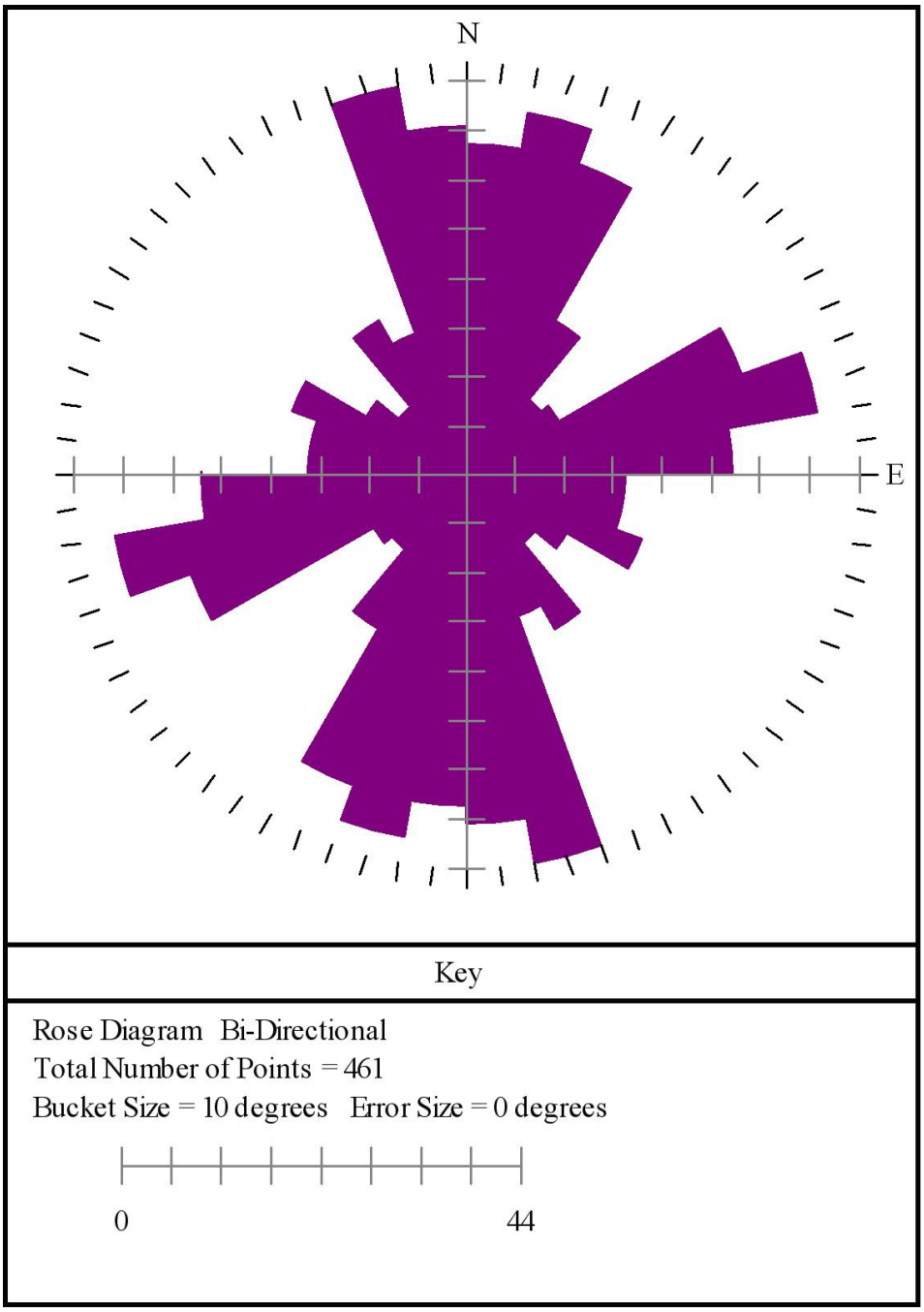

Figure 3.7 – Rose diagram of fracture orientation from all folds.

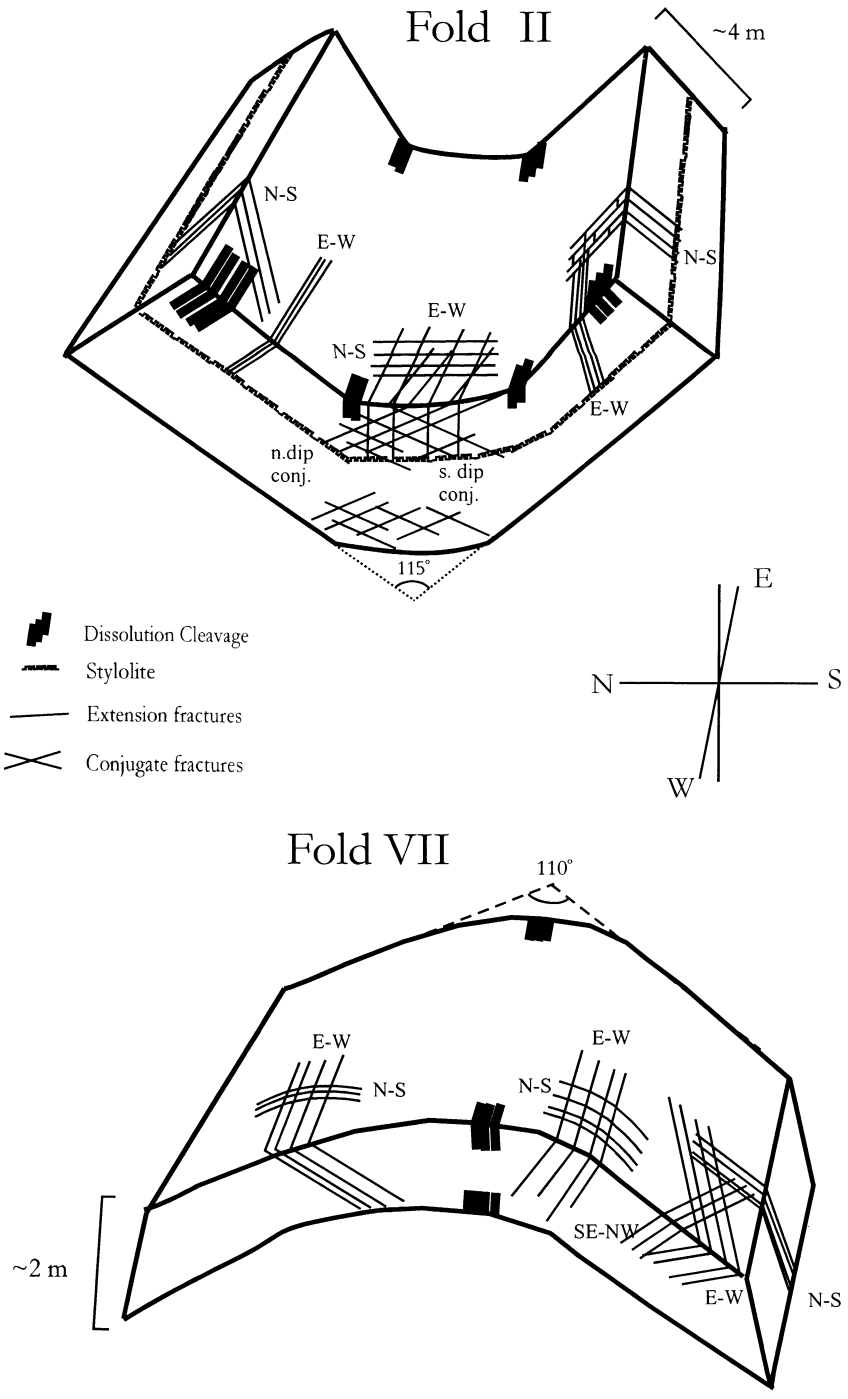

Figure 3.8 – Schematic rendering of features associated with folds. (After Brinton, 2002).

Table 3.1 – Summary of the fracture data.

Fracture Set	SP	Lith.	Form.	Bed	Fold	Interl. Angle	Avrg. Spacing	Avrg. Length	Avrg. Height
				m		deg.	m	m	m
FR-7-9-1NS	L	Ps	Alapah	3			0.277	0.458	1.971
FR-7-9-1EWcj	L	Ps	Alapah	3			0.100	0.288	0.827
FR-7-9-1conj	L	Ps	Alapah	3			0.480	0.143	0.325
FR-7-9-1MNS	L	Ps	Alapah	3			1.467	6.000	8
FR-7-9-2EW	L	Ps/Gr	uAlapah	3			0.079	0.231	0.338
FR-7-9-2NS	L	Ps/Gr	uAlapah	3			1.063	0.680	4.4
FR-7-9-3EW	L	Ps/Gr	uAlapah	1			0.224	0.230	1.51
FR-7-9-3NS	L	Ps/Gr	uAlapah	1			0.136	0.238	0.425
FR-7-10-1EW	Hs	Ps/Gr	Alapah	1.5	II	125	0.310	0.165	0.582
FR-7-10-1EWS	Hs	Ps/Gr	Alapah	1.5	II	125	0.143	0.085	0.296
FR-7-10-1EWN	Hs	Ps/Gr	Alapah	1.5	II	125	0.176	0.101	0.386
FR-7-10-1NS	Hs	Ps/Gr	Alapah	1.5	II	125	0.136	3.467	0.687
FR-7-12-1NS	L	Ms	Wahoo	1.7			0.064	0.095	0.832
FR-7-13-1ANS	L	Md	Wahoo	2.4			0.072	0.130	0.98
FR-7-13-1BEW	L	Md	Wahoo	2.4			0.258	0.171	0.686
FR-7-13-1Sh	L	Md	Wahoo	2.4			0.125	0.300	999
FR-7-13-2Sh	L	Md	Wahoo	2.4			0.010	0.200	999
FR-7-14-1NS	L	Md/Ws	uWahoo	1.5			0.150	0.088	1.113
FR-7-14-1EW	L	Md/Ws	uWahoo	1.5			0.203	0.083	0.517
FR-7-14-1MicEW	L	Md/Ws	uWahoo	1.5			0.018	0.101	0.2
FR-7-14-2MNS	L	Ws	uWahoo	1.5			0.553	0.053	2.286
FR-7-14-2MicNS	L	Ws	uWahoo	1.5			0.038	0.010	0.617
FR-7-14-2MeNS	L	Ws	uWahoo	1.5			0.233	0.027	0.291
FR-7-19-1EW	L	Gr	uWahoo	1.5	II	125	0.123	0.109	0.377
FR-7-19-1NS	L	Gr	uWahoo	1.5	II	125	0.240	0.413	0.82
FR-7-19-2NS	L	Gr	Alapah	2.5	II	125	0.500	0.700	1.9
FR-7-19-2EW	L	Gr	Alapah	2.5	II	125	0.130	0.425	0.625
NS-7-26-2a	L	Ps/Gr	UN	4			0.160	0.225	2.083
NS-7-26-2NS	L	Ps/Gr	UN	4			0.069	1.138	2.063
NS-7-26-2MNS	L	Ps/Gr	UN	4			0.600	1.000	4
NS-7-27-1a	L	Ws/Gr	uAlapah	4	VII	90	0.358	1.760	0.2
NS-7-27-1vert	L	Ws/Gr	uAlapah	4	VII	90	0.175	0.980	0.003
NS-7-27-1conj	L	Ws/Gr	uAlapah	4	VII	90	0.325	0.480	0.003
NS-7-27-2a	Ha	Ws/Gr	UN	4	VII	90	0.143	0.260	0.96
NS-7-27-2b	Ha	Ws/Gr	UN	4	VII	90	0.100	0.304	0.786
NS-7-27-4a	L	Ws/Ps	UN	N/A	VII	90	2.250	0.600	1.4
NS-7-27-4b	L	Ws/Ps	UN	N/A	VII	90	0.920	2.333	4
NS-7-29-1NS	L	Ps/Gr	Alapah	2.5	V	100	0.273	0.350	0.05
NS-7-29-1EW	L	Ps/Gr	Alapah	2.5	V	100	0.092	0.732	0.05
NS-7-29-1A	L	Ps/Gr	Alapah	2.5	V	100	0.375	0.589	0.05
NS-7-29-2NS	Ha	Ps/Gr	Alapah	3	V	100	0.084	0.409	0.509
NS-7-29-2EW	Ha	Ps/Gr	Alapah	3	V	100	0.080	0.370	0.15

Table 3.1 – (continued).

Fracture Set	SP	Lith.	Form.	Bed	Fold	Interl. Angle	Avrg. Spacing	Avrg. Length	Avrg. Height
				m		deg.	m	m	m
NS-7-29-2MNS	Ha	Ps/Gr	Alapah	3	V	100	1.300	1.040	2.8
NS-7-29-2MEW	Ha	Ps/Gr	Alapah	3	V	100	1.700	0.520	3.4
NS-7-29-3NS	L	Ws/Ps	Alapah	0.4	V	100	0.304	4.645	0.4
NS-7-29-3a	L	Ws/Ps	Alapah	0.4	V	100	0.453	0.450	0.4
SS-8-2-2a	L	Ps	Wahoo	2	VIII	110	0.045	1.000	0.5
SS-8-2-3a	Ha	Ps	Wahoo	0.2	VIII	110	0.253	0.200	0.15
SS-8-2-3b	Ha	Ps	Wahoo	0.1	VIII	110	0.250	0.567	0.2
SS-8-3-1a	L	Ps	Wahoo	0.7			0.175	0.314	0.55
SS-8-3-2SW	L	Ps	Wahoo	2			0.233	0.271	0.2
SS-8-3-2NW	L	Ps	Wahoo	2			0.100	0.176	0.9
SS-8-4-1EW	L	Ps	Wahoo	1	VIII B	160	0.181	0.115	0.525
SS-8-4-1NS	L	Ps	Wahoo	1	VIII B	160	0.074	0.288	0.567
SS-8-4-2NS	Ha	Ps	Wahoo	1.5	VIII B	160	0.050	0.431	0.2
SS-8-4-2EW	Ha	Ps	Wahoo	1.5	VIII B	160	0.184	0.153	0.2
SS-8-4-2ConjA	Ha	Ps	Wahoo	1.5	VIII B	160	0.180	0.450	0.7
SS-8-4-2ConjB	Ha	Ps	Wahoo	1.5	VIII B	160	0.320	0.447	0.7
SS-8-4-3EW	Hs	Ps	Wahoo	3	VIII B	135	0.075	0.130	0.13
SS-8-4-3NS	Hs	Ps	Wahoo	3	VIII B	135	0.090	0.079	0.13
SS-8-6-1NS	L	Ps	Wahoo	0.5			0.097	0.650	0.638
SS-8-6-1EW	L	Ps	Wahoo	0.5			0.097	0.556	0.225
SS-8-6-1BNS	L	Ps	Wahoo	0.5			0.225	0.243	0.629
SS-8-6-1BEW	L	Ps	Wahoo	0.5			0.190	0.262	0.6

III.3. Brinton's Analysis of Fracture Properties

Brinton (2002) described the fracture data at each location and performed a detailed fold-by-fold analysis of the fracture data. Fractures of similar orientation were compared between folds of close proximity. The relative age of the fractures was assessed by studying the termination of one fracture on another fracture, assuming that the more through-going fracture set predates the other set. The following is a brief summary of Brinton's (2002) fold-by-fold analysis:

- There is reliable evidence that the EW fracture sets predominantly pre-date the NS fracture sets.
- The EW fractures pre-dated or formed early during folding, and that the NS fractures formed late during, or after folding.
- The EW fractures have greater density in the hinge of the folds as compared to the limb. Fracture spacing in both orientations become more variable in fold hinges.

Linear statistical analyses also were performed on an area-wide scale on all the data, including fracture data from the entire study area. The purpose was to analyze the roles of stratigraphy and folding in the development of fractures. Assuming that the effects of geologic factors on fracturing are independent of each other, Brinton lumped all fractures together for investigating the effects of lithology, bed thickness, and interlimb angle on the fracture spacing. For example, to evaluate the effect of lithology on fracture spacing, he compared the average fracture spacing of all fractures, grouped into appropriate lithologic classifications. Similarly, the average fracture spacing is plotted against bed thickness or interlimb angle to evaluate the effect of bed thickness or degree of folding on fracture density. The following is a summary of Brinton's (2002) area-wide scale analysis.

- Wackestone shows the smallest fracture spacing, followed by packestone, then by grainstone. Mudstones show the greatest average fracture spacing.
- Lumping all data and plotting against bed thickness shows no influence of the bed thickness on fracture spacing.
- Fracture density in the hinges is slightly higher than in the limbs.
- As the interlimb angle decreases (i.e., folds get tighter), the fracture spacing increases. This correlation is weak and would be considered unreliable.

- Fracture spacing and its variance for NS and EW orientations are similar. The orientation of the NS fractures becomes more uniform with decreasing interlimb angle while such a relationship does not exist for the EW fractures.

Brinton's (2002) analysis of the fracture data in the northeastern Brooks Range suggests that fracture spacing is controlled by lithology. The bed thickness and the degree of folding do not have a significant effect on fracturing. No reliable pattern relating fracture distribution with the amount of folding was detected.

Several issues were raised from Brinton's analysis:

1- The area-wide analysis of the effect of a particular parameter on the fracture spacing is based on the assumption that other parameters either have no effect or have equal effect on fracture spacing at each value of the parameter in question. The sparseness of the fracture data, however, may magnify or dampen the effect of one particular parameter on the fracture spacing.

2- The fracture length and height were never used to see if folding or other geologic parameters affect the fracture properties.

In next chapters, I will present further results of the statistical analysis of the fracture properties. The effects of folding and structural position on fracture size will be analyzed. Conventional statistical analysis and neural network will be used to analyze the fracture spacing.

CHAPTER IV

STATISTICAL ANALYSIS

This chapter extends the fracture property statistical analysis made by Brinton (2002). The fracture spacing, height, and length for fractures in two orientations are studied. The fractures are grouped with regard to different values of interlimb angle, bed thickness, structural position and fracture orientation. The t-test for mean value, Kolmogorov-Smirnov test for general difference of distribution, and bootstrapping to evaluate differences in medians are used in assessing the effects of bed thickness, degree of folding, and structural position on the fracture spacing.

This analysis suggests that the geologic parameters have complex effects on the fracture spacing distribution. The fracture spacing increases and becomes more variable as the interlimb angle decreases. The fracture length increases as interlimb angle decreases, especially for NS fractures. The local structural setting seems to have an important role in the fracture spacing and fracture size distributions. The complexity of the effects of geologic parameters on the fracture spacing suggest that conventional statistical analysis is insufficient and that a different method is needed.

IV.1. Fracture Spacing

IV.1.1. Summary of Fracture Spacing Data

One main objective of the fracture analysis is to evaluate the effects of mechanical stratigraphy and folding on fracture spacing. I assume that mechanical stratigraphy and folding are represented by the bed thickness, the lithology, the formation, the interlimb angle, and the structural position in fold.

An ideal analysis of the effect of a particular geologic parameter on the fracture spacing requires that other parameters are fixed. For example, the effects of the degree

of folding on the fracture spacing are best examined for a layer of a single lithology, with constant thickness, at the same position in folds of different interlimb angles. This, however, can not be fulfilled because of the limited amount of fracture data. In the following sections, the fracture data are grouped into different groups representing different values of the geologic parameters. Comparing the fracture spacing between groups, I want to examine following questions.

1- Does fracture spacing increase with bed thickness?

2- Does fracture spacing increase with interlimb angle?

3- Is fracture spacing in limbs of the fold significantly different from that in the hinge of the fold?

Table 4.1 summarizes the main statistical characteristics of the fracture spacing for NS and EW fractures, lumped together from all 5 folds (Chapter III). Both fracture sets have very similar statistics. Figure 4.1 shows the cumulative distribution plots for both fracture sets. These plots and statistical tests show that both fracture sets are statistically similar at a 95% confidence level.

Both sets appear to have similar behavior with respect to the effects of bed thickness and tightness of the fold. A plot of fracture spacing versus bed thickness (Figure 4.2) shows that, as bed thickness increases, fracture spacing and its variability in both orientation increases. This behavior agrees with the fracture density-bed thickness reported in the literature (Harris et al., 1960; Ladeira and Price, 1981; Huang and Angelier, 1989; Narr and Suppe, 1991). A plot of fracture spacing versus interlimb angle (Figure 4.3) however shows a trend different from that expected if the fractures are related to folding: the average spacing increases, and the spacing becomes more variable with decreasing interlimb angle. The results of the literature review in Chapter II suggested that the average fracture spacing at any location can be affected by different factors. It is therefore important to investigate the effects of a particular geologic factor on the average fracture spacing by keeping others at fixed values.

Table 4.1 – Fracture spacing summary.

	EW fracture	NS fracture	Difference, %
Number of fractures	176	215	-
Average, m	0.26	0.28	6.7
Median, m	0.14	0.15	7.1
Standard deviation, m	0.455	0.370	-18.6
90^{th} percentile, m	0.45	0.65	44.4

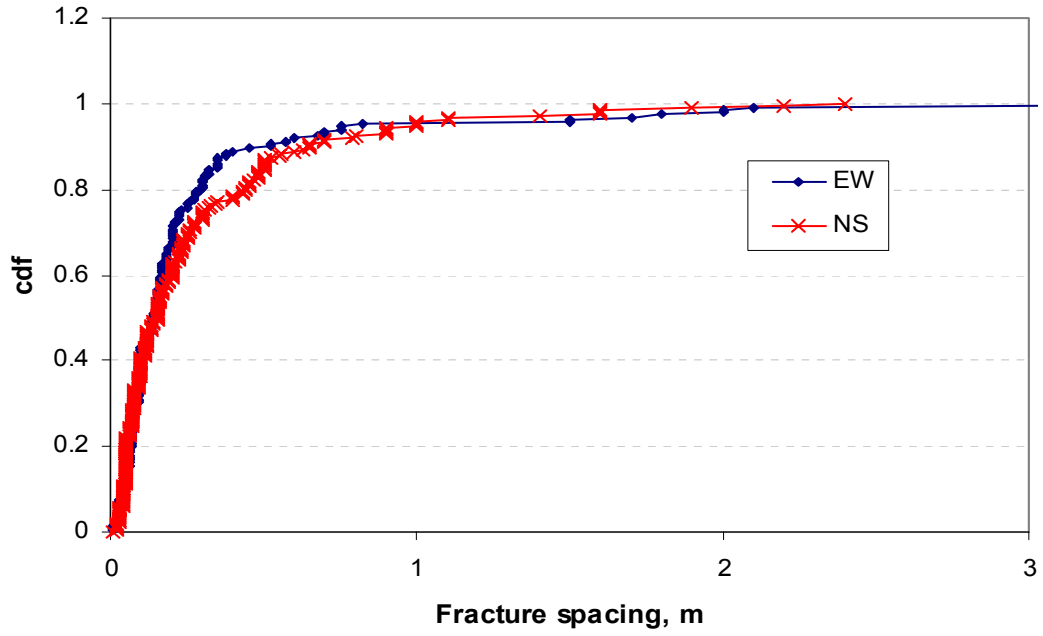

Figure 4.1 – Cumulative distribution of fracture spacing for two orientations, all fracture data.

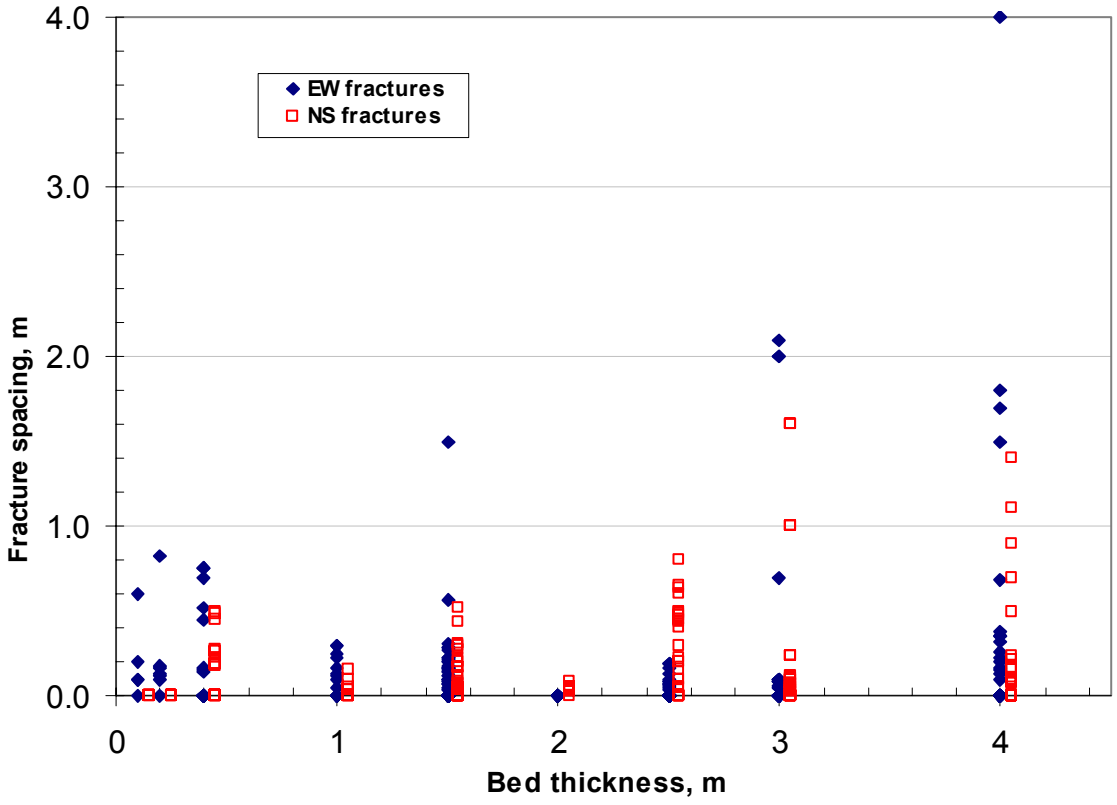

Figure 4.2 – Fracture spacing versus bed thickness for two orientations. The fracture spacing increases with the bed thickness.

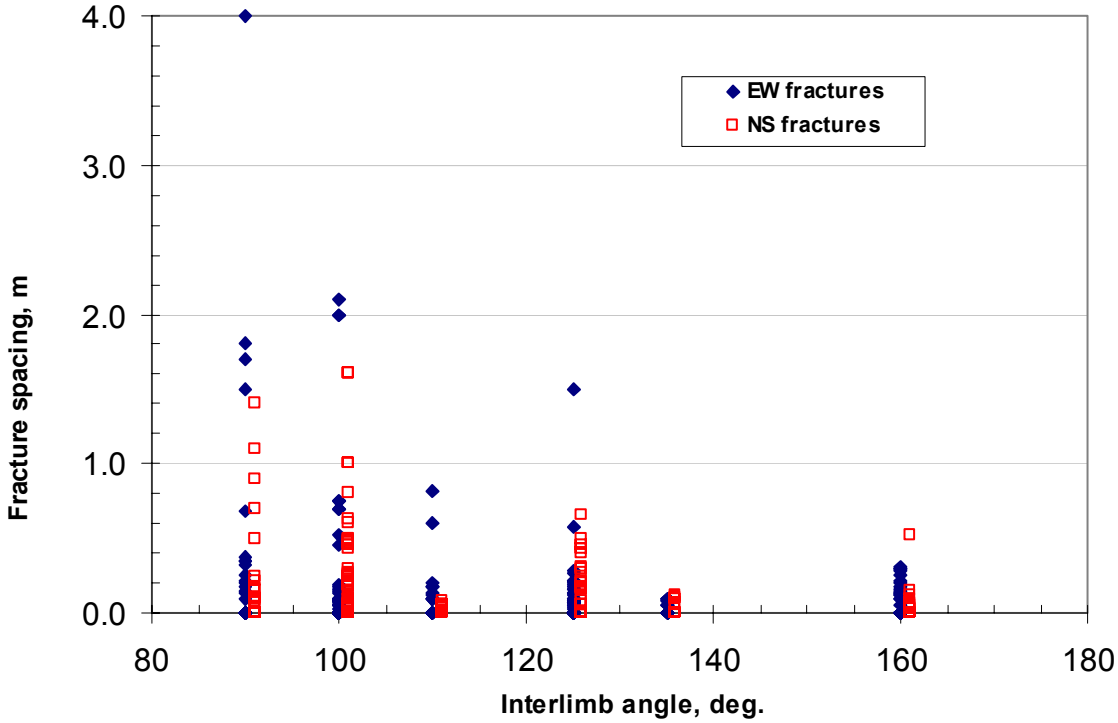

Figure 4.3 – Fracture spacing versus interlimb angle for two orientations. As interlimb angle decreases, fracture spacing and its variability increase.

IV.1.2. Regrouping of the Fracture Data

The limited data prevents us from investigating the effects of a single geologic factor with other being constant. We in fact do not have enough data for examining the effect of single geologic parameters on average fracture spacing with all other parameters being fixed. One approach that may partially correct this situation is to treat continuous variable as a categorical. For example, instead of analyzing the effect of bed thickness on the average fracture spacing as a continuous for the whole range of bed thickness, we can examine how average fracture spacing differs in thin bed and in thick

bed. In such a case, bed thickness becomes a categorical variable with some arbitrary boundary defining which value of bed thickness belongs to the "thin bed" and which value belongs to the "thick bed". By doing this, the number of fracture data in each category of bed thickness becomes large enough for studying the effect of other parameters on the average fracture spacing within each bed thickness group, now being considered fixed. Treating continuous variable as a discrete has following advantages:

- it increases the amount of data in each group and thus, will improve the statistical significance of the analysis.
- the assumption of the fixed value of a variable can now be applied within each group of that variable for studying the effect of other variables.

The major concerns of this approach are as follows.

- It loses the detailed effect of the exploratory variable on the response variable within each group. Because of this, treating a continuous variable as a discrete is meaningful only when the effect of this variable on the response variable is monotonically between two consecutive regions of this variable.
- It is difficult to choose the points dividing the range of a variable into different regions. If we choose to depict the relationship between this variable and the response variable, then the boundary should be a point that maximizes the difference between subsets of data from each region. If we choose to improve the significance of the analysis for other parameters within each group, then the number of data points in each group should be considered.

For our fracture data, I assume that following parameters can affect average fracture spacing: the degree of folding, the bed thickness, the structural position on a fold, the lithology, and the fracture orientation. We in fact already treat several continuous variables as discrete including following.

- Lithology is a continuous variable representing the distribution of the rock components and texture within the rock matrix.
- Structural position is a continuous variable representing the linear distance across a fold.

By the same token we can also treat bed thickness and degree of folding as the discrete variables for further analysis.

IV.1.2.1. Interlimb Angle

Theoretical and experimental studies indicate that the fracture spacing of a single layer decreases with degree of folding (Harris et al., 1960; Lisle, 1994; Jamison, 1997; Henning et al., 2000). We expected that the fracture spacing monotonically decreases with the interlimb angle under the condition that homogeneous layer folded from the flat laying condition and would not change back to unfolded condition.

Visual inspection of Figure 4.3 suggests that the interlimb angle of about 110° can serve as a boundary for two regions of degree of folding. To be more precise, I compared the average fracture spacing of the resulted datasets using t-test (Jensen et al., 1997). Figure 4.4 shows t-statistic of the distribution of the difference in means and the ratio of data points in these subsets as a function of the point dividing interlimb angle. Large t-statistics means large difference between average fracture spacing of two subsets. The ratio of data points equal 1 means that two sets have the same number of data. The results suggest that, the interlimb angle of 105° maximizes the difference between two subsets and has a good proportion of data points in them. This value is chosen as the boundary dividing interlimb angle into two categories: tight folds with $\alpha < 105°$ and open folds with $\alpha \geq 105°$ (α is the interlimb angle).

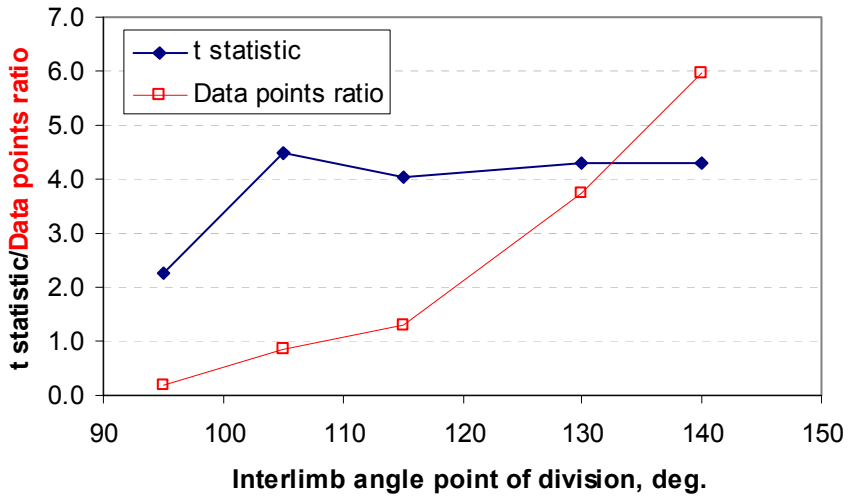

Figure 4.4 – t-statistic of difference in average fracture spacing and the ratio of data points between two groups of interlimb angle.

IV.1.2.2. Bed Thickness

Many studies, based on experiments and field observations, indicated that fracture spacing increases with the thickness of fractured layer (e.g., Narr and Suppe, 1991; Wu and Pollard, 1995). That is, under the same condition, fractures in thin beds have smaller average fracture spacing than in thick beds. Theoretical studies (e.g., Pollard and Segall, 1987) also suggest that the fracture spacing in a homogeneous medium is proportional to the layer thickness. The proportional coefficient is determined by parameters such as the properties of the fractured and neighboring layers. Assuming that the properties of neighboring layers are similar for different fractured layers, the monotonicity of the relationship between fracture spacing and bed thickness can be applied and bed thickness can be divided into categories.

T-statistics for the difference in average fracture spacing and the ratio of data points are calculated for two groups of fracture spacing as a function of the value

dividing bed thickness into categories. The results (Figure 4.5) suggest that the bed thickness of 2.2 m maximizes the difference between two subsets and has a good proportion of data points in them. This value is chosen as the boundary dividing bed thickness into two categories: thin beds (h≤2.2 m) and thick beds (h>2.2 m).

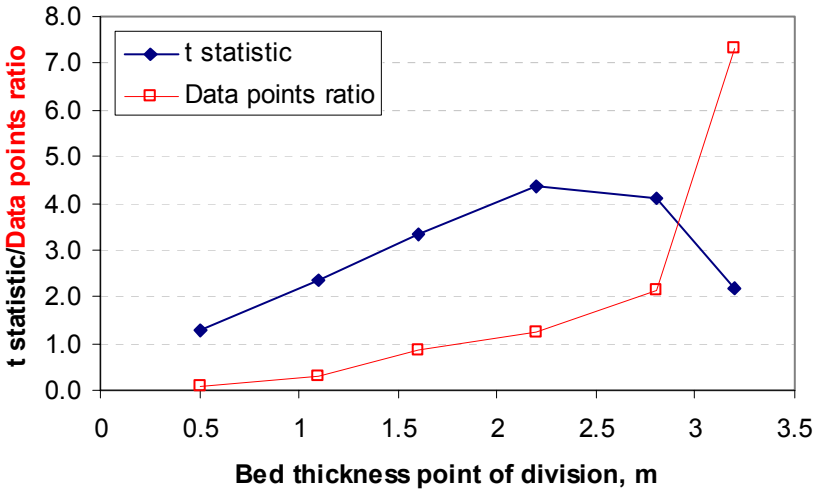

Figure 4.5 – t-statistic of difference in average fracture spacing and the ratio of data points between two groups of bed thickness.

IV.1.3. Statistical Tools for Analysis

I use box plots (Siegel and Morgan, 1996) and sample cumulative distributions of resulting subsets for visual comparison among subsets. Along with graphical comparisons, I applied several statistical tests to quantify and assess the effects of geologic factors on fracture spacing. I used the t-test for the differences in mean, the Kolmogorov-Smirnov (KS) test for the differences between distributions, and bootstrapping for differences in median (Neave and Worthington, 1988) to assess the

statistical significance of the difference between datasets. The bootstrapping procedure is carried as followed:

1- draw with replacement a sample of size N from each dataset to be compared;

2- determine sample medians of bootstrapped samples;

3- calculate the difference between medians obtained in step 2; and

4- repeat the step 1 to 3 for 999 times.

These 1000 differences form the distribution of the difference in median between two datasets. An α-level confidence interval includes all differences between the $\alpha/2$ and $1-\alpha/2$ percentiles of the distribution. The datasets are said to have different medians if their bootstrapped confidence interval excludes the value of zero.

Following sections presented the results of these analyses for fracture spacing.

IV.1.4. Analysis Results

IV.1.4.1. Interlimb Angle and Bed Thickness

Figure 4.6 shows the box plot of fracture spacing for the subsets of data according to different groups of bed thickness and interlimb angle. It appears that the fracture spacing is not affected by the value of bed thickness, as it seems to be in Figure 4.2. Within each range of interlimb angle, fracture spacing remains relatively unchanged for variations in bed thickness. This effect contrasts with the often-reported relationship between fracture spacing and bed thickness. On Figure 4.4, we also see that the fracture spacing increases for both subsets of bed thickness as the interlimb angle decreases. This relationship is contrary to the expectation that fracturing would be enhanced by folding i.e., fracture spacing is expected to be smaller for the tighter folds (i.e., small interlimb angle). The observed relationship between fracture spacing and interlimb angle in these detachment folds suggests that the fractures may not be closely or wholly related

to the folding. At the 95% confidence level, all three statistical tests confirmed what we observed graphically, i.e.:

- Bed thickness does not have a significant effect on the fracture spacing distribution.
- As the interlimb angle decreases, the fracture spacing increases and becomes more variable.

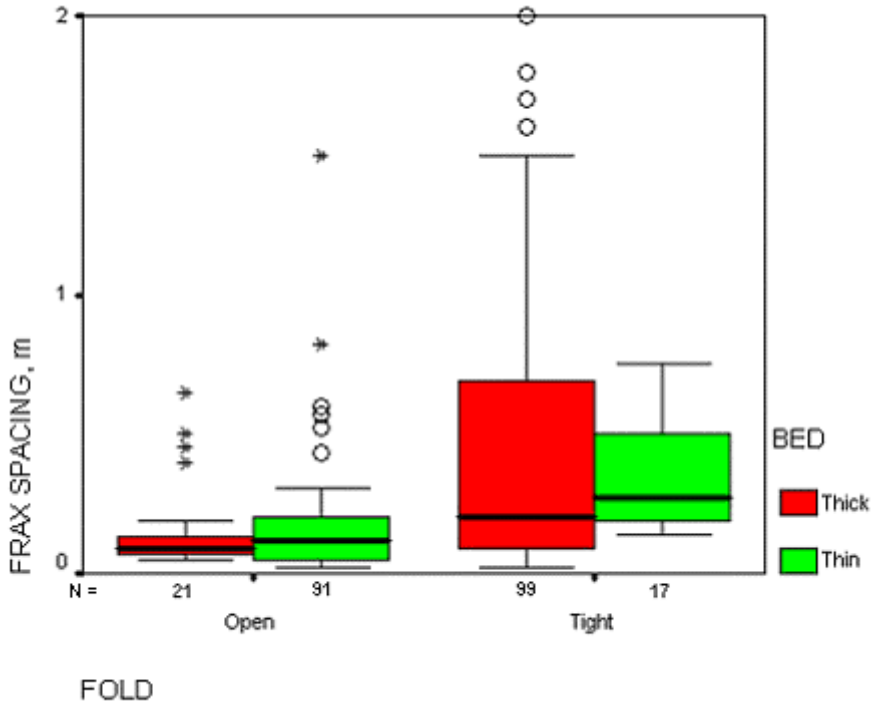

Figure 4.6 – Box plot of fracture spacing for two groups of interlimb angle. Fracture spacing and its variability increase as the interlimb angle decreases for both groups of bed thickness. The lower edge of each shaded box represents the 25th percentile of the dataset, the upper edge represents the 75th percentile. The heavy line is the median of the sample. The "whiskers" at the two ends of each box connect data points lying within 1.5 lengths of the box. The circles are the adjacent values and the stars are the outliers. (Siegel and Morgan, 1996).

IV.1.4.2. Fracture Spacing with Respect to Interlimb Angle and Orientation

The results of comparing the two fracture sets indicated that the fracture spacing of both sets are statistically similar. Dividing the fracture data into subsets reveals more subtle effect of folding on fracture spacing distribution. The box plots of fracture spacing for the two fracture sets with respect to interlimb angle show that fracture spacing in both fracture sets appears to behave similarly as the interlimb angle changes (Figure 4.7). Fracture spacing in both the NS and EW fracture sets increases and becomes more variable as the interlimb angle decreases. A t-test confirms this. The KS test and test on median, however, reveal that the distribution and the median of the fracture spacing are significantly different for the two fracture orientations with large interlimb angle. In folds with large interlimb angles, the median of the EW fractures (0.13 m) is significantly larger than the median of the NS fractures (0.07 m).

IV.1.4.3. Fracture Spacing with Respect to Interlimb Angle and Structural Position

The position of the sample location on the fold also has an effect on the fracture spacing distributions. Fracture spacings in limbs of folds with small interlimb angle are significantly larger than in hinges of folds with small interlimb angles and in folds with large interlimb angles (Figure 4.8). The t-test suggests that the average fracture spacing both on the limbs and the hinges of folds with small interlimb angle is significantly larger than in folds with large interlimb angle. The KS test indicates that the fracture spacing distributions are significantly different for all subsets, except for the fractures in hinges of fold with different interlimb angles.

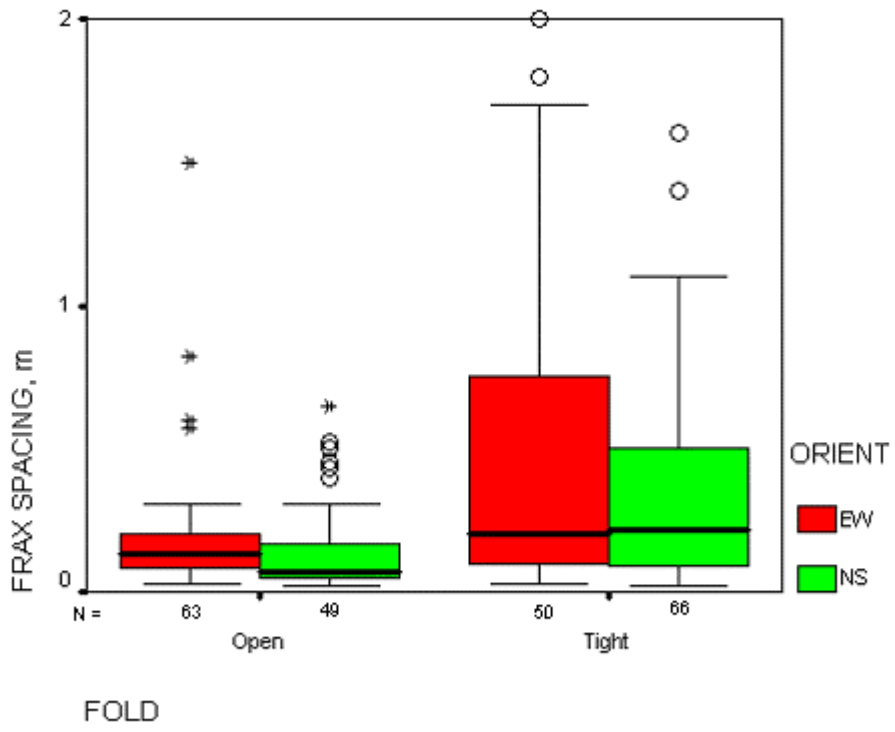

Figure 4.7 – Box plot of fracture spacing for different interlimb angle and orientation. As folding increases, fracture spacing and its variability increases in both fracture sets.

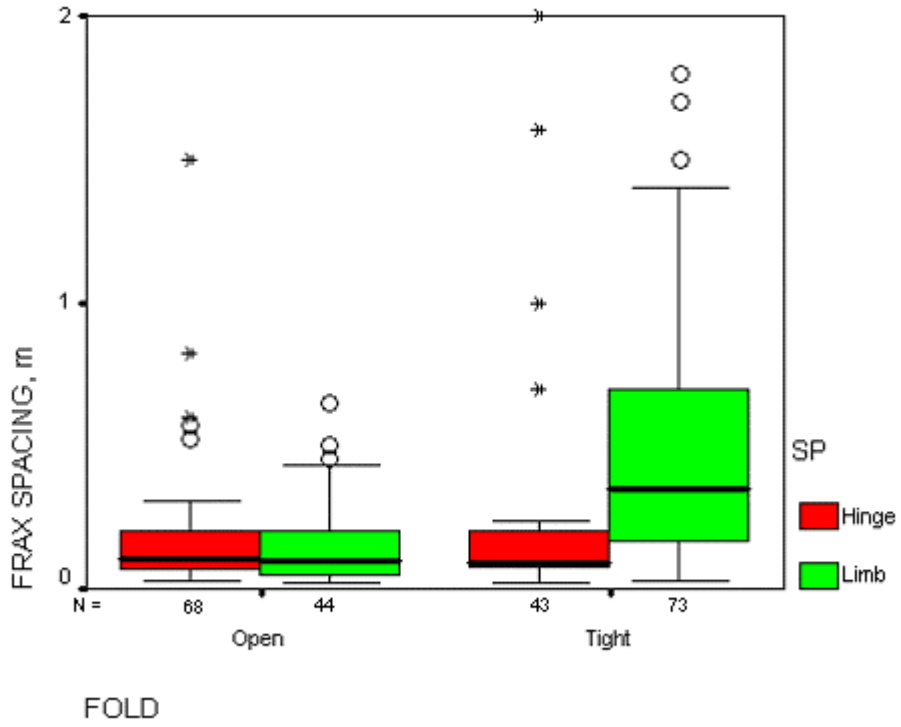

Figure 4.8 – Box plot of fracture spacing for different interlimb angle and structural position. As folding increases (fold changes from open to tight), fracture spacing and its variability increases in both limbs and hinges, especially in limbs.

IV.1.4.4. Fracture Spacing with Respect to Orientation and Structural Position

Grouping the fracture sets with respect to different structural positions on the folds shows insignificant difference between the sets. However, the NS fractures in limb and in hinge appear to be significantly different (Figure 4.9). Combining this analysis with that shown in Figures 4.7 and 4.8 suggests that the apparent contradictory effect of folding on the fracture spacing may be due to excessive influence of the data from the fold limbs. That is, for all possible combinations of bed thickness and interlimb angle with structural position, the one in fold limbs shows greatest fracture spacing.

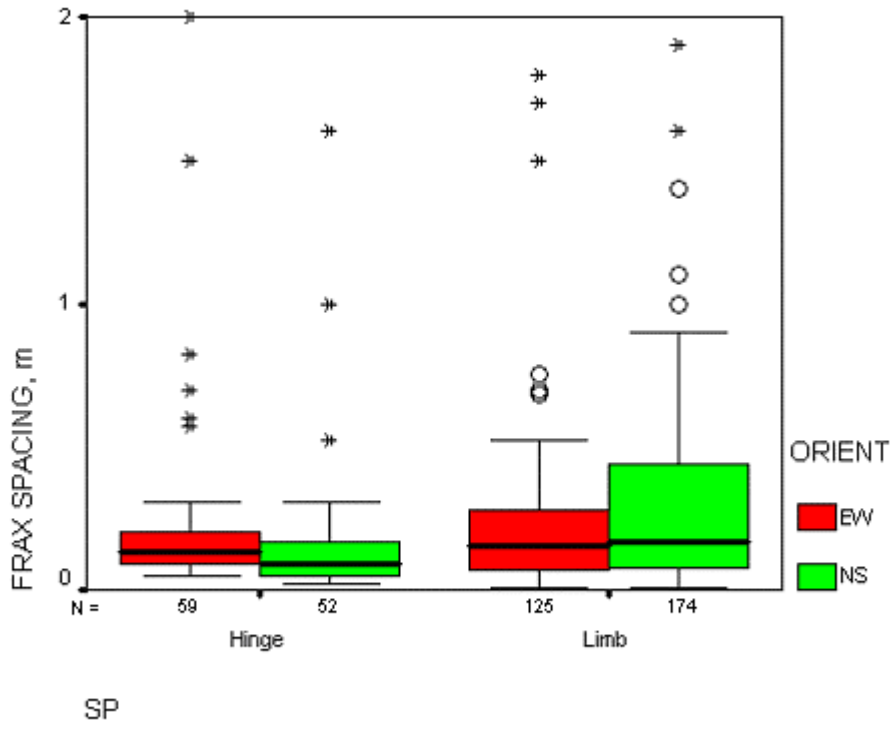

Figure 4.9 – Box plot of fracture spacing for two orientations at different position on fold.

IV.1.4.5. Fracture Spacing with Respect to Bed Thickness and Structural Position

Comparing the fracture spacing of the datasets from two groups of bed thickness and structural position suggests that fracture spacing in thick beds and on fold limbs is significantly larger than fracture spacing in other combination of parameters. Figure 4.10 shows that the fracture spacing distribution in thick beds and fold limbs is significantly skewed in the direction of large fracture spacing.

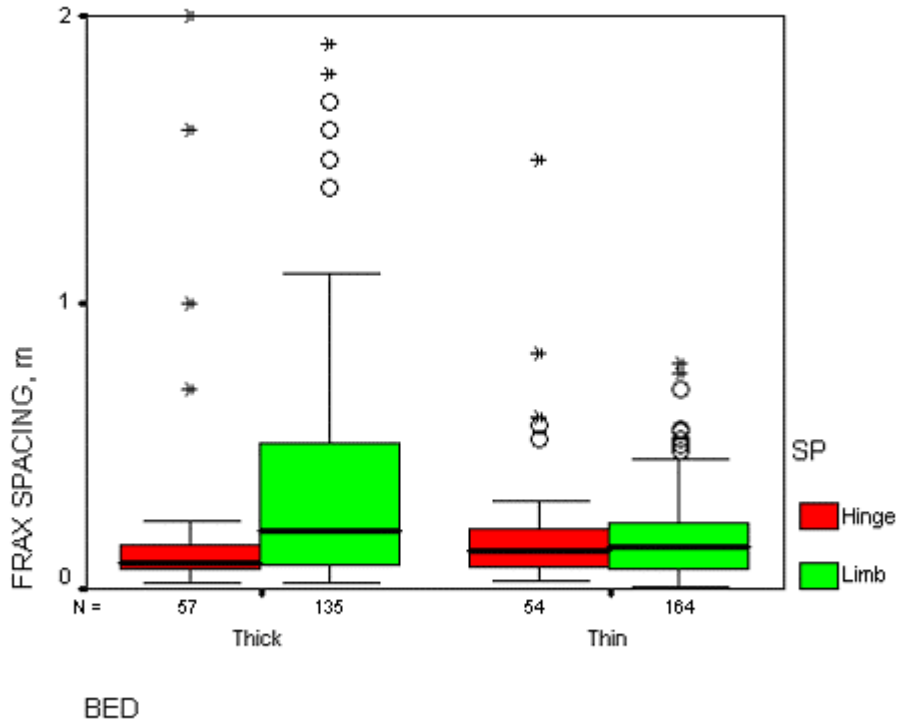

Figure 4.10 – Box plot of fracture spacing for two groups of bed thickness at different position on fold.

IV.1.5. Summary

Table 4.2 shows the summary of the statistical assessment of the difference between different subsets of data. The results are the p-value of the t-test, Kolmogorov-Smirnov test and the bootstrapped difference in median.

Table 4.2 – Summary of the statistical assessment of fracture spacing subsets.

		p value		
Set 1	Set 2	**t-test**	**KS**	**Median***
EW-Tight folds	EW-Open folds	0.999	0.999	D
NS-Tight folds	NS-Open folds	1.000	0.999	D
EW-Thin beds	EW-Thick beds	0.981	0.827	nd
NS-Thin beds	NS-Thick beds	1.000	1.000	D
EW-Limb	EW-Hinge	0.210	0.752	nd
NS-Limb	NS-Hinge	0.942	0.998	nd
Tight folds-Thin beds	Tight folds-Thick beds	0.914	0.948	nd
Open folds-Thin beds	Open folds-Thick beds	0.036	0.434	nd
Tight folds-Limb	Tight folds-Hinge	0.935	1.000	D
Open folds-Limb	Open folds-Hinge	0.493	0.693	nd
Tight folds-EW	Tight folds-NS	0.950	0.742	nd
Open folds-EW	Open folds-NS	0.779	0.998	D
Thin beds-Limb	Thin beds Hinge	0.482	0.220	nd
Thick beds-Limb	Thick beds-Hinge	0.948	1.000	D
Thin beds-Tight folds	Thin beds-Open folds	0.999	1.000	D
Thick beds-Tight folds	Thick beds-Open folds	1.000	0.982	D
Thin beds-EW	Thin beds-NS	0.896	0.783	nd
Thick beds-EW	Thick beds-NS	0.134	0.993	nd
Limb-Thin beds	Limb-Thick beds	1.000	1.000	nd
Hinge-Thin beds	Hinge-Thick beds	0.771	0.987	nd
Limb-EW	Limb-NS	0.053	0.945	nd
Hinge-EW	Hinge-NS	0.707	0.988	nd
Limb-Tight folds	Limb-Open folds	1.000	1.000	D
Hinge-Tight folds	Hinge-Open folds	0.947	0.462	nd

*) D means difference and nd means no difference at 95% confidence level.

The comparison of the fracture spacing for different combinations of geologic factors in this section suggests that the local structural position may have strong effect on the fracture spacing. In particular, the fracture spacing in thick beds and on the limbs of tight folds is significantly larger than for other combination of parameters used in this study (Figures 4.8, 4.10). The contradictory relationship between folding and fracture spacing as seen in Figure 4.3 can be mainly attributed to the fractures associated with

this combination of parameters. Table 4.3 summarizes the average p-value of the test with respect to each geologic factors and their ranking. All tests suggest that in general, folding has the most significant role in controling the fracture fracing. It is worth noting that the effect of folding from the tests is contradictory with that from literature: fracture spacing is large in tight folds than in open folds. The effect of other factors on fracture spacing is different for different tests.

Table 4.3 – Ranking of the geologic factors.

	Average p-value		Rank		
	t-test	KS	t-test	KS	Median*
Folding	0.99	0.91	1	1	1
Bed thickness	0.68	0.87	3	3	3
Structural position	0.78	0.78	2	4	2
Fracture orientation	0.59	0.91	4	2	3

In summary, the analysis in this section suggests that:

1- the two fracture sets behave similarly with regard to the degree of folding and other parameters;

2- the folding has significant effect on the fracture spacing;

3- the fracture spacing is weakly affected by bed thickness;

4- the fracture spacing on the limbs of tight folds is significantly larger than the fracture spacing in other groups;

5- the fracture spacing on the limbs within thicker bed is significantly larger than the fracture spacing in other groups; and

6- the fracture spacing is a complex function of different geologic factors and that lumping all fracture data into one large dataset may not be helpful for investigating the effects of a particular geologic factor on fracture density.

Dividing fracture data into subsets can only partially overcome the problem of combining different geologic factors in the analysis. For example, the effect of bed thickness and interlimb angle on the fracture spacing shown in Figure 4.4 may be affected by the structural position, lithology or fracture orientation. Dividing fracture data according to the orientation and structural position shows that these parameters do affect the fracture spacing (e.g., Figures 4.8, 4.9) differently for different values of bed thickness and structural position. The conclusion about the effects of single geologic parameters on the fracture spacing is, in fact, the conclusion about the combined effects of other parameters. Ideally, the effect of single geological factor on fracture distributions must be assessed while other factors are fixed. With this level of data division, there is evidence that large fracture spacing on the limb of tight folds and within thick beds contributes to the apparent overall behavior of fracture spacing with regard to degree of folding or bed thickness. Further division of fracture data into smaller subsets for a single geological factor, however, is restricted by the number of the available data.

More detailed analysis of the effects of single geological factor on fracture spacing will be done with the use of neural network. The application of neural network will be described in the next two chapters.

IV.2. Fracture Size

IV.2.1. Summary of Fracture Size Data

In modeling the connectivity of the fracture system, fracture size should be specified along with the fracture density. It is typically inadequate to deterministically describe the system of fractures in the formation. Instead, the major fracture characteristics, including fracture orientation, fracture spacing, fracture size or trace

length and aperture are represented by statistical distributions. The following section presents the fracture size analysis for the data described in Chapter III. An analysis similar to the one performed on fracture spacing will be presented to give an idea of how fracture size is distributed with bed thickness and folding.

The cumulative distribution function of fracture height is shown in Figure 4.11. Table 4.4 summarizes the general statistics of both NS and EW fractures for fracture heights. The plot and data summary indicate significant difference in height distributions of the two sets.

The cumulative distribution function of fracture length is shown in Figure 4.12. Table 4.5 summarizes the general statistics of both NS and EW for fracture lengths. The plot and data summary also indicate significant difference in length distributions of the two sets.

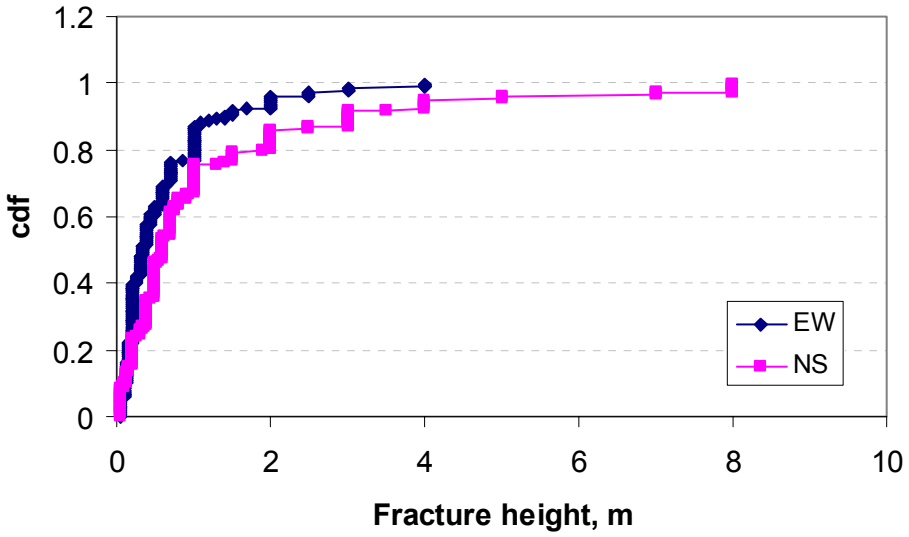

Figure 4.11 – Cumulative distribution of fracture height for two orientations, all fracture data.

Table 4.4 – Fracture height summary.

	EW fracture	NS fracture	Difference, %
Number of fractures	203	250	-
Average, m	0.595	1.165	96
Median, m	0.34	0.6	76
Standard deviation, m	0.708	1.639	131
90^{th} percentile, m	1.4	3.0	114

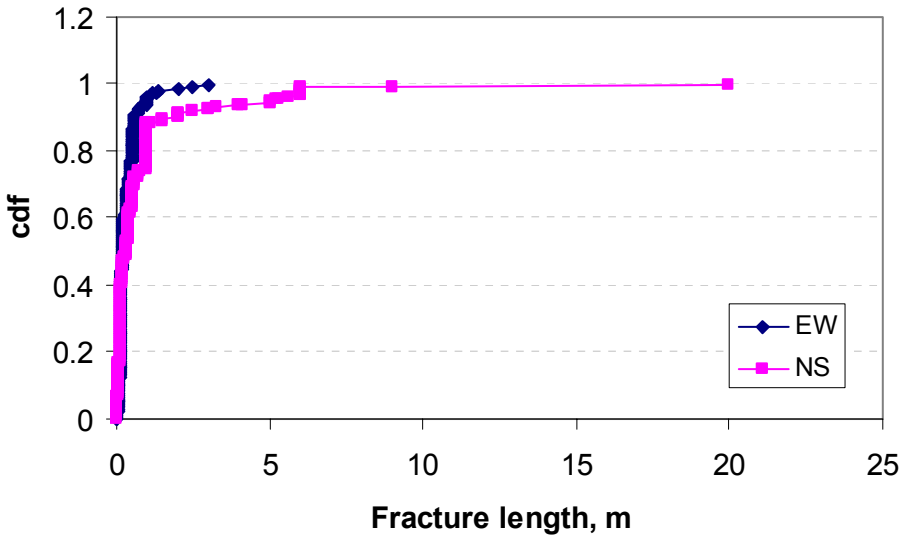

Figure 4.12 – Cumulative distribution of fracture length for two orientations, all fracture data.

Table 4.5 – Fracture length summary.

	EW fracture	NS fracture	Difference, %
Number of fractures	192	247	-
Average, m	0.327	0.853	161
Median, m	0.2	0.3	50
Standard deviation, m	0.382	1.848	383
90^{th} percentile, m	0.6	2.0	233

Examination of cumulative distribution plots and the data in Tables 4.4 and 4.5 suggests that there are more large fractures with NS than with EW strike. All statistical tests indicate significant differences between the NS and EW sets. The NS fractures are generally more developed in size than EW fractures.

It is worth noting that the fracture length and height can be heavily affected by several types of error involving the fracture size measurement. Chiles and de Marsily (1993) discussed several types of bias that can affect the fracture measurement, including censoring error, truncation error, and the bias caused by the scale of the survey. Censoring error occurs when a fracture termination is not observed; the recorded length is shorter than the true length. Truncation error occurs when small fractures are not recorded due to the resolution of the survey.

For the data available in this study, the fracture length was either taken on the bedding plane or on the exposed face of the formation: 40% of total fracture length data were measured on bedding planes and 60% were measured on exposed faces. Clearly, fractures lengths that were measured on exposed face are not reliable. Similarly, fracture heights that were measured on bedding plane represent only the minimum possible values. In several instances, an arbitrary value has been assigned to all fractures at the same location.

Figure 4.13 shows the histogram of fracture height normalized to the value of bed thickness for all fractures. This plot suggests that the majority of fractures terminates within the fractured layer and only ~20% of fractures have the height to bed thickness ratio greater than 1. From the field observations, ~50% of fractures are described as terminated at least at one bedding plane. This fact, combined with Figure 4.13 suggests that either fractures are initiated very near the bedding plane or the reported fracture heights are heavily truncated. Even 50% of fractures are reported to be terminated at bedding plane, bed thickness does not seem to have a major effect on controlling the fracture height since majority of fractures have height less than the thickness of fractured layer. Figure 4.14 shows the similar histogram of fracture length normalized to the bed thickness. A majority fraction of fractures have length smaller than the bed thickness.

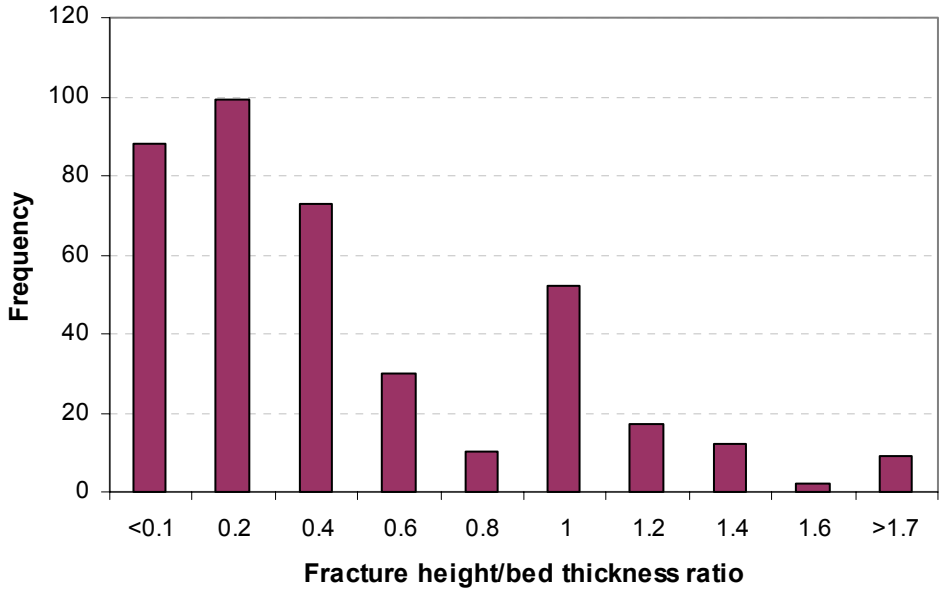

Figure 4.13 – Histogram of fracture height normalized to the bed thickness.

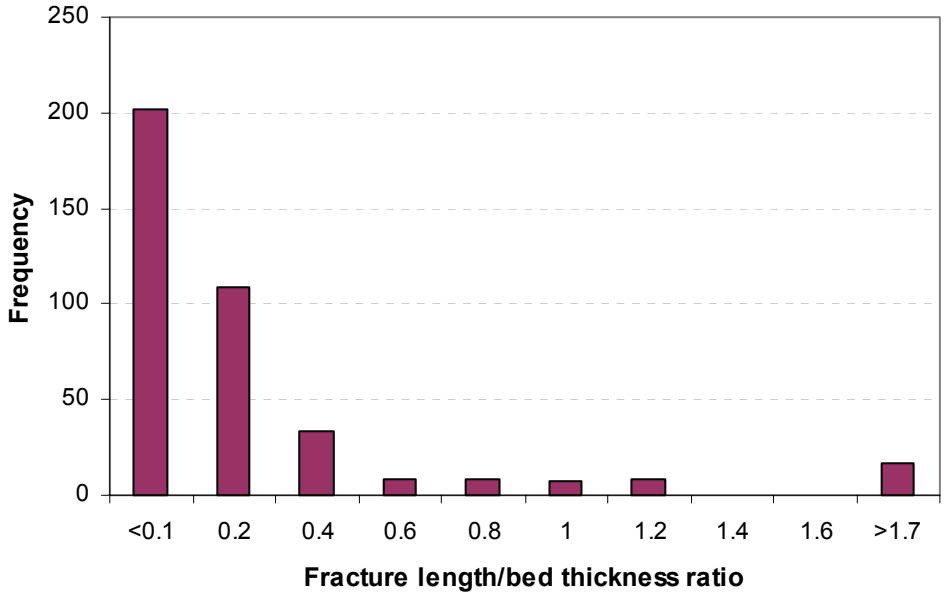

Figure 4.14 – Histogram of fracture length normalized to the bed thickness.

It is worth noting that, to my knowledge, there is no theoretical or experimental ground for the relationship between fracture size (length and height) and geologic factors. Intuitively, however one would expect that folding enhances fracturing and the fracture length and height would be greater in tight folds as compared to that in open folds. I present the comparison of our fracture length and fracture height at different values of interlimb angle and for different position on the fold.

IV.2.2. Fracture Height Versus Interlimb Angle and Structural Position

Figures 4.15-4.16 show the box plot of the fracture height for the two fracture sets with regard to interlimb angle and structural position. No significant difference was observed between fracture height of different datasets. These results suggest that the

effect of the degree of folding and the structural position on fracture height is not significant.

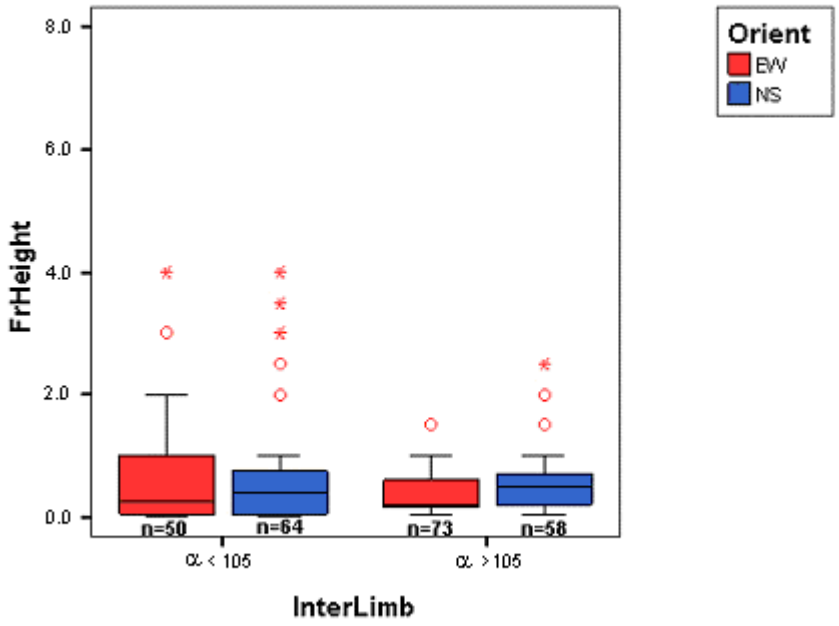

Figure 4.15 – Fracture height of the two fracture sets from folds of different interlimb angle.

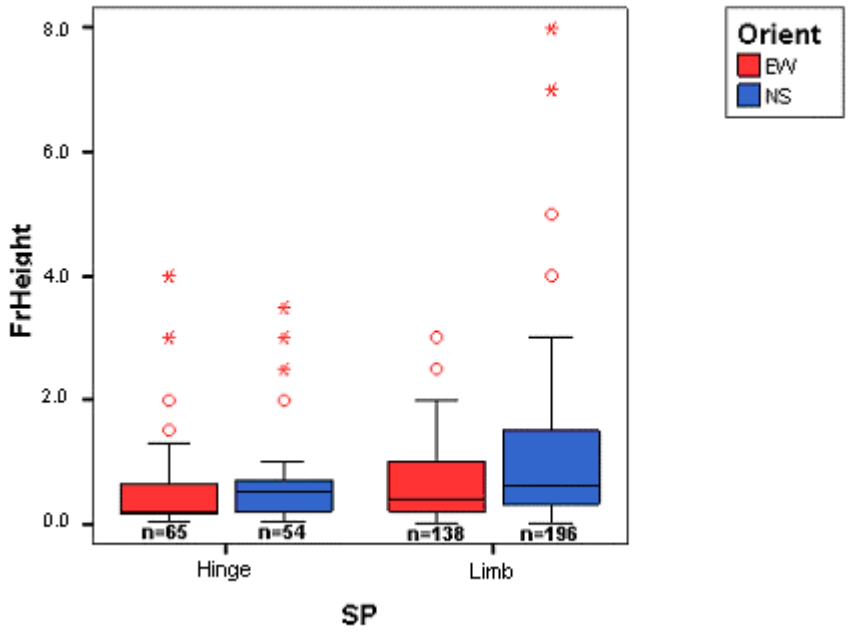

Figure 4.16 – Fracture height of the two fracture sets in different structural position.

IV.2.3. Fracture Length Versus Interlimb Angle and Structural Position

Figures 4.17-4.18 show box plot of fracture length at different value of interlimb angle and structural position. Unlike the fracture height, the fracture length increases with folding. Fracture length in the fold limbs is slightly larger and more variable than in the hinges, especially for NS fractures.

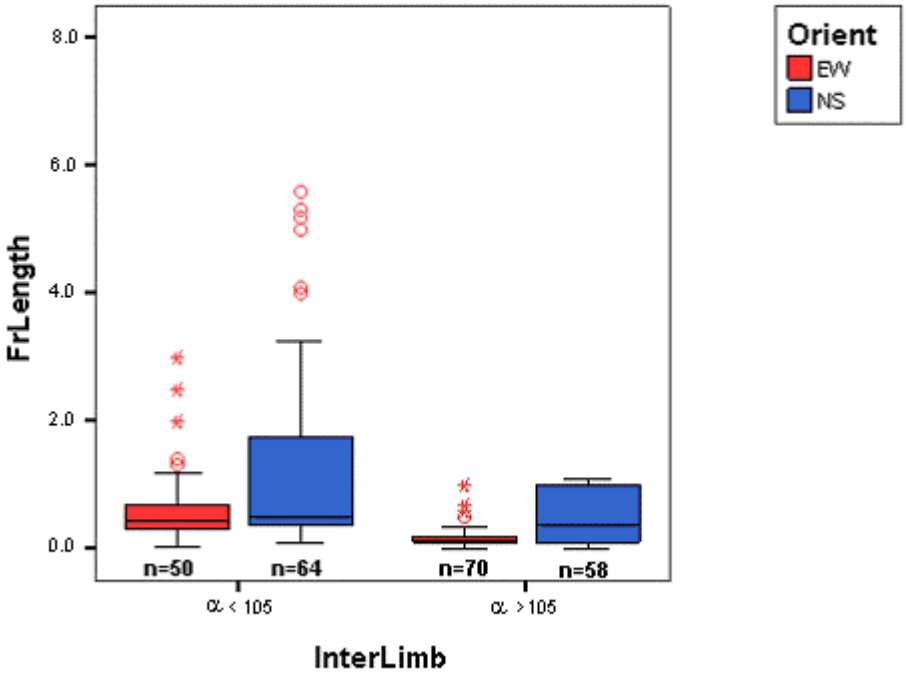

Figure 4.17 – Fracture length of the two fracture sets in different interlimb angle. Fracture length is larger in tight folds as compared to open folds.

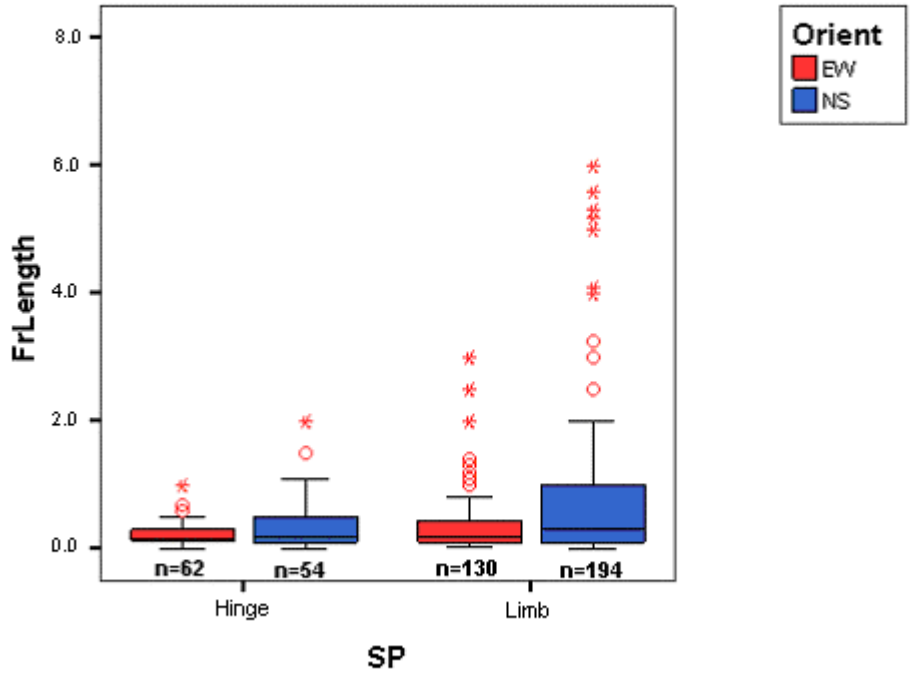

Figure 4.18 – Fracture length of the two fracture sets in different structural position. Fracture length in limbs is larger than in hinges.

IV.2.4. Summary

The analysis of fracture height and fracture length indicates that the behavior of both NS and EW fractures is similar with regard to the interlimb angle. The fracture height does not seem to be affected by the structural position in the fold, while the fracture length is more variable in fold limbs for both fracture sets.

Whereas the fracture height does not seem to relate to folding, fracture length is larger and more variable in tight folds than in open folds for both fracture sets. This implies that folding enhances the fracture length in both sets, and if that is true, then the

bed boundary plays an important in controlling the fracture height. This reflects the fact that 50% of fractures are reported to terminate at the bedding plane.

The behavior of fracture length with regard to folding is in contrast to the behavior of fracture spacing: folding does not appear to increase fracture density but does significantly affect fracture length. Assuming that the truncation error affects the fracture length measurement equally at any sample location, this analysis leads to following conclusion: the fracture system in the region of study is so over-saturated so that additional shortening of formation caused by folding does not change the fracture spacing but enhances the fracture development in length. Since the bedding plane can be a boundary for the fracture development, the analysis of fracture length could be more helpful in assessing the effect of folding on fracture development. However, it is very difficult to measure the fracture length on the exposed face of the formation. The result of the analysis could be more reliable if the fracture length is measured on the bedding planes.

CHAPTER V

TESTING OF NEURAL NETWORKS ON KNOWN FUNCTIONS

As discussed in Chapter II, the problem of developing neural networks when there are few data is difficult, and no general solution has been identified. Here, I examine the network building and validation process in the case of scarce data and where the underlying relationship between the variables is known. This analysis will give us some guidance when we apply the NNs to the Lisburne data in Chapter VI. In particular, we now investigate: (1) the effect of choosing different activation functions on the output of the network; (2) the effect of different initial weights on the cross validation method; and (3) the possibility to assess the network prediction error.

The results of the investigation suggest that the network prediction depends on the activation function used for the output unit and on the initial values of the network weights. Using the linear activation function reproduces the true relation and is less biased than the sigmoidal and Gaussian activation functions. When the number of available data is small, different initial weights for network training produces different network predictions. In these cases, applying multiple network training during the cross validation process helps to eliminate the effect of the initial weights on the result of the network configuration selection. For small datasets, the multiple initial weights of the leave one out training method can be used to assess the network prediction error.

V.1. Leave One Out Cross Validation and Prediction Error

V.1.1. Leave One Out Cross Validation

This model selection method is based on the argument that increasing model complexity need not result in a better description of the underlying function due to increasing estimation error. To find an appropriate degree of complexity, it is appealing

to compare the prediction error of different model specification. For FNNs with one hidden layer, the model selection process consists of selecting the optimum number of hidden nodes in the hidden layer (or the optimum *network configuration*).

To calculate the prediction error, a resampling technique is used. In conventional statistical analysis, this technique is often used to assess the variability of estimates using incomplete datasets (Jensen et al., 1997). Those datasets are built from available data by sampling with replacement (bootstrapping method) or by removing v observations from available data (jackknifing method) (Lewis and Orav, 1989).

The cross validation technique uses the resampled data generated by the bootstrapping or jackknifing methods for network training. The data not used to train are used to estimate the prediction error. This process is outlined as follows.

- Start with a simple network configuration. Use the resampling technique to build a number of datasets from the available data.
- Train the network using resampled datasets. The training of the network using each dataset produces a set of network weights. The resulting network weights are used to calculate the prediction error on the data that do not participate in the network training. The average of the prediction error from all datasets is the cross validation error for the given network configuration.
- Add a hidden node in the network and repeat the previous step.
- Compare the cross validation error obtained from different network configurations. The best network configuration is the one that gives the minimum prediction error.

In this chapter, I will examine the leave one out (LOO) cross validation method for network selection and for prediction error assessment. This method uses jackknifing to build datasets for network training and validation.

For a dataset of N points, the LOO cross validation method builds N subsets of size N-1 by removing one point from the original dataset. For each network

configuration, the network is trained N times, using one subset of data each time. The trained network is then used to calculate the prediction error on the remaining data point. $\bar{y}_i = f(w, x_{-i})\big|_{x=x_i}$ is the predicted value at x_i by the network trained with x_i left out and the squared prediction error is

$$SPE_i = (\bar{y}_i - y_i)^2, \tag{5.1}$$

where y_i is the true observed value of the response variable at x_i.

Repeating the training for N times, we can calculate the mean squared prediction error, E_{CV}, for all N points that have been left out,

$$E_{CV} = \frac{1}{N}\sum_{i=1}^{N} SPE_i \tag{5.2}$$

This is the cross validation (CV) error for the given network configuration. By determining the smallest E_{CV} among different network configurations, characterized by different numbers of hidden nodes in the hidden layer, we select the optimal network configuration. The scarcity of data, which is the main reason for using CV, however, leads to different prediction errors when using different initial weights for the network training. Moody and Utans (1992) suggest that the training during model selection process be carried on different resampled subsets with the same set of initial weights. This, however, artificially forces all networks to be defined around one random set of weights and different results still can be obtained for different sets of initial weights.

Considering the fact that network prediction can be affected by initial weights, I propose multiple realizations of the network training for selecting the optimum network configuration. That is, the prediction error for each network configuration is re-estimated M times (M>1), each time with different initial weights. The average CV-error resulting from M realizations is used to select the best network configuration.

The model selection process is as follows.

1- Specify initial network configuration.

2- Calculate E_{CV}^{i} for M times and take the average $\hat{E}_{CV} = \frac{1}{M}\sum_{i=1}^{M} E_{CV}^{i}$.

3- Include one additional hidden unit in the network.

4- Calculate $\hat{E}_{CV}$ of the extended network as in step 2.

5- If the $\hat{E}_{CV}$ is smaller than the previous model, then chose this model and repeat the step 3. If $\hat{E}_{CV}$ is greater than the previous model, then discard this model and chose the last model as the optimum network configuration.

V.1.2. Network Prediction Error

Once the optimum network configuration is chosen, the weights obtained for the optimum network can be used for prediction. It is worth noting that we have N sets of weights, each set corresponds to one LOO subset used in training. The prediction model, therefore, is not a single network model but a number of network realizations, which are called *CV-networks*. The network prediction at given values of input variables is the average of the values predicted by these CV-networks. The CV-networks also give a way to assess the variability of the network prediction (Hwang and Ding, 1997).

The average network prediction is:

$$\bar{y} = \frac{1}{N}\sum_{i=1}^{N} \bar{y}_{CVi} \tag{5.3}$$

where $\bar{y}_{CVi}$ is the predicted value of the network, trained with the observation *i* left out.

The CV-variance of the network prediction is:

$$\hat{s}^2 = \frac{1}{(N-1)}\sum_{i=1}^{N} (\bar{y}_{CVi} - \bar{y})^2 \tag{5.4}$$

Assuming that the prediction error is normally distributed, the prediction confidence interval of the average network prediction can be constructed as:

$$I_p = \left(\bar{y} - t_{df}^{\alpha/2}\,\hat{s}/\sqrt{N}\,,\bar{y} + t_{df}^{\alpha/2}\,\hat{s}/\sqrt{N}\right) \tag{5.5}$$

where $t_{df}^{\alpha/2}$ is the "t value" from Student's distribution with confidence level α, df = N-1 degrees of freedom, and $\hat{s}$ is the standard error of the average network prediction, estimated from CV-networks. This prediction interval I_p is determined from networks, trained with leave one out subsets of data, and is termed the leave one out (LOO) prediction interval.

In the following section, I will illustrate the model selection method based on LOO cross validation and will examine the network prediction error behavior on a known function. The feed forward neural network will be used for constructing the approximation of the function given sample from that known function. The goal is to assess some issues that are pertinent for the case of small datasets before applying neural networks in the Lisburne situation. Those issues are: 1) the choice of activation function, 2) the effect of multiple network training on the results of the model selection process.

The following one-variable and two-variable functions were used to test the LOO procedure:

$$y = -0.3x^2 + 2x + 1 \tag{5.6}$$

and

$$y = -0.3x_1^2 + 2x_1 + 0.05x_2^3 + 0.2x_1x_2 + 1 \tag{5.7}$$

V.2. One Variable Function

The plot of Eq. 5.6 in the range from 0 to 6 is shown in Figure 5.1.

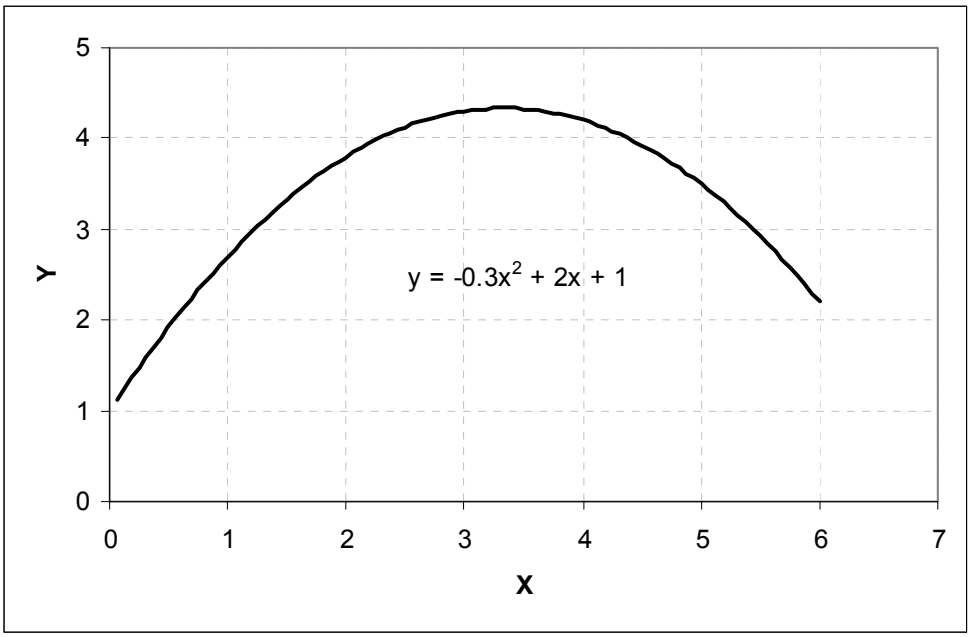

Figure 5.1 – One variable function for x from 0 to 6.

A feed forward network was used to approximate this function, using (x, y) pairs of values. The network has three layers: input layer, one hidden layer, and output layer. The input layer has one unit representing the bias and one unit representing the variable x. The sigmoidal activation function is used at hidden units. The network is trained using backpropagation learning algorithm with varying learning rate and a fixed momentum of 0.8. Before training, the learning rate is set at 0.1 and the network weights are initialized to a random value between -0.1 and 0.1. During training, the learning rate increases or decreases by a factor of 1.1 if the training error between iterations decreases or increases, respectively. The training mean square error is updated every 50 iterations. The network training stops when the change of mean squared error between two updates is less than a threshold value of 0.001 within the maximum of 10000 iterations. The reason for checking the mean squared error after 50 iterations is to eliminate the premature stopping when the error stabilizes or even increases for several

iterations before reaching true minimum. A program in Visual Basic was written to perform the network training and prediction.

The (x, y) pairs were produced by randomly generating 10 values of x ranging from 0 to 6. For each value of x, a value of y is calculated according to Eq. 5.6. These data will be used in training the network. One testing set of 50 data points with x randomly generated in the range from 0 to 6 and with one point at x=7 is created for assessing the prediction error of the network.

V.2.1. Choice of Activation Function

Typically, the same activation function is used for all neurons in any particular layer of a neural network. Nonlinear functions are required in one layer to achieve the advantage of FFNs compared to linear correlation (Fausett, 1994). FNNs usually use the sigmoidal function at the hidden layer. The selection of which activation function to use at the output layer is arbitrary, and mainly determined by computational considerations (Bishop, 1995; Ripley, 1996). I will examine the network behavior for three activation functions commonly used at the output layer: sigmoidal, Gaussian, and linear. For this purpose, the neural network is trained on the same training dataset, shown in Figure 5.2, with three different activation functions at the output node. Three hidden nodes are used in the hidden layer. The sigmoidal function is used at every hidden node. To eliminate the effect of the initial weights, the network training is performed 10 times for each dataset. The trained network is used to predict the value of y for x in the testing dataset. Figures 5.3 to 5.5 show the prediction of the network with the three different activation functions.

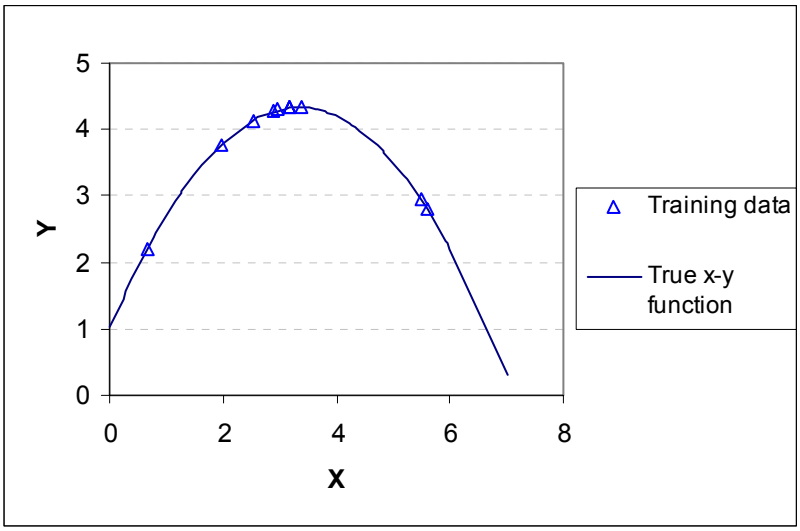

Figure 5.2 – Data for training: small set of 10 points.

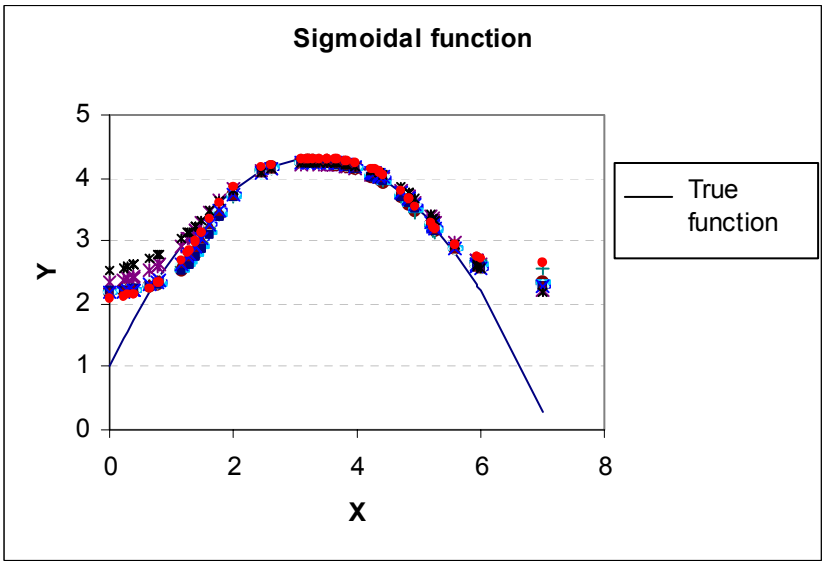

Figure 5.3 – Prediction of the true x-y relationship with sigmoidal function.

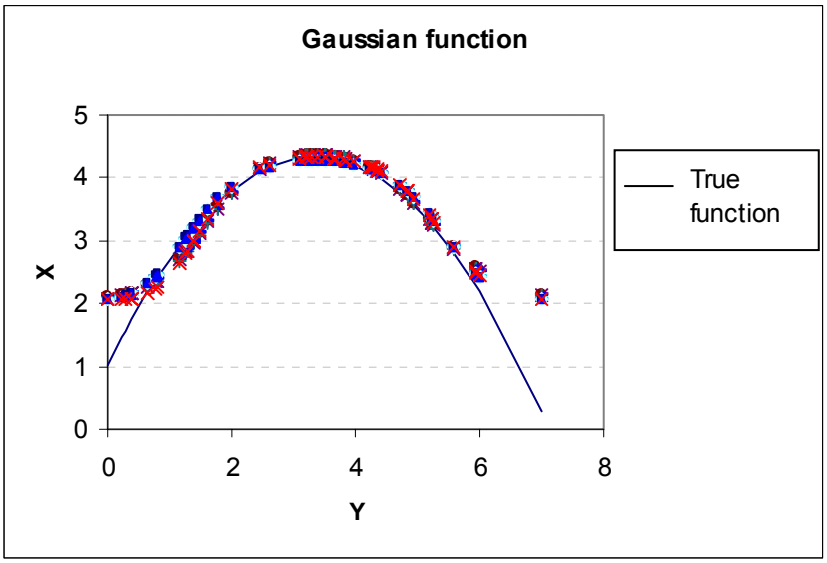

Figure 5.4 – Prediction of the true x-y relationship with Gaussian function.

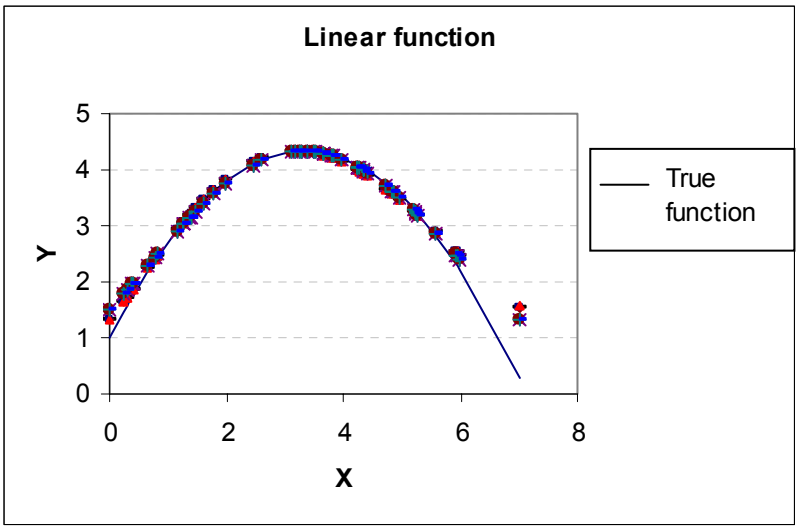

Figure 5.5 – Prediction of the true x-y relationship with linear function.

The plots of the network prediction for three different activation functions show that the linear function gives closer network predictions than the other two, especially for the data beyond the training data. The plots also show that the network predictions slightly depend on the initial weights.

To eliminate the effect of training data, I perform the above analysis for 10 different datasets. Each set consists of 10 randomly generated data points with x ranging from 0 to 6. For each set, the network is trained multiple times and is used to predict the value of y in the testing dataset. Two measurements are calculated for each function: mean squared prediction error for the data lying within the range of the training data (MSPE1) and mean squared prediction error for the data lying outside of the range of training data (MSPE2). These two measurements represent the ability of network to correlate the data and to extrapolate beyond the range of training data. The results (Table 5.1) suggest that the linear activation function gives closer predictions and faster convergence speed, compared to the other two.

Table 5.1 – Network prediction error for different activation functions, small dataset.

	Small dataset (N=10)		
	MSPE1	MSPE2	Number of Iterations
Sigmoidal	0.0216	0.8928	1855
Gaussian	0.0093	0.6629	1154
Linear	0.0071	0.2145	658

Similar analysis has been done for larger datasets (N=30 data points, Table 5.2). As expected, MSPE1 does not differ significantly for different activation functions. The extrapolation error MSPE2 of the network however, suggests that the linear and the Gaussian functions outperform the sigmoidal function.

Table 5.2 – Network prediction error for different activation functions, large dataset.

Function	Large dataset (N=30)		
	MSPE1	MSPE2	Number of Iterations
Sigmoidal	0.0096	1.0852	3256
Gaussian	0.0085	0.5911	1852
Linear	0.0087	0.5511	1354

The results of the analysis of the activation function for the univariate problem suggest several things:

- Network training with the linear activation function is faster than with sigmoidal and Gaussian activation functions.
- The linear activation function gives better network predictions when extrapolating beyond the range of training data.
- The effect of the activation function on network prediction depends on the number of data for training. Within the range of the training data, all functions give similar prediction error in case of large training dataset. For the case of small training datasets, the linear function produces the smallest prediction error.

The linear activation function will be used in subsequent analysis for the one variable function.

V.2.2. Small Dataset

V.2.2.1. Model Selection

I apply the LOO cross validation method for a dataset of 10 points with x randomly generated in the range from 0 to 6. The initial network configuration has two hidden nodes. The training parameters are similar to the ones described in the previous section. The linear activation function will be used at the output node. A minimum of 2 and a maximum of 8 hidden nodes is permitted. To illustrate the effect of multiple network realizations on the CV-error, the CV-error calculation for the whole range of network configurations (number of hidden node ranging from 2 to 8) is repeated 5 times.

Figure 5.6 shows the behavior of the mean squared error during training as a function of the number of hidden nodes in the model. Five curves on the plot correspond to five different runs. Small networks (two hidden nodes) do not give a small training error. For networks with 4 or more hidden nodes, the training error does not change significantly with added network complexity.

Figure 5.7 shows the behavior of the CV-error as a function of the added complexity to the network. The results suggest that the prediction error drastically decreases for the first two added hidden nodes and then stabilizes or slowly increases. Different network realizations at each configuration produce slightly different CV errors. The plots on Figures 5.6 and 5.7 suggest that the effect of initial weights is stronger on the CV-error than on the training error. That is, networks with similar training error may behave differently when used for prediction. Since the prediction ability of the network is of central concern, it is important to find the solution which provides the smallest prediction error.

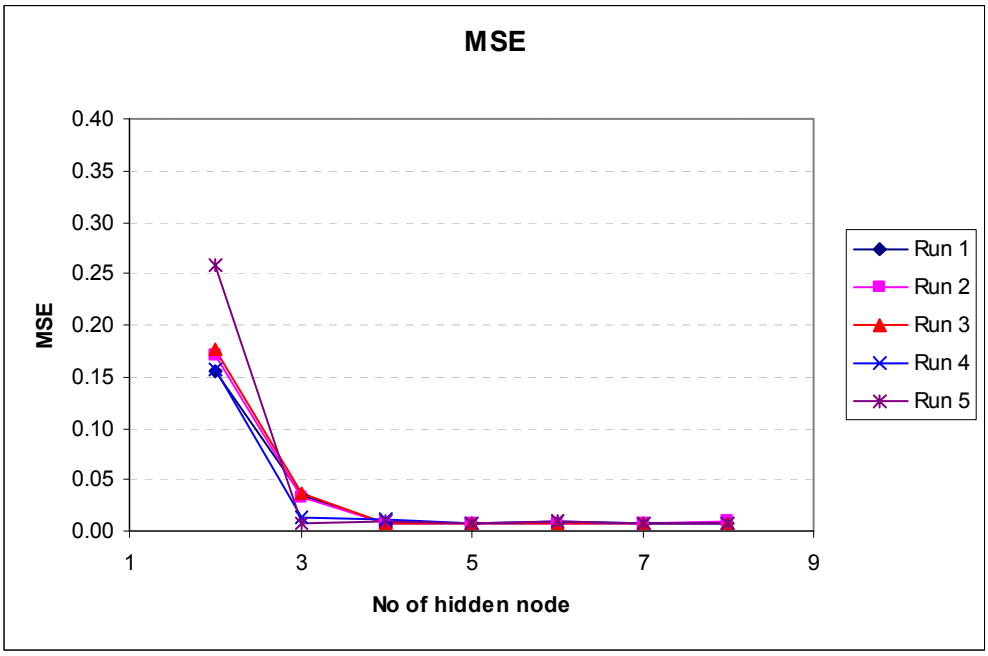

Figure 5.6 – Mean square error on the training dataset as a function of the network complexity.

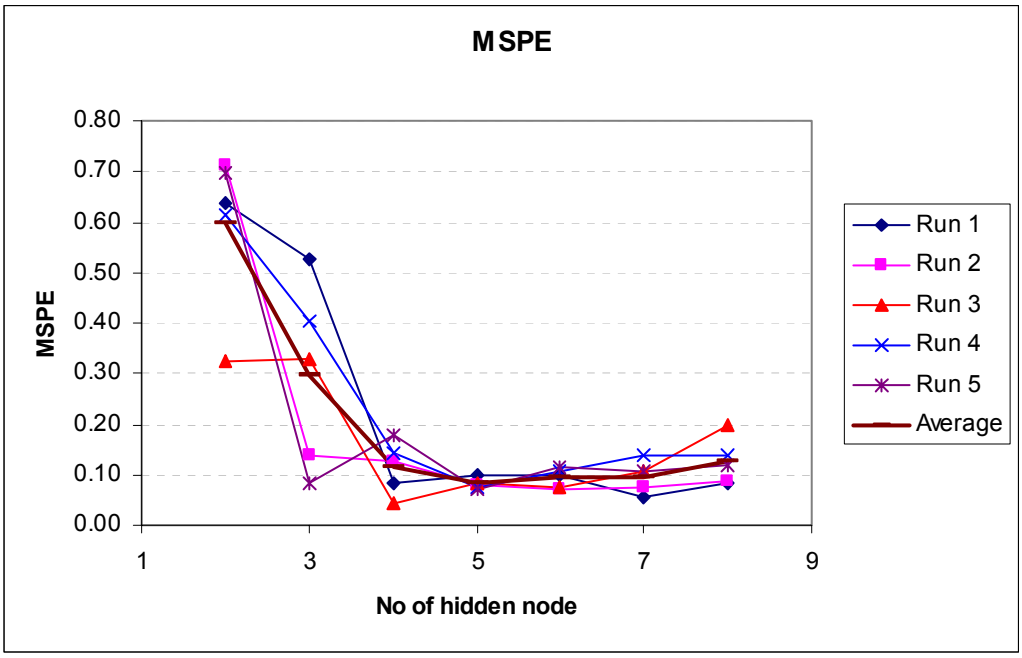

Figure 5.7 – CV-error for different runs shows that it is affected by the initial network weights.

Table 5.3 shows the CV-error for different network configurations at different runs. The results show that automatically applying of the model selection process resulted in optimum configuration with the number of hidden node varying from 4 to 7. Had we carried out the model selection process with multiple network realizations, the resulting optimum network configuration would have 5 hidden nodes.

Table 5.3 – CV-error for small dataset, one variable function.

	Number of hidden node in the model						
	2	3	4	5	6	7	8
Run 1	0.639	0.529	0.082	0.099	0.100	**0.057**	0.081
Run 2	0.713	0.138	0.128	0.078	**0.070**	0.074	0.087
Run 3	0.325	0.330	**0.045**	0.083	0.076	0.106	0.199
Run 4	0.614	0.406	0.143	**0.075**	0.108	0.140	0.139
Run 5	0.699	0.083	0.180	**0.073**	0.116	0.105	0.118
Average	0.598	0.297	0.116	**0.082**	0.094	0.096	0.125

*) Bold indicates the minimum among all network configurations

V.2.2.2. Network Prediction Variability

Network weights obtained from LOO training for configuration of 5 hidden nodes were used to predict the value of the function at 50 values of x in the testing dataset. Figure 5.8 shows the network prediction with the LOO prediction interval at the confidence level α=95%. The prediction interval is wide in the region where no data are available and is small in the region where abundant data exist. Comparing to the true values of the function, 49 true values are within the LOO confidence limits (98%). If the testing dataset include only points within the range of x used for model selection, then 100% true values are within the LOO confidence limits.

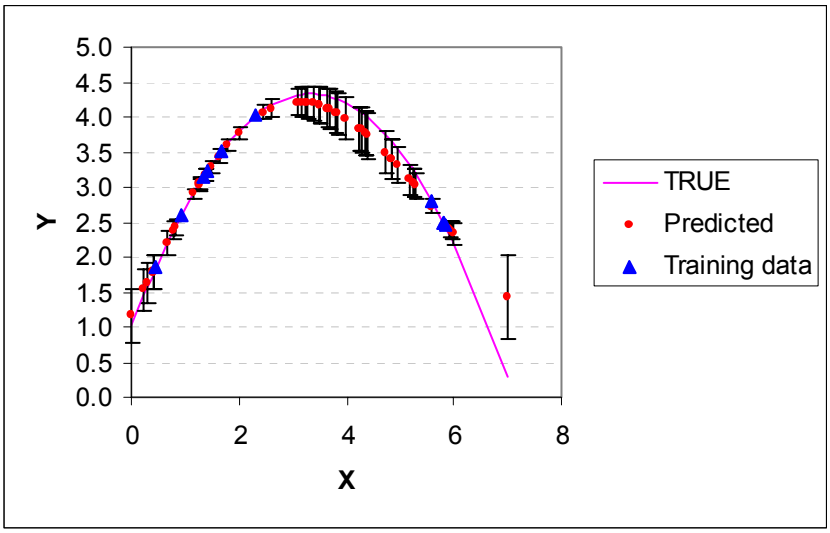

Figure 5.8 – Average LOO network prediction for the data in the testing dataset: small dataset for one variable function. Out of 50 points, 49 are within 95% confidence limits.

To eliminate the effects of data distribution in the training set, the model selection algorithm was run for 10 different sets of data with x randomly generated from 0 to 6. In all cases, E_{CV} depends on the initial weights of the network. The average E_{CV} is therefore evaluated with the number of realization M=5. The resulting optimum network configuration for these cases has hidden nodes varied between 4 and 6. The sets of weights obtained at the optimum network configuration were used to predict y values, given x in the testing dataset. Comparing with the true values, all cases give satisfactory results: the number of points falling within 95% confidence limits is always greater than 48 out of 50.

V.2.3. Large Dataset

A similar analysis, applied to the case of a large data set (N=30 data points) suggests that the results of the model selection slightly depend on the initial weight (Figure 5.9). The CV-error slightly varies with different initial network weights (Figure

5.10). This results in three different optimum network configurations based on 5 runs of the selection algorithm (Table 5.4). The average CV error from 5 realizations is smallest when 6 hidden nodes are in the model. The degree of determination for the network with 6 and 8 hidden nodes is 1.67 and 1.25 respectively. Thus, for the case of large datasets, a single run of the network configuration selection still leads to different optimum network configurations, but the change in the degree of determination of the system is not as big as for the case of small dataset.

The LOO network prediction is shown in Figure 5.11 with 95% confidence limits. In this case, 47 points out of 50 (94%) are within the prediction limit. This is slightly smaller than the nominal value (95%). If we exclude the point with x=7 from testing dataset, then 96% of points are within the confidence limit.

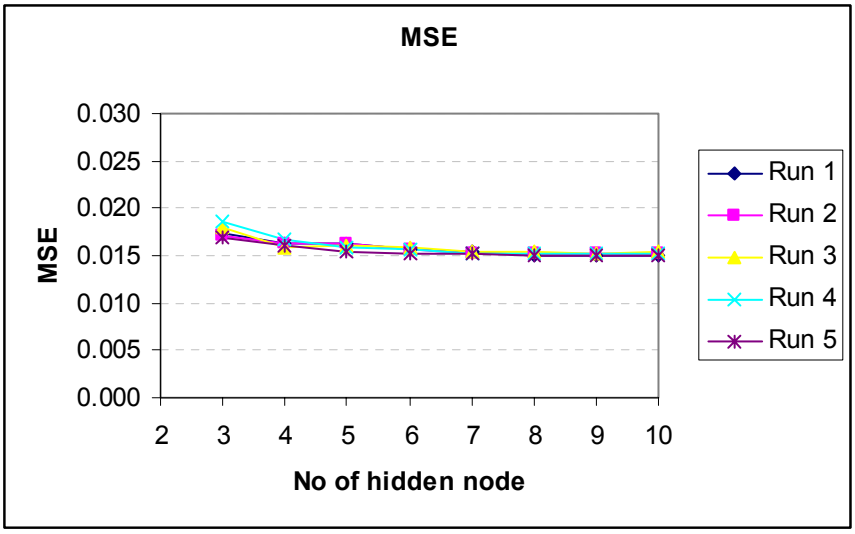

Figure 5.9 – Mean square error on the training dataset as a function of the network complexity: large dataset with N=30 points.

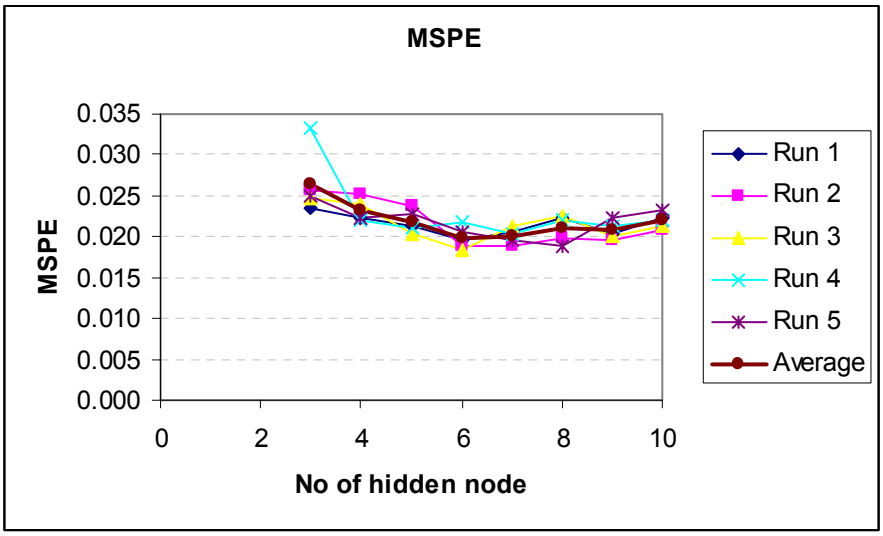

Figure 5.10 – CV-error of the network selection: large dataset with N=30 points.

Table 5.4 – CV-error for large dataset, one variable function.

	Number of hidden nodes in the model							
	3	4	5	6	7	8	9	10
Run 1	0.024	0.022	0.021	**0.019**	0.021	0.022	0.020	0.022
Run 2	0.026	0.025	0.024	**0.019**	0.019	0.020	0.020	0.021
Run 3	0.025	0.024	0.020	**0.018**	0.021	0.022	0.020	0.021
Run 4	0.033	0.022	0.021	0.022	**0.020**	0.022	0.021	0.022
Run 5	0.025	0.022	0.023	0.021	0.020	**0.019**	0.022	0.023
Average	0.026	0.023	0.022	**0.020**	0.020	0.021	0.021	0.022

*) Bold indicates the minimum among all network configurations

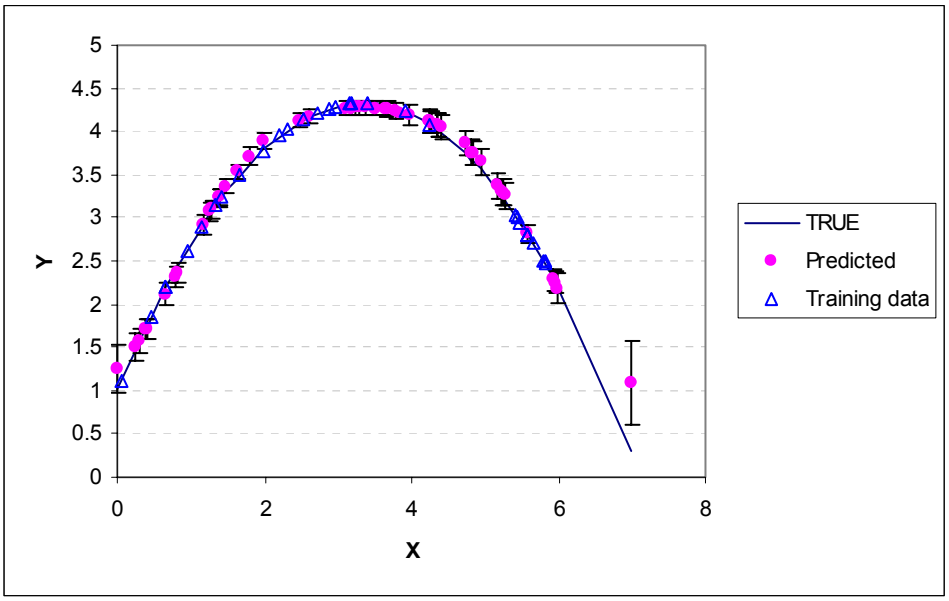

Figure 5.11 – Average LOO network prediction for the data in the testing dataset: large dataset for one variable function. Out of 50 points, 47 are within 95% confidence limits.

Comparing the results of the analysis for small and large datasets suggests several things:

- For large data sets, the CV-error is smaller than for small dataset. Adding hidden nodes in the model does not result in a significant change of the CV-error.
- In these examples, the network with 4 hidden neurons in case of small dataset has a degree of determination of 0.83, and having the average CV error of 0.116, while the network with 10 hidden neurons in case of large dataset has a degree of determination of 1 and having an average CV error of 0.02 (5 times different). That is, networks with similar degree of determination may represent underlying relationship with different degrees of satisfaction. This suggests that, together with the degree of determination as defined in Eq. 2.7

($D_1 = \frac{N}{X_p}$, with X_p is the number of weights), another quantity may be used to represent the ability of the neural network to model data. This quantity may be the ratio of available data N over the number of explanatory variables X:

$$D_2 = \frac{N}{X}. \quad (5.8)$$

In this example, D_2 for small dataset is 10, and for large dataset is 30, regardless of the network configuration. Combining $D_3 = D_1 D_2$ may even a better choice for judging how well a network can represent data. For the aforementioned examples, D_3 is 8.3 and 30 respectively.

V.3. Two Variable Function

I apply the above analysis for the two-variable function given by Eq. 5.7 (Figure 5.12). The small dataset for training consists of 14 data points with x_1, x_2 randomly chosen from 0 to 6. A separate testing dataset consists of 50 data points with x_1 and x_2 randomly chosen from 0 to 6. The network with two input nodes and four hidden nodes is used. The parameters for network training are the same as for the one variable function case. 10 different training sets, each consists of 14 data points were used for assessing the network prediction behavior with regard to different activation functions. The results (Table 5.5) suggest that the linear activation function gives closer predictions and faster convergence speed, compared to the other two.

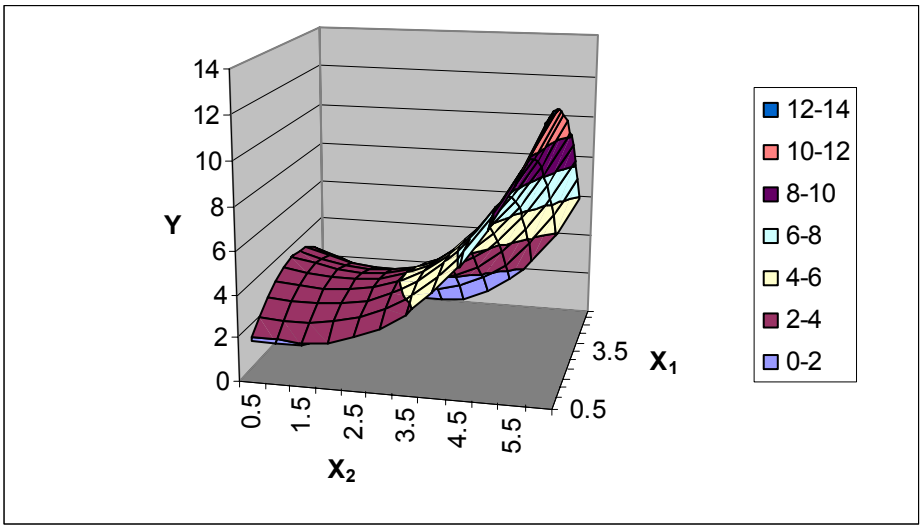

Figure 5.12 – Two variable function with x_1 and x_2 ranging from 0 to 6.

Table 5.5 – Prediction behavior for different activation functions.

	Small dataset (N=14)		
	MSPE1	MSPE2	Number of Iterations
Sigmoidal	0.760	3.016	8766
Gaussian	0.367	4.352	7243
Linear	0.281	1.680	5612

The linear activation function is used for model selection and for prediction variability analysis, similar to the one for one variable function. The average mean squared error during the LOO training is shown in Figure 5.13. The CV-error is shown in Figure 5.14 as a function of the number of hidden node in the model.

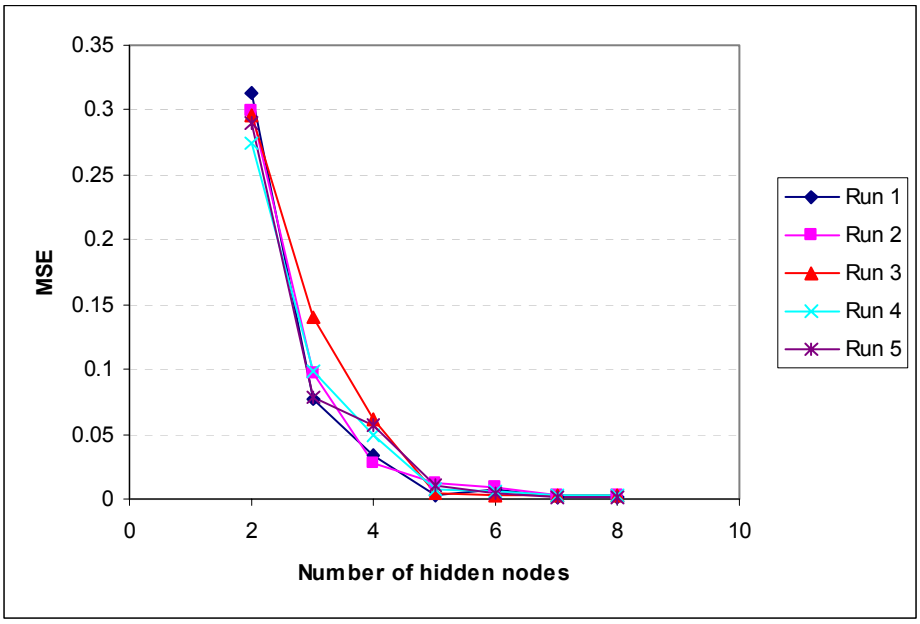

Figure 5.13 – Mean squared error on training dataset as a function of number of hidden nodes in the model.

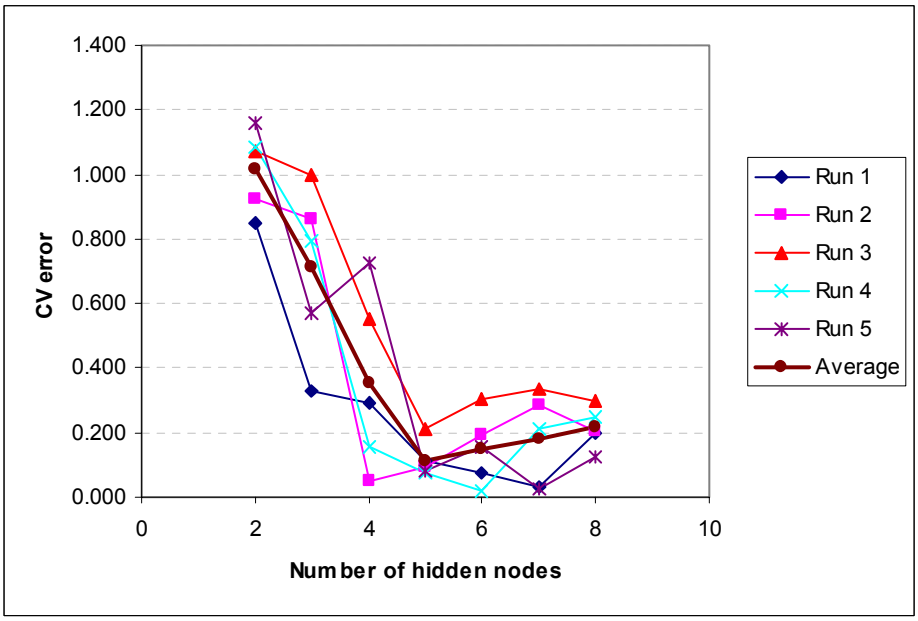

Figure 5.14 – CV-error as a function of number of hidden nodes in the model.

The CV-error shows that the network with 5 hidden nodes has the smallest average prediction error (Figure 5.14). The degree of determination D_1 for this configuration is 0.93. The "second" degree of determination D_2 is 7. The combined D_3 is 6.5. Without multiple realizations for network selection, the optimum configuration can have 4 to 7 hidden nodes, depending on the initial network weights (Table 5.6).

The LOO network prediction is plotted against the true value of the function in testing dataset (Figure 5.15). 46 true values out of 50 (92%) fall within the 95% confidence limit. This is slightly lower than the nominal value (95%). However, if we test only data points within the range of x_1, x_2 used in model selection, then 100% true values fall within the 95% confidence limits.

Table 5.6 – CV-error for large dataset, two variable function.

	Number of hidden nodes in model						
	2	3	4	5	6	7	8
Run 1	0.850	0.326	0.293	0.114	0.075	**0.033**	0.198
Run 2	0.921	0.859	**0.051**	0.095	0.190	0.285	0.106
Run 3	1.071	0.999	0.551	**0.211**	0.303	0.334	0.296
Run 4	1.082	0.793	0.158	0.072	**0.021**	0.213	0.147
Run 5	1.161	0.572	0.724	0.079	0.152	**0.024**	0.122
Average	1.017	0.709	0.355	**0.114**	0.148	0.178	0.174

*) Bold indicates the minimum among all network configurations

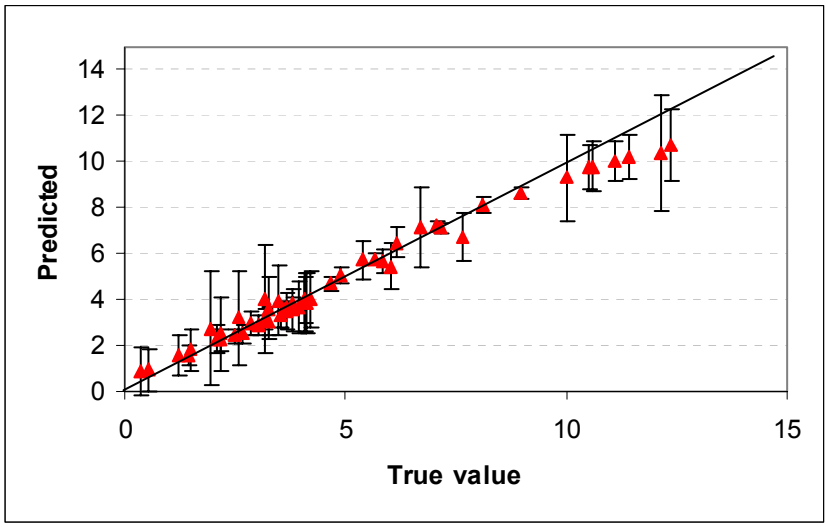

Figure 5.15 – Average LOO network prediction for the data in the testing dataset: small dataset for two variable function. Out of 50 points, 46 are within 95% confidence limits.

The analysis of the LOO network prediction for another 5 randomly generated sets of data, each consisting of 14 data points, produces similar behavior:

- The CV-error calculated in the model selection process depends on the initial weights of the network.
- The LOO prediction interval gives a good coverage of the true values of function. The number of points falling within 95% confidence limits is between 46 and 48 out of 50 (92% to 96%). If the testing dataset includes only points within the range of x_1, x_2 used in model selection, then 97% to 100% true values fall within the 95% confidence limits.

It is worth noting that the network prediction depends on several factors: the optimization algorithm, the convergence criterion, and the activation function used by network. The number of realizations in LOO network training also can affect the estimated network prediction interval. In our test, I run the network training 5 times for each jackknifed dataset. More accurate estimation of prediction interval can be obtained

by increasing the number of network realization at the cost of increasing the computational time.

While the jackknifing parameter estimation and prediction interval method works well for the estimator that is linear combination of available data (Lewis and Orav, 1989), such methods may not well suited for neural networks which use nonlinear function. Thus, the uncertainty related to the estimated LOO prediction interval may be problem dependent. In our tests, I examine the behavior of the network prediction variance for two functions. The results show that, with the given network parameters, the multiple LOO method produces satisfactory prediction intervals. If the testing dataset include only points within the range of available data, then the true values always fall within the estimated confidence intervals. The extrapolation beyond the training data reduces the number of points falling within the estimated confidence intervals.

Because of the nonlinear nature of the network estimates, extending the results to more complex relationships of high dimension may introduce uncertainty in the LOO estimated prediction interval. In any cases, the results of this study suggest that the LOO estimated prediction interval is a valuable tool for assessing the uncertainty of the network prediction, especially when we need to compare different network predicted values. Given the scarcity of the data, this method may be the only resort to addressing this problem.

I have introduced another quantity for assessing the "degree of determination" of the network. This quantity can be helpful in addressing the generalization ability of different network configurations. In cases where the rigorous model selection algorithm is used, the comparison of different model is based solely on prediction error. The use of this quantity, similar to the one in Eq. 2.7, therefore is limited in giving the user an idea about the relationship between available data and the number of unknown.

V.4. Summary

The results of investigation in this chapter suggest following:

- In case of small dataset for training, the network behavior depends on the activation function. In our tests, the linear activation function had an equal or better prediction performance than either the sigmoidal or the Gaussian functions. To my knowledge, this observation has not been reported in literature.
- In case of large dataset for training, the network behavior is insensitive to the choice of activation function. The choice of the activation function is determined mostly by the computational consideration. Similar suggestions regarding the selection of activation function were made in literature (e.g., Ripley, 1996).
- The network behavior depends on the initial weights of the network, especially for the case of small datasets. In such cases, multiple realizations of the network training and using all resulting sets of weights for prediction help to uniquely select the optimal network configuration.
- The LOO cross validation is not only a valuable technique for validating the network configuration, but also provides a way to assess the prediction error of the network. Because of the unidentifiable nature of neural network modeling, the information about prediction errors is valuable for evaluating the effectiveness of the model.
- One drawback of the cross validation model selection is that it may become computationally burdensome. Suppose that t is the time for one network training pass and NC is the number of configurations to be examined, then the time required for multiple LOO cross validation is NCxNxMxt where t depends on the number of data for training. The total training time for small dataset in the two-variable function example is almost 5 hr on a PC 1.6 GHz.

The model selection procedure and the approach for prediction error assessment described in this chapter will be used for analyzing the relationship between fracture spacing and different geologic factors in the next chapter.

CHAPTER VI

NEURAL NETWORK ANALYSIS OF FRACTURE SPACING DATA

Statistical analysis of the fracture density in Chapter IV shows that bed thickness does not have a significant effect on fracture density and that the structural position and fracture orientation may play an important role in fracture distribution. Because of the limited number of data, conventional linear statistical analysis can only partially address the effect of individual geologic parameters on the fracture density. This chapter presents the use of artificial neural networks to investigate the collective effect of geologic parameters on the fracture density.

The neural network used in this study is the multilayer feed forward network. Bed thickness, lithology, structural position on the fold, stratigraphic position, fracture orientation, and degree of folding are the inputs and average fracture spacing is the output of the network. The back propagation algorithm is used to train the network on the given data and observed fracture density. The multiple leave-one-out cross validation method is used for selecting the best network configuration and for estimating the network prediction confidence interval. The resulting method produces a population of network predictions for each given input pattern and allows using conventional statistical tests to assess the significance of the effect of input parameters on fracture spacing. The results of the neural network analysis suggest (1) that the effect of geologic parameters on fracture distribution is complex and (2) the lithology and local stratigraphic setting play an important role in fracture distribution.

VI.1. Neural Networks

VI.1.1. Network Parameters

The feed forward neural network consists of three layers (Figure 6.1**)**. I assume that the fracture spacing in each orientation may be affected by bed thickness, lithology, structural position on the fold, degree of folding, and the stratigraphic position. The basis for this assumption is the effect of folding and mechanical stratigraphy on fracture distributions reported in the literature (see Chapter II). Thus, the input layer of the network consists of 7 neurons, representing a bias unit and 6 input parameters: bed thickness, lithology, structural position on the fold, degree of folding (which is expressed by the magnitude of interlimb angle), orientation, and formation. The number of hidden units in the hidden layer is a subject for selection. The multiple LOO cross validation method described in Chapter V will be used to select the best network configuration. The output layer consists of one unit representing the average fracture spacing. The sigmoidal activation function is applied for all units in the hidden layer. The linear activation function is used for the output unit. It shows several advantages over sigmoidal and Gaussian functions in cases of sparse datasets, such as less biased predictions, both in interpolation and extrapolation outside of the training data (Chapter V). The back propagation algorithm is used with varying learning rate (between 0.02 and 0.2) and fixed momentum of 0.8. The network training is stopped when the absolute change of mean squared error for every 50 iterations is less than 0.0001.

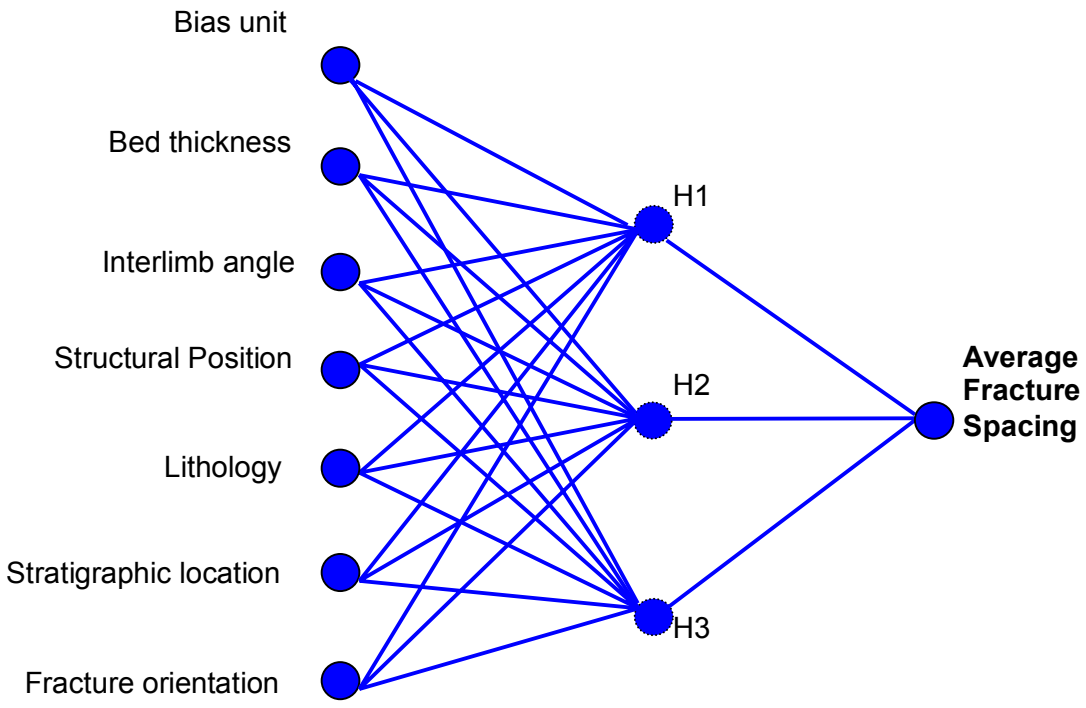

Figure 6.1 – Feed forward neural network to study the effect of geologic factors on fracture spacing in exposed detachment folds of Lisburne Group in northeastern Alaska.

VI.1.2. Fracture Spacing Data

The fracture data and associated geologic parameters were defined by geologists at the University of Alaska. A detailed description of the geological setting and fracture data were given in Chapter III. The fracture data were collected from 5 detachment folds with interlimb angles ranging from 90 deg. to 160 deg. Only extensional fractures are included in the analysis. Bed thickness ranges between 0.1 m and 4 m. To assist the convergence of the training and the analysis of the network connection weights, the bed thickness and interlimb angle are scaled to the range between 0 and 1 as follows:

$$x_{new} = \frac{x - x_{\min}}{x_{\max} - x_{\min}}.$$

Structural position on the fold, formation, and fracture orientation are categorical variables and are represented by discrete numbers as follows:

- for structural position: -1 represents the limb, 1 represents the hinge;
- for fracture orientation: -1 represents EW orientation, 1 represents NS orientation; and
- for stratigraphic location: -1 represents Wahoo limestone, 1 represents Alapah Limestone.

Lithology is a special case of categorical variable. While other categorical variables take only two values, lithology can have several discrete values. Two approaches can be used for assigning values to lithology: (1) treating each value as one variable; or (2) assigning values in the continuous sense. Each method has its advantages and disadvantages. Treating each value of lithology as one variable will increase the number of weights in the model, hence, decrease the degree of determination of the system. Assigning values to the variable in the continuous sense may create a false sense of the continuity among these values, hence, may have adverse effect on the behavior of the network. In our case, the lithology of the available data consists mainly of two types: packstone and grainstone. Therefore, the lithology is treated as one variable with packstone represented by -1, grainstone represented by 1. For all categorical variables, 0 represents the status where the value of the variable is undefined.

A total of 25 data patterns are available for network analysis (Table 6.1). Each input pattern consists of one set of values for bed thickness, interlimb angle, lithology, structural position, orientation, and stratigraphic position. A training pattern is the values for all input variables and associated average fracture spacing.

Table 6.1 – Fracture data used in neural network analysis.

Bed thickness, m	Interlimb angle, deg.	Structural position	Lithology	Formation	Orientation	Average fracture spacing, m
1.5	125.0	1	-1	1	-1	0.245
1.5	125.0	1	-1	1	1	0.123
1.5	125.0	-1	1	-1	-1	0.123
1.5	125.0	-1	1	-1	1	0.240
2.5	125.0	-1	1	1	1	0.500
2.5	125.0	-1	1	1	-1	0.130
4	90.0	-1	-1	1	1	0.341
4	90.0	-1	-1	1	-1	0.175
4	90.0	1	1	0	-1	0.143
4	90.0	1	1	0	1	0.100
2.5	100	-1	1	1	1	0.319
2.5	100	-1	1	1	-1	0.092
3	100	1	1	1	1	0.464
3	100	1	1	1	-1	0.561
0.4	100	-1	-1	1	1	0.304
0.4	100	-1	-1	1	-1	0.453
2	110	-1	-1	-1	1	0.045
0.2	110	1	-1	-1	-1	0.253
0.1	110	1	-1	-1	-1	0.250
1	160	-1	-1	-1	-1	0.181
1	160	-1	-1	-1	1	0.074
1.5	160	1	-1	-1	1	0.131
1.5	160	1	-1	-1	-1	0.182
3	135	1	-1	-1	-1	0.075
3	135	1	-1	-1	1	0.090

VI.1.3. Optimal Network Configuration

The multiple LOO cross validation method described in Chapter V is used to select the best network configuration and to assess the network prediction error. The algorithm starts with the network having 1 hidden node and iteratively adds a new node into model. For each configuration, the LOO cross validation error is calculated based on the leave one out prediction. The algorithm stops when the average cross validation error starts to increase. Figure 6.2 shows the average cross validation error as a function of the number of hidden nodes in the model. The best network configuration, corresponding to smallest CV-error, consists of 3 hidden nodes.

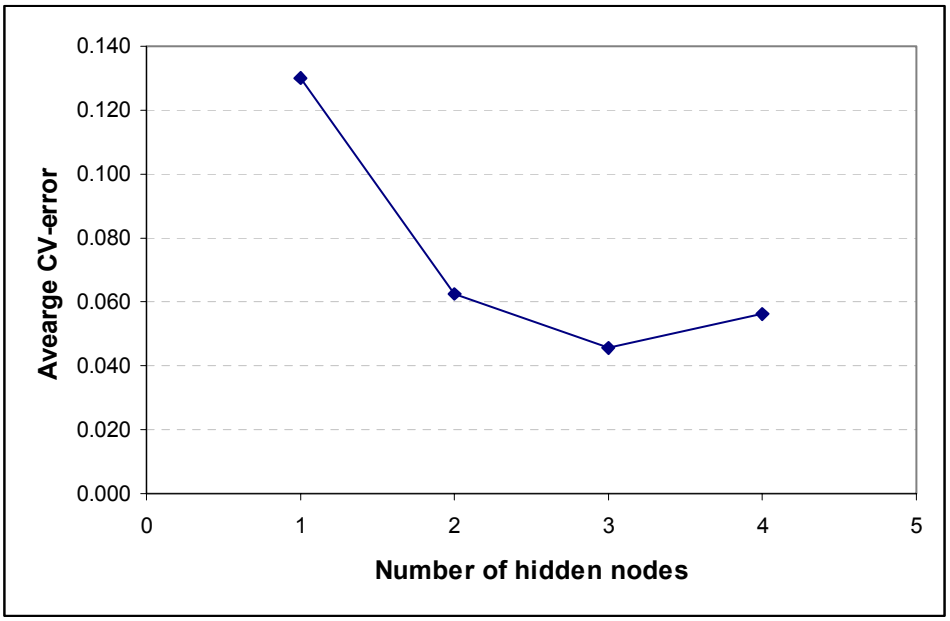

Figure 6.2 – Average CV-error as a function of the number of hidden nodes in the model.

In the next sections, I will examine the behavior of the network prediction for the best network configuration and will explore the effect of each input geologic parameter on fracture spacing.

VI.1.4. Network Sensitivity Analysis

Analyzing the network result for multiple-variable relationships is not straight-forward (Chapter II). The network outputs are impossible to be viewed graphically due to the multi-dimensionality of the model. The problem is worse if there are multiple values of network prediction for each given input pattern.

If the network is used purely for prediction, the network output is simply calculated for all network weights, stored during training. The prediction value of the network is the average from all the network outputs. The variance of the prediction value is assessed from the distribution of the network output at given input pattern (Figure 6.3)

In our case, we want to investigate the effect of input geologic parameters on the network output (average fracture spacing). This can be done by plotting the network output at different input patterns. For example, the average fracture spacing at an interlimb angle of 100 deg., lithology of packestone, NS fractures, in the limbs of the fold is calculated for several values of bed thickness, ranging from 0.25 m to 3.75 m, while fixing other parameters (Figure 6.4). Similarly, the fracture spacing at bed thickness of 1 m, lithology of packestone, NS fracture, in limb of the fold is calculated for several values of interlimb angle, ranging from 90 deg. to 160 deg. (Figure 6.5).

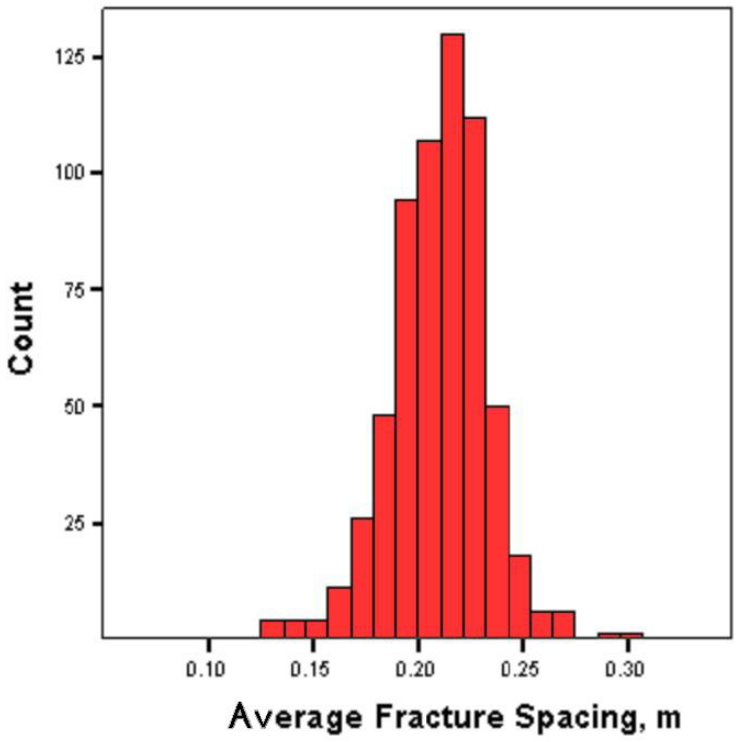

Figure 6.3 – Distribution of the average fracture spacing as predicted by the neural network for EW fracture at bed thickness of 1 m, interlimb angle of 100 deg., and the structural position is the hinge in the Wahoo formation.

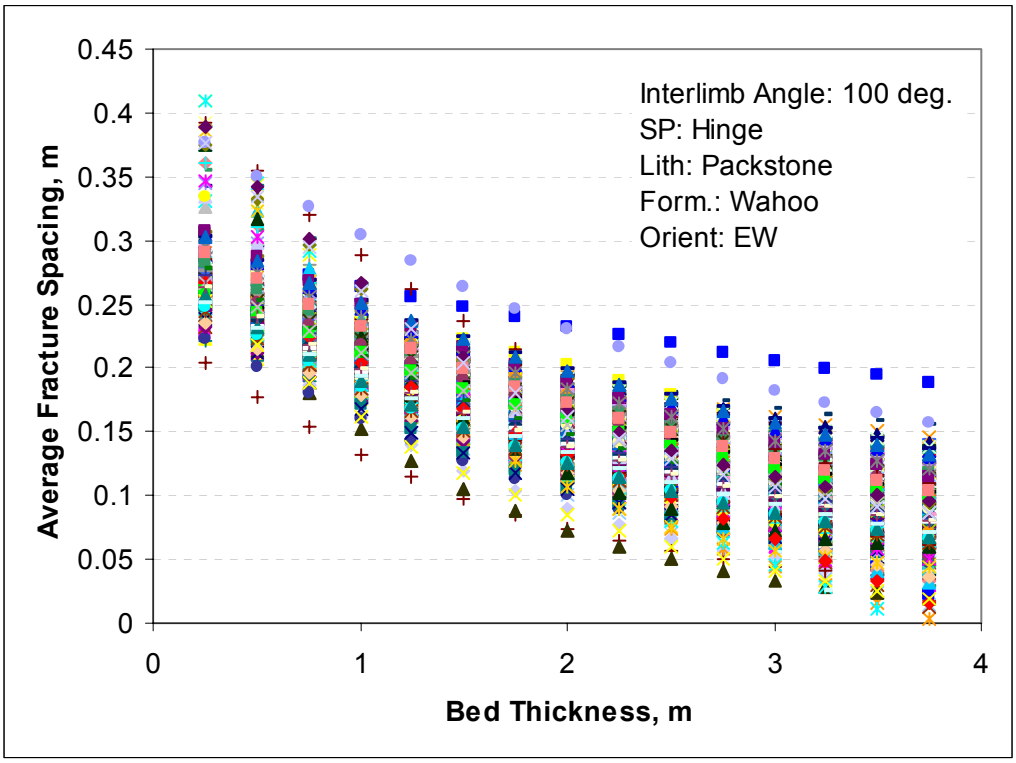

Figure 6.4 – Fracture spacing as a function of bed thickness at interlimb angle of 100 deg. Other parameters are: hinge, packstone, Wahoo formation, and EW orientation.

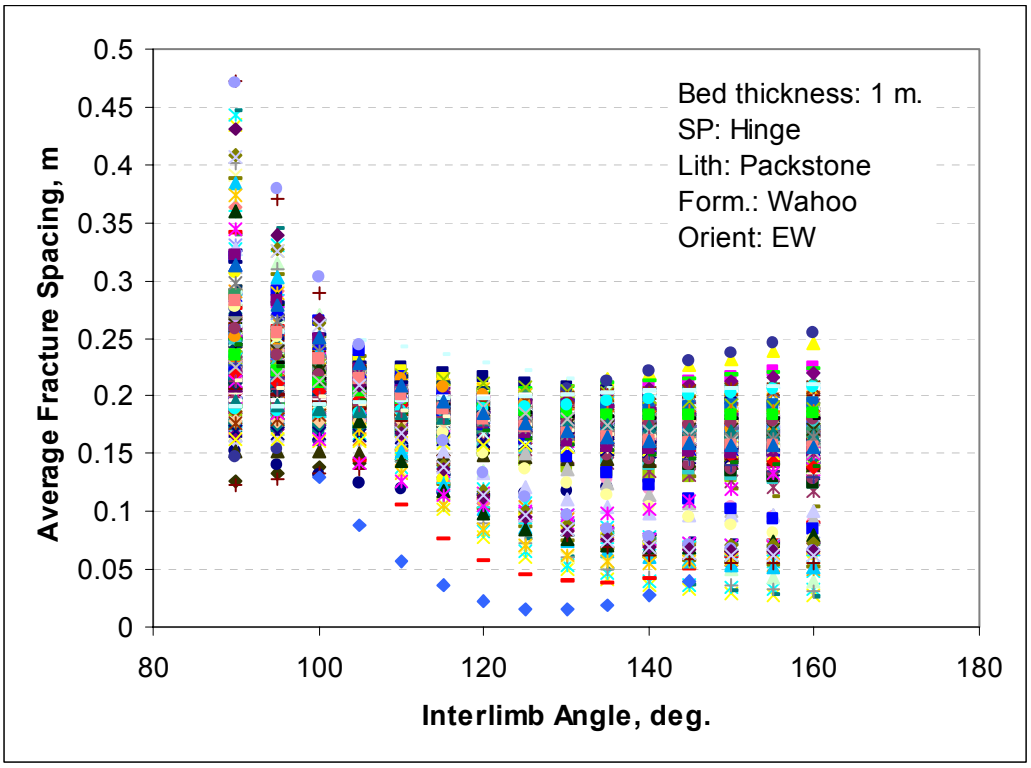

Figure 6.5 – Fracture spacing as a function of interlimb angle at bed thickness of 1 m. Other parameters are: Hinge, Packstone, Wahoo formation, and EW orientation.

Examining the relationships of fracture spacing as a function of bed thickness (Figure 6.4) and interlimb angle (Figure 6.5) suggests that the variance of the network prediction is not constant. It is smaller at and around the points where data exist for training than in the regions of no data. In most cases, the fracture spacing varies monotonically with respect to bed thickness and interlimb angle. The trend of this relationship is not unique. In some cases, the graph shows that fracture spacing decreases with bed thickness; in another cases, the fracture spacing levels out or increases with bed thickness. The same holds true for the relationship between fracture spacing and interlimb angle.

We want to assess the statistical significance of the effect of each geological parameter on the fracture spacing. In particular, we want to answer these questions:

1- How does the bed thickness affect the fracture spacing?

2- How does the interlimb angle affect the fracture spacing?

3- How does the structural position and lithology affect the fracture spacing?

Because the relationships between fracture spacing and geological parameters may be nonlinear (e.g., Figures 6.4, 6.5), conventional tests using the linear correlation coefficient are not appropriate. Instead, I assessed the statistical significance by following the same approach as the statistical analysis in Chapter IV: by testing statistical differences between groups of data, derived from the different values of the input variables.

For discrete variables, this approach will cover all possible values of that variable. For the continuous variables such as bed thickness and interlimb angle, different numbers of groups can be used for assessing the significance of each variable on the network output (Lek et al., 1996). We are interested in judging whether the average fracture spacing in tight folds is different comparing to the average fracture spacing in open folds. Similarly, how does the average fracture spacing in thin beds compare to the spacing in thick beds. Thus, the statistical significance of the bed thickness and interlimb angle on the average fracture spacing will be assessed by considering two groups of bed thickness and two groups of interlimb angle. A bed thickness of 1 m represents thin beds, and a bed thickness of 3 m represents thick beds. Similarly, an interlimb angle of 100 deg. represents tight folds, and an interlimb angle of 140 deg. represents open folds.

As a result, we have $64=2^6$ subsets of fracture data. Each subset of data represents a single combination of input geologic parameters considered in this model. For example: one subset is fracture spacing in thin beds (h = 1 m), in hinges of tight folds (interlimb angle of 100 deg.), the lithology is packstone, the orientation is NS, and the formation is the Wahoo. I use the paired t-test to assess the statistical significance of

the difference between datasets of average fracture spacing (Siegel and Morgan, 1996). Each data pair consists of two datasets of average fracture spacing predicted by the neural network for two values of a particular geologic factor. For example, to infer the effects of bed thickness on fracture spacing, I compare the average fracture spacing in thin beds (h = 1 m) and in thick beds (h = 3 m), while keeping all other geologic parameters in the model (interlimb angle, structural position, lithology, formation, and fracture orientation) at the constant value. The prediction variabilities for each subset are estimated from the network predictions at the given geologic parameters using LOO.

The following sections present the results of statistical assessments of the network predictions with regard to the geologic factors. For each pair of average fracture spacings, the paired difference is calculated and the one sample t-test is used to see whether the average of the paired differences is significantly different from 0. The test can be formulated in two ways: 1) test if there is a significant difference between sets and 2) test if the first set is greater/smaller than the second set. The difference between the two formulations of the test is the confidence level in the test: the test for difference uses a two-tail confidence level while the test for the direction of the difference uses a one-tail confidence level.

VI.2. Results of Network Analysis

VI.2.1. Effects of Bed Thickness

Table 6.2 presents the results of the t-test for all possible combinations of two values of bed thickness with other geologic parameters in the neural network model. The effect of bed thickness on fracture spacing is characterized by the difference between average fracture spacing at bed thicknesses of 1 m and 3 m, while other parameters in the model are fixed. The column labeled as *p-value* in Table 6.3 presents the significance level for the hypothesis that the average fracture spacing in thin beds is *larger* than the average fracture spacing in thick beds. The p-value of 0.5 indicates no difference between average fracture spacings. The p-value less than 0.5 indicates that

the average fracture spacing in thin beds is smaller than in thick beds. The column labeled as "test result" presents the result of the paired t-test at a 95% confidence level: the value of 1 indicates that the average fracture spacing in thin beds is statistically greater than in thick beds; and the value of -1 indicates that the average fracture spacing in thin beds is statistically smaller than in thick beds. The value of 0 indicates that there is not enough evidence to conclude about the difference at the confidence level of 90%. The reason for using two different confidence levels is that the test for differences uses a two-tail test value while the test for the direction of difference uses a one-tail test value.

The effect of bed thickness on fracture distribution is not clear. In all 32 possible combinations of interlimb angle (two groups), structural position, lithology, fracture orientation, and formation, there are 5 instances where fracture spacing in thin beds (h = 1 m) is larger than fracture spacing in thick beds (h = 3 m); 0 instances where fracture spacing in thin beds is smaller than fracture spacing in thick beds; and 27 instances where there is no significant difference between fracture spacings for the two bed thicknesses. The differences between fracture spacing in thin beds and in thick beds occurred in combinations with EW fractures and with tight folds (4 cases occurred in fold with the interlimb angle of 100 deg., only 1 case in fold with the interlimb angle of 140 deg.). Out of these 5 cases where fracture spacing in thin beds was statistically greater than in thick beds, there is no preference with regard to other geologic factors: 3 cases occurred in hinges, 2 cases in limbs; 3 in the Wahoo, 2 in the Alapah; 3 in packstone, 2 in grainstone.

Statistical analysis of the fracture density in Chapter IV shows that bed thickness does not have a significant effect on fracture density. Compared to the statistical analysis results in Chapter IV, the neural network provides more detailed effects of bed thickness on fracture spacing. Neural network analysis indicates that the effect of bed thickness on fracture spacing is different for different combinations of other geologic parameters but in general, there was no significant difference in fracture spacing between thin and thick beds.

Table 6.2 – Result of t-test for the effect of bed thickness on fracture spacing.

Int. Angle, deg.	Structural Position	Lihthology	Formation	Orient.	Mean (H1) m	Mean (H2) m	p-value	t test result*
100	Hinge	Packstone	Alapah	NS	0.307	0.282	**0.563**	0
100	Hinge	Packstone	Alapah	EW	0.638	0.423	**0.791**	0
100	Hinge	Packstone	Wahoo	NS	0.065	0.033	**0.754**	0
100	Hinge	Packstone	Wahoo	EW	0.209	0.100	**0.997**	**1**
100	Hinge	Grainstone	Alapah	NS	0.446	0.412	**0.571**	0
100	Hinge	Grainstone	Alapah	EW	0.759	0.522	**0.786**	0
100	Hinge	Grainstone	Wahoo	NS	0.113	0.076	**0.765**	0
100	Hinge	Grainstone	Wahoo	EW	0.242	0.121	**0.984**	**1**
100	Limb	Packstone	Alapah	NS	0.308	0.308	**0.506**	0
100	Limb	Packstone	Alapah	EW	0.307	0.151	**0.994**	**1**
100	Limb	Packstone	Wahoo	NS	0.120	0.067	**0.728**	0
100	Limb	Packstone	Wahoo	EW	0.179	0.040	**0.811**	0
100	Limb	Grainstone	Alapah	NS	0.390	0.387	**0.517**	0
100	Limb	Grainstone	Alapah	EW	0.349	0.183	**0.991**	**1**
100	Limb	Grainstone	Wahoo	NS	0.148	0.096	**0.711**	0
100	Limb	Grainstone	Wahoo	EW	0.181	0.042	**0.813**	0
140	Hinge	Packstone	Alapah	NS	0.199	0.242	**0.303**	0
140	Hinge	Packstone	Alapah	EW	0.283	0.223	**0.694**	0
140	Hinge	Packstone	Wahoo	NS	0.083	0.071	**0.580**	0
140	Hinge	Packstone	Wahoo	EW	0.156	0.089	**0.955**	**1**
140	Hinge	Grainstone	Alapah	NS	0.304	0.351	**0.309**	0
140	Hinge	Grainstone	Alapah	EW	0.357	0.286	**0.706**	0
140	Hinge	Grainstone	Wahoo	NS	0.123	0.110	**0.567**	0
140	Hinge	Grainstone	Wahoo	EW	0.173	0.105	**0.934**	0
140	Limb	Packstone	Alapah	NS	0.295	0.322	**0.354**	0
140	Limb	Packstone	Alapah	EW	0.179	0.095	**0.851**	0
140	Limb	Packstone	Wahoo	NS	0.132	0.094	**0.678**	0
140	Limb	Packstone	Wahoo	EW	0.157	0.037	**0.787**	0
140	Limb	Grainstone	Alapah	NS	0.370	0.400	**0.362**	0
140	Limb	Grainstone	Alapah	EW	0.199	0.118	**0.854**	0
140	Limb	Grainstone	Wahoo	NS	0.162	0.126	**0.650**	0
140	Limb	Grainstone	Wahoo	EW	0.157	0.039	**0.782**	0

*) 1 indicates that fracture spacing in H1 (h = 1 m) is statistically greater than in H2 (h = 3 m), -1 indicates that fracture spacing in H1 is statistically smaller than in H2, and 0 indicates no difference between subsets.

This relationship is opposite to that often reported in the literature (Ladeira and Price, 1981; Huang and Angelier, 1989; Narr and Suppe, 1991). From the breakdown of the number of cases where the differences occurred, we can say that the EW fractures in the limbs of Wahoo formation are more likely to have fracture spacing in thin beds greater than in thick beds. Hanks et al. (1997) found no reliable relationship between fracture spacing and bed thickness for flat-lying Lisburne Carbonates in the northeastern Brooks Range.

It is worth noting that the choice of the bed thickness values used for fracture spacing comparison may affect the analysis results. The p-value in Table 6.2 may change if we choose to compare the average fracture spacing in beds of 1 m and 4 m. However, considering the fact that fracture spacing monotonically varies with the bed thickness (e.g., Figure 6.4), choosing different bed thickness values for fracture spacing comparison might not significantly alter the analysis results. The bed thicknesses of 1 and 3 m ware chosen to avoid the possible boundary effects in calculating fracture spacing using networks. The same arguments are applied when analyzing the effects of folding on fracture spacing.

VI.2.2. Effects of Folding

Table 6.3 shows the result of the t-test for all possible combinations of two values of interlimb angle with other geologic parameters in the model. At the confidence level of 90%, all cases show no significant difference between the average fracture spacings in tight and in open folds. Even at the confidence level of 80%, only 2 out of 32 cases (6%) show significant differences between average fracture spacings in tight and in open folds. The average value of the p-value for all 32 cases is 0.63, which is only slightly greater than 0.5. These results indicate that fracturing may not be closely related to the folding, or that it already had reached its saturation status prior to folding so that the folding does not change the fracture spacing distribution (Bai and Pollard, 2000).

Table 6.3 – Result of t-test for the effect of folding on fracture spacing.

Bed Thick. m	Structural Position	Lihthology	Form.	Orient.	Mean (α1) m	Mean (α2) m	p value	t test result*
1	Hinge	Packstone	Alapah	NS	0.307	0.199	**0.757**	0
3	Hinge	Packstone	Alapah	NS	0.282	0.242	**0.612**	0
1	Hinge	Packstone	Alapah	EW	0.638	0.283	**0.879**	0
3	Hinge	Packstone	Alapah	EW	0.423	0.223	**0.918**	0
1	Hinge	Packstone	Wahoo	NS	0.065	0.083	**0.401**	0
3	Hinge	Packstone	Wahoo	NS	0.033	0.071	**0.366**	0
1	Hinge	Packstone	Wahoo	EW	0.209	0.156	**0.808**	0
3	Hinge	Packstone	Wahoo	EW	0.100	0.089	**0.600**	0
1	Hinge	Grainstone	Alapah	NS	0.446	0.304	**0.774**	0
3	Hinge	Grainstone	Alapah	NS	0.412	0.351	**0.667**	0
1	Hinge	Grainstone	Alapah	EW	0.759	0.357	**0.876**	0
3	Hinge	Grainstone	Alapah	EW	0.522	0.286	**0.918**	0
1	Hinge	Grainstone	Wahoo	NS	0.113	0.123	**0.442**	0
3	Hinge	Grainstone	Wahoo	NS	0.076	0.110	**0.375**	0
1	Hinge	Grainstone	Wahoo	EW	0.242	0.173	**0.804**	0
3	Hinge	Grainstone	Wahoo	EW	0.121	0.105	**0.669**	0
1	Limb	Packstone	Alapah	NS	0.308	0.295	**0.565**	0
3	Limb	Packstone	Alapah	NS	0.308	0.322	**0.442**	0
1	Limb	Packstone	Alapah	EW	0.307	0.179	**0.892**	0
3	Limb	Packstone	Alapah	EW	0.151	0.095	**0.813**	0
1	Limb	Packstone	Wahoo	NS	0.120	0.132	**0.413**	0
3	Limb	Packstone	Wahoo	NS	0.067	0.094	**0.341**	0
1	Limb	Packstone	Wahoo	EW	0.179	0.157	**0.682**	0
3	Limb	Packstone	Wahoo	EW	0.040	0.037	**0.537**	0
1	Limb	Grainstone	Alapah	NS	0.390	0.370	**0.587**	0
3	Limb	Grainstone	Alapah	NS	0.387	0.400	**0.450**	0
1	Limb	Grainstone	Alapah	EW	0.349	0.199	**0.881**	0
3	Limb	Grainstone	Alapah	EW	0.183	0.118	**0.813**	0
1	Limb	Grainstone	Wahoo	NS	0.148	0.162	**0.403**	0
3	Limb	Grainstone	Wahoo	NS	0.096	0.126	**0.332**	0
1	Limb	Grainstone	Wahoo	EW	0.181	0.157	**0.694**	0
3	Limb	Grainstone	Wahoo	EW	0.042	0.039	**0.533**	0

*) 1 indicates that fracture spacing in α1 (α = 100 deg.) is statistically greater than in α2 (α = 140 deg.), -1 indicates that fracture spacing in α1 is statistically smaller than in α2, and 0 indicates no difference between subsets.

VI.2.3. Effects of Structural Position

Table 6.4 shows the result of the paired t-test for all possible combinations of two values of structural position on fold with other geologic parameters in the model. 2 out of 32 possible cases show that average fracture spacing in limbs is significantly smaller than in hinges at the confidence level of 95%. Both two cases occurred for the EW fractures in the Alapah Formation. The other 30 cases show no significant difference between the average fracture spacing in limb and the average fracture spacing in hinge. The average p-value for the hypothesis that average fracture spacing in the limbs is larger than average fracture spacing in the hinges is 0.427, which is only slightly different from 0.5. This suggests that, in general, the structural position does not have a significant effect on the average fracture spacing.

Analyzing the effect of the structural position in combination with other parameters suggests that the structural position may have a systematic effect on the average spacing of the fractures in different orientations: the average p-value is 0.63 for the hypothesis that the average fracture spacing of the NS fractures in the limbs is larger than in hinges. The average p-value for the hypothesis that the average fracture spacing of the EW fractures in the limb is larger than in the hinge is 0.22. That is, the NS fractures in the hinges tend to be more closely spaced than in the limbs while the EW fractures in the limb tend to be more closely spaced than in the hinge. In combination with other parameters, the structural position has no preferential effect on the fracture spacing.

Table 6.4 – Result of t-test for the effect of structural position on fracture spacing.

Bed Thick. M	Int. Angle deg.	Lihthology	Form.	Orient.	Mean (L) m	Mean (H) m	p value	t test result*
1	100	Packstone	Alapah	NS	0.308	0.307	**0.504**	0
3	100	Packstone	Alapah	NS	0.308	0.282	**0.608**	0
1	100	Packstone	Alapah	EW	0.307	0.638	**0.112**	0
3	100	Packstone	Alapah	EW	0.151	0.423	**0.005**	**-1**
1	100	Packstone	Wahoo	NS	0.120	0.065	**0.712**	0
3	100	Packstone	Wahoo	NS	0.067	0.033	**0.629**	0
1	100	Packstone	Wahoo	EW	0.179	0.209	**0.371**	0
3	100	Packstone	Wahoo	EW	0.040	0.100	**0.274**	0
1	100	Grainstone	Alapah	NS	0.390	0.446	**0.388**	0
3	100	Grainstone	Alapah	NS	0.387	0.412	**0.398**	0
1	100	Grainstone	Alapah	EW	0.349	0.759	**0.082**	0
3	100	Grainstone	Alapah	EW	0.183	0.522	**0.000**	**-1**
1	100	Grainstone	Wahoo	NS	0.148	0.113	**0.656**	0
3	100	Grainstone	Wahoo	NS	0.096	0.076	**0.593**	0
1	100	Grainstone	Wahoo	EW	0.181	0.242	**0.304**	0
3	100	Grainstone	Wahoo	EW	0.042	0.121	**0.224**	0
1	140	Packstone	Alapah	NS	0.295	0.199	**0.815**	0
3	140	Packstone	Alapah	NS	0.322	0.242	**0.758**	0
1	140	Packstone	Alapah	EW	0.179	0.283	**0.225**	0
3	140	Packstone	Alapah	EW	0.095	0.223	**0.184**	0
1	140	Packstone	Wahoo	NS	0.132	0.083	**0.783**	0
3	140	Packstone	Wahoo	NS	0.094	0.071	**0.644**	0
1	140	Packstone	Wahoo	EW	0.157	0.156	**0.503**	0
3	140	Packstone	Wahoo	EW	0.037	0.089	**0.313**	0
1	140	Grainstone	Alapah	NS	0.370	0.304	**0.704**	0
3	140	Grainstone	Alapah	NS	0.400	0.351	**0.647**	0
1	140	Grainstone	Alapah	EW	0.199	0.357	**0.120**	0
3	140	Grainstone	Alapah	EW	0.118	0.286	**0.127**	0
1	140	Grainstone	Wahoo	NS	0.162	0.123	**0.707**	0
3	140	Grainstone	Wahoo	NS	0.126	0.110	**0.579**	0
1	140	Grainstone	Wahoo	EW	0.157	0.173	**0.412**	0
3	140	Grainstone	Wahoo	EW	0.039	0.105	**0.289**	0

*) 1 indicates that fracture spacing in L (Limb) is statistically greater than in H (Hinge), -1 indicates that fracture spacing in Limb is statistically smaller than in Hinge, and 0 indicates no difference between subsets.

VI.2.4. Effects of Lithology

Table 6.5 shows the result of the paired t-test for all possible combinations of two values of lithology with other geologic parameters in the model. All 32 possible combinations of parameters show no significant difference between fracture spacing in packstone and in grainstone at the confidence level of 90%. Analysis of the p-value, however, suggests that the fracture spacing in packstone is systematically smaller than in grainstone. The average p-value is 0.26 and the range is from 0.08 to 0.49. This effect of lithology is undetectable at the 90% confidence level. In fact, if the confidence level is lowered to 80%, then 5 out of 32 cases will have significant differences of average fracture spacing in packstone, compared to that in grainstone.

VI.2.5. Effects of Stratigraphic Position

The position of the fold in the stratigraphic column has a consistent effect on fracture distribution (Table 6.6). At the confidence level of 90%, 16 out of 32 possible cases show significant differences between average fracture spacing in the Wahoo and in the Alapah. The p-values of the hypothesis that the fracture spacing in Wahoo is larger than in Alapah range from 0.0 to 0.4 with the average of 0.085. If the stratigraphic position (Wahoo or Alapah Formation) represents the interaction between layers within the stratigraphic unit and how these layers are packed to form this single unit, then this factor plays an important role in the fracture spacing. In general, the Alapah Formation is interbedded and is more lithologically heterogeneous than the Wahoo Formation (Hanks et al., 1997; Whalen, 2000).

Table 6.5 – Result of t-test for the effect of lithology on fracture spacing.

Bed Thick. m	Int. Angle deg.	Structural Position	Form.	Orient.	Mean (P) m	Mean (G) m	p value	t test result*
1	100	Hinge	Alapah	NS	0.307	0.446	**0.162**	0
3	100	Hinge	Alapah	NS	0.282	0.412	**0.125**	0
1	100	Hinge	Alapah	EW	0.638	0.759	**0.160**	0
3	100	Hinge	Alapah	EW	0.423	0.522	**0.117**	0
1	100	Hinge	Wahoo	NS	0.065	0.113	**0.300**	0
3	100	Hinge	Wahoo	NS	0.033	0.076	**0.296**	0
1	100	Hinge	Wahoo	EW	0.209	0.242	**0.328**	0
3	100	Hinge	Wahoo	EW	0.100	0.121	**0.360**	0
1	100	Limb	Alapah	NS	0.308	0.390	**0.094**	0
3	100	Limb	Alapah	NS	0.308	0.387	**0.089**	0
1	100	Limb	Alapah	EW	0.307	0.349	**0.243**	0
3	100	Limb	Alapah	EW	0.151	0.183	**0.237**	0
1	100	Limb	Wahoo	NS	0.120	0.148	**0.269**	0
3	100	Limb	Wahoo	NS	0.067	0.096	**0.269**	0
1	100	Limb	Wahoo	EW	0.179	0.181	**0.479**	0
3	100	Limb	Wahoo	EW	0.040	0.042	**0.473**	0
1	140	Hinge	Alapah	NS	0.199	0.304	**0.186**	0
3	140	Hinge	Alapah	NS	0.242	0.351	**0.147**	0
1	140	Hinge	Alapah	EW	0.283	0.357	**0.228**	0
3	140	Hinge	Alapah	EW	0.223	0.286	**0.203**	0
1	140	Hinge	Wahoo	NS	0.083	0.123	**0.302**	0
3	140	Hinge	Wahoo	NS	0.071	0.110	**0.298**	0
1	140	Hinge	Wahoo	EW	0.156	0.173	**0.383**	0
3	140	Hinge	Wahoo	EW	0.089	0.105	**0.387**	0
1	140	Limb	Alapah	NS	0.295	0.370	**0.081**	0
3	140	Limb	Alapah	NS	0.322	0.400	**0.084**	0
1	140	Limb	Alapah	EW	0.179	0.199	**0.314**	0
3	140	Limb	Alapah	EW	0.095	0.118	**0.278**	0
1	140	Limb	Wahoo	NS	0.132	0.162	**0.268**	0
3	140	Limb	Wahoo	NS	0.094	0.126	**0.267**	0
1	140	Limb	Wahoo	EW	0.157	0.157	**0.493**	0
3	140	Limb	Wahoo	EW	0.037	0.039	**0.466**	0

*) 1 indicates that fracture spacing in P (Packstone) is statistically greater than in G (Grainstone), -1 indicates that fracture spacing in Packstone is statistically smaller than in Grainstone, and 0 indicates no difference between subsets.

Table 6.6 – Result of t-test for the effect of stratigraphic position on fracture spacing.

Bed Thick. m	Int. Angle deg.	Structural Position	Lihthology	Orient.	Mean (W) m	Mean (A) m	p value	t test result*
1	100	Hinge	Packstone	NS	0.065	0.307	**0.101**	0
3	100	Hinge	Packstone	NS	0.033	0.282	**0.014**	**-1**
1	100	Hinge	Packstone	EW	0.209	0.638	**0.065**	0
3	100	Hinge	Packstone	EW	0.100	0.423	**0.001**	**-1**
1	100	Hinge	Grainstone	NS	0.113	0.446	**0.068**	0
3	100	Hinge	Grainstone	NS	0.076	0.412	**0.002**	**-1**
1	100	Hinge	Grainstone	EW	0.242	0.759	**0.047**	**-1**
3	100	Hinge	Grainstone	EW	0.121	0.522	**0.000**	**-1**
1	100	Limb	Packstone	NS	0.120	0.308	**0.005**	**-1**
3	100	Limb	Packstone	NS	0.067	0.308	**0.001**	**-1**
1	100	Limb	Packstone	EW	0.179	0.307	**0.101**	0
3	100	Limb	Packstone	EW	0.040	0.151	**0.083**	0
1	100	Limb	Grainstone	NS	0.148	0.390	**0.001**	**-1**
3	100	Limb	Grainstone	NS	0.096	0.387	**0.000**	**-1**
1	100	Limb	Grainstone	EW	0.181	0.349	**0.067**	0
3	100	Limb	Grainstone	EW	0.042	0.183	**0.065**	0
1	140	Hinge	Packstone	NS	0.083	0.199	**0.104**	0
3	140	Hinge	Packstone	NS	0.071	0.242	**0.050**	**-1**
1	140	Hinge	Packstone	EW	0.156	0.283	**0.188**	0
3	140	Hinge	Packstone	EW	0.089	0.223	**0.165**	0
1	140	Hinge	Grainstone	NS	0.123	0.304	**0.048**	**-1**
3	140	Hinge	Grainstone	NS	0.110	0.351	**0.025**	**-1**
1	140	Hinge	Grainstone	EW	0.173	0.357	**0.092**	0
3	140	Hinge	Grainstone	EW	0.105	0.286	**0.120**	0
1	140	Limb	Packstone	NS	0.132	0.295	**0.046**	**-1**
3	140	Limb	Packstone	NS	0.094	0.322	**0.011**	**-1**
1	140	Limb	Packstone	EW	0.157	0.179	**0.405**	0
3	140	Limb	Packstone	EW	0.037	0.095	**0.295**	0
1	140	Limb	Grainstone	NS	0.162	0.370	**0.017**	**-1**
3	140	Limb	Grainstone	NS	0.126	0.400	**0.004**	**-1**
1	140	Limb	Grainstone	EW	0.157	0.199	**0.294**	0
3	140	Limb	Grainstone	EW	0.039	0.118	**0.249**	0

*) 1 indicates that fracture spacing in W (Wahoo) is statistically greater than in A (Alapah), -1 indicates that fracture spacing in Wahoo is statistically smaller than in Alapah, and 0 indicates no difference between subsets.

VI.2.6. Effects of Orientation

Table 6.7 shows the result of the test for fracture spacing with respect to fracture orientation. There are 28 instances where there is no significant difference in fracture spacing between fracture sets at a confidence level of 90% and 4 instances where fracture spacing in the EW orientation is smaller than in the NS orientation at the confidence level of 95%. All these 4 cases occur in the limbs of the fold and in the Alapah Formation.

The average p-value for the hypothesis that the average fracture spacing in EW orientation is larger than in NS orientation is 0.53, which suggests that, in general, the orientation does not affect the average fracture spacing. However, the wide range of the p-values (from 0.002 to 0.95) with the standard deviation of 0.33 suggests that the effects of the orientation are highly variable and depend on other parameters.

The combination of the fracture orientation and other parameters suggests that the differences between fracture spacing in the EW and NS orientations is systematically different in the limb and in the hinge. In the limb, the average p-value for the hypothesis that the average fracture spacing in EW orientation is larger than in NS direction is 0.76. In the hinge, the average p-value for the hypothesis that the average fracture spacing in EW direction is larger than in NS direction is 0.30. That is, in the limb, the average fracture spacing of EW fractures is larger than the average spacing of NS fractures whereas, in the hinge, the average fracture spacing of EW fractures is smaller than the average spacing of NS fractures.

Table 6.7 – Result of t-test for the fracture spacing in different orientation.

Bed Thick. m	Int. Angle deg.	Structural Position	Lihthology	Form.	Mean (EW) m	Mean (NS) m	p value	t test result*
1	100	Hinge	Packstone	Alapah	0.638	0.307	**0.914**	0
3	100	Hinge	Packstone	Alapah	0.423	0.282	**0.912**	0
1	100	Hinge	Packstone	Wahoo	0.209	0.065	**0.902**	0
3	100	Hinge	Packstone	Wahoo	0.100	0.033	**0.797**	0
1	100	Hinge	Grainstone	Alapah	0.759	0.446	**0.910**	0
3	100	Hinge	Grainstone	Alapah	0.522	0.412	**0.876**	0
1	100	Hinge	Grainstone	Wahoo	0.242	0.113	**0.923**	0
3	100	Hinge	Grainstone	Wahoo	0.121	0.076	**0.810**	0
1	100	Limb	Packstone	Alapah	0.307	0.308	**0.492**	0
3	100	Limb	Packstone	Alapah	0.151	0.308	**0.012**	**-1**
1	100	Limb	Packstone	Wahoo	0.179	0.120	**0.803**	0
3	100	Limb	Packstone	Wahoo	0.040	0.067	**0.377**	0
1	100	Limb	Grainstone	Alapah	0.349	0.390	**0.304**	0
3	100	Limb	Grainstone	Alapah	0.183	0.387	**0.002**	**-1**
1	100	Limb	Grainstone	Wahoo	0.181	0.148	**0.697**	0
3	100	Limb	Grainstone	Wahoo	0.042	0.096	**0.260**	0
1	140	Hinge	Packstone	Alapah	0.283	0.199	**0.724**	0
3	140	Hinge	Packstone	Alapah	0.223	0.242	**0.442**	0
1	140	Hinge	Packstone	Wahoo	0.156	0.083	**0.945**	0
3	140	Hinge	Packstone	Wahoo	0.089	0.071	**0.723**	0
1	140	Hinge	Grainstone	Alapah	0.357	0.304	**0.648**	0
3	140	Hinge	Grainstone	Alapah	0.286	0.351	**0.341**	0
1	140	Hinge	Grainstone	Wahoo	0.173	0.123	**0.781**	0
3	140	Hinge	Grainstone	Wahoo	0.105	0.110	**0.473**	0
1	140	Limb	Packstone	Alapah	0.179	0.295	**0.104**	0
3	140	Limb	Packstone	Alapah	0.095	0.322	**0.010**	**-1**
1	140	Limb	Packstone	Wahoo	0.157	0.132	**0.661**	0
3	140	Limb	Packstone	Wahoo	0.037	0.094	**0.279**	0
1	140	Limb	Grainstone	Alapah	0.199	0.370	**0.054**	0
3	140	Limb	Grainstone	Alapah	0.118	0.400	**0.007**	**-1**
1	140	Limb	Grainstone	Wahoo	0.157	0.162	**0.473**	0
3	140	Limb	Grainstone	Wahoo	0.039	0.126	**0.213**	0

*) 1 indicates that fracture spacing in EW orientation is statistically greater than in NS orientation, -1 indicates that fracture spacing in EW orientation is statistically smaller than in NS orientation , and 0 indicates no difference between subsets.

VI.2.7. Summary

Table 6.8 summarizes the results of the effects of the geologic parameters on the average fracture spacing using a neural network. Assuming that bed thickness, degree of folding, structural position on the fold, lithology, formation, and fracture orientation are the major factors in fracturing, the effects of each parameter have been assessed using a neural network and applying statistical tests on the network predictions.

Table 6.8 – Summary of statistical test on fracture spacing, estimated by neural network.

Variable	Hypothesis	No of accepted out of 32
Bed	Fracture spacing in thin bed is greater than in thick bed	5
	Fracture spacing in thin bed is smaller than in thick bed	0
	No difference, at α=90%	27
Interlimb angle	Fracture spacing in tight fold is greater than in open fold	0
	Fracture spacing in tight fold is smaller than in open fold	0
	No difference, at α=90%	32
SP	Fracture spacing in limb is greater than in hinge	0
	Fracture spacing in limb is smaller than in hinge	2
	No difference, at α=90%	30
Lithology	Fracture spacing for packstone is greater than in grainstone	0
	Fracture spacing for packstone is smaller than in grainstone	0
	No difference, at α=90%	32
Formation	Fracture spacing in Wahoo is greater than in Alapah	0
	Fracture spacing in Wahoo is smaller than in Alapah	16
	No difference, at α=90%	16
Orientation	Fracture spacing of EW fractures is greater than of NS fractures	0
	Fracture spacing of EW fractures is smaller than of NS fractures	4
	No difference, at α=90%	28

The investigation shows that fracture spacing is related to the combined effect of several geologic characteristics. The neural network can model the combined effect of these geologic characteristics and can assess the effects of particular geologic parameter on fracture spacing. Given the scarcity of the fracture data, the conventional statistical analysis has to lump the data and, therefore, can not assess the effects of particular geologic parameter on fracture spacing (Chapter IV). The result of network analysis may provide a basis with which to rank the geologic parameters according to their effects on fracture spacing.

From the number of cases that have significant difference in Tables 6.2-6.7, the most important parameter that affects the fracture spacing is the formation, followed by bed thickness, fracture orientation, and structural position on fold. The numbers of cases with significant difference between average fracture spacing are 16, 5, 4, and 2 respectively for these parameters.

Both the degree of folding and the lithology (packstone and grainstone) statistically are not significant in affecting the fracture spacing with no cases of significant difference. This way of ranking the parameters, however, depends on the confidence level used in the tests.

Another way of ranking the parameter is based on the average p-value: in applying the paired t-test, the p-value of 0.5 indicates no difference between two sets. A p-value greater than 0.5 indicates that the first set is greater than the second set, while a p-value less than 0.5 indicates that the first set is smaller than the second. The average p-value for all possible data pairs of each parameter, therefore, represents the effect of that parameter on the fracture spacing (Table 6.9).

Table 6.9 – Result of the parameters ranking.

	Paired t-test		p-value				
	# of different case at a=95%	Rank	average $p-p_0$	max	min	Stdev	Rank
Bed thickness	5	2	0.71	0.997	0.303	0.201	3
Interlimb angle	0	5	0.63	0.918	0.332	0.195	4
Structural Position	-2	4	0.43	0.815	0.000	0.247	5
Lithology	0	5	0.26	0.493	0.081	0.120	2
Formation	-16	1	0.09	0.405	0.000	0.101	1
Orientation	-4	3	0.53	0.945	0.002	0.326	6

According to this method of assessment, the most significant parameter is the formation (with p_{avrg}=0.09), followed by lithology, bed thickness, degree of folding, structural position, and fracture orientation (with p_{avrg} equals 0.26, 0.71, 0.63, 0.43, and 0.53, respectively). This way of ranking does not depend on the confidence level used in the tests. In fact, the two methods of ranking parameters yields the same result if the confidence level of 50% is used in the method based on the results of paired t-test.

Compared to the ranking based on the t-test at 95% confidence level, formation does not change its ranking. This supports the conclusion that stratigraphic position has a consistent effect on the fracture spacing. From the 5th place in the t-test method, the lithology changes its ranking to the 2nd place in the p-value method. The range of the p-value suggests that lithology has a consistent effect on fracture spacing: in all combinations of parameters, the fracture spacing in packstone is smaller in grainstone with the p-value ranges from 0.081 to 0.493. However, this effect is not statistically detectable at the one-tail confidence level of 95%.

Another parameter with the big change of its ranking is the fracture orientation. According to the results of the paired t-test, the fracture orientation ranks 3rd in relating with the fracture spacing. Analysis of the average p-value suggests that the fracture orientation is the least influential parameter ($p_{EW>NS}$ =0.53). This is in accordance with the conventional statistical analysis in Chapter IV. However, the large range of the p-value (from 0.002 to 0.945 with the standard deviation of 0.326) suggests that the effect of fracture orientation is not systematic: the difference of the fracture spacing in EW and NS orientations depends on the combination of other parameters, especially the structural position. In the hinges, EW fracture spacing is larger than NS fractures ($p_{EW\ in\ hinge\ >\ NS\ in\ hinge}$ = 0.758) while in the limb, EW fracture spacing is smaller than NS fractures ($p_{EW\ in\ limb\ <\ NS\ in\ limb}$ = 0.704). For fractures in each orientation, EW fractures in the limbs are more densely spaced than EW fractures in the hinges ($p_{EW\ in\ hinge\ >\ EW\ in\ limb}$ = 0.779), and NS fractures in the hinges are more densely spaced than the NS in the limbs ($p_{NS\ in\ limb\ >\ NS\ in\ hinge}$ = 0.632). This analysis indicates that the structural position relates to the fracture spacing selectively with regard to the fracture orientation.

VI.3. Comparison with Conventional Statistical Analysis

Table 6.10 summarizes the results for the parameter ranking of the statistical t-test analysis and the neural network analysis of fracture spacing. In grouping fracture data into subsets, I extend the t-test analysis in Chapter IV to cover the effect of lithology and stratigraphic position. In using conventional statistical analysis, the degree of folding has the greatest effect on fracture spacing whereas, in neural network analysis, folding appears to have a smaller effect on fracture spacing. In neural network analysis, bed thickness appears to be the third important factor after stratigraphic position and lithology in controlling the fracture density, whereas it ranks fourth after the degree of folding, the stratigraphic position, and the structural position in applying conventional statistical analysis. In both methods, the fracture orientation is the least important factor in controlling the fracture spacing.

The difference in the rank of geologic parameters between two methods can be explained by the fact that, we lump the fracture data into subsets in using conventional statistical analysis (Chapter IV). Because these subsets represent the combination of different parameters, any conclusion about the effects of a single parameter on controlling the fracture spacing could be biased. Neural networks, on the other hand, can trace the effects of a single parameter on the fracture spacing with other parameters fixed.

Table 6.10 – Summary of the statistical and neural network analysis for fracture spacing.

	Parameter rank	
	t-test	Neural network
Bed thickness	4	3
Interlimb angle	1	4
Structural position	3	5
Lithology	5	2
Stratigraphic position	2	1
Orientation	6	6

The analysis in this chapter demonstrates the following advantages of the neural network:

- it produces a detailed functional relationship between average fracture spacing and geologic parameters without lumping the effect of other parameters; and
- it provides the capability to analyze the effects of the single parameter on fracture spacing with the statistical confidence.

As a result, the neural network analysis provides more insight into the relationship between average fracture spacing and geologic parameters with statistical

confidence. For all combinations of geologic parameters considered in the model, there are several conclusions.

- The general effect of bed thickness on fracture spacing is opposite to the relationship often reported in the literature. Neural network analysis shows that fracture spacing is either larger in thin beds than in thick beds (15.6% at the confidence level of 95%) or it does not significantly differ (84.4% at the confidence level of 90%).
- The degree of folding does not have a significant effect on fracture spacing (100% at the confidence level of 90%).
- The effect of the lithology on fracture spacing is systematic but undetectable at the confidence level of 95%. In general, the average fracture spacing in packstone is smaller than in grainstone (12.5% at the confidence level of 90%, 31.3% at the confidence level of 80%).
- Position in the stratigraphic column has the most consistent effect on fracture distribution. The fracture spacing in the Wahoo Formation is consistently smaller than in the Alapah Formation (50% smaller, 0% larger at the confidence level of 95%; 69% smaller, 0% larger at the confidence level of 80%).
- The effect on fracture spacing of structural position on the fold is closely related to the fracture orientation. Fracture spacing can be larger in the limb than in the hinge or vice versa, depending on the fracture orientation. In the limbs, fracture spacing of the EW fracture set is smaller than the NS fracture set whereas, in the hinges, NS fractures are more densely spaced than EW fractures. Note that the fold axis is in EW orientation.

VI.4. Discussion on the Sampling Requirement

One important question in designing a study is to determine the amount of data required for the analysis. As discussed in Chapter II, the degree of determination of the

system D_1 is often used to judge the effectiveness of the system in modeling the data. As a rule of thumb, D_1 of at least 2 is suggested in using neural networks (Bishop, 1995). However, the optimal network configuration is data driven and cannot be determined *a-priori*. Thus, this measurement could not be used to determine the required amount of data for the analysis.

Another quantity to measure the degree of determination of the system is the ratio of the data to the number of explanatory variables of the model D_2 (Eq. 5.8). This quantity does not depend on the network configuration but depends on the number of exploratory variables of the model. Thus, it is important to identify the possible important variables of the model before collecting data for analysis. For the fracture system in this study, the degree of determination D_1 is 1 and D_2 is 4.2. With these values of determination, the network produces significant prediction variability (Figures 6.4, 6.5). Using multiple realizations of the cross validation technique, one still can assess the prediction variability and investigate the relationship among variables at the price of wide confidence interval of the network prediction.

It is worth noting that 4 out of 6 variables in our model are discrete variables with only 3 possible values. For the model with continuous explanatory variables, a larger degree of determination D_2 is required to represent the whole range of each. The question of how big D_2 should be in designing the data collection process depends on several factors such as the nature of the possible relationship between explanatory and response variables, the range of change for each explanatory variable, and the tolerance to the prediction variability of the model. Unfortunately, these factors are highly problem dependent and could not easily determined. In any case, careful analysis of the possible theoretical or experimental relationship between each explanatory and response variable is essential in determining the required amount of data for analysis.

CHAPTER VII

FRACTURE NETWORK CONDUCTIVITY ASSESSMENT

This chapter presents the result of the analysis of flow conductivity of a fracture system consisting of two orthogonal fracture sets, similar to those observed in the Lisburne Group. I used FracMan to model the fracture system and to calculate the flow conductance of the fracture system along the principal orientation of each fracture set. The effects of fracture properties such as fracture size, fracture spacing, and transmissivity on system isotropy were investigated.

The results of this investigation suggest that, given two fracture sets with similar spacing characteristics, significant anisotropy can be observed because of the difference in fracture length. The set with the greater length plays an important role not only for flow along its principle direction but also in the orthogonal direction.

VII.1. Overview

The fracture data used in this study were collected from several locations with different combinations of geological parameters. At each location, two major fracture sets, EW and NS striking, were identified and their properties were characterized. All possible combinations of geological parameters resulted in a large number of cases, which is difficult to handle. FracMan, on other hand, is limited to a maximum number of fractures in the model and with the given fracture density. In this study, it can only model the fracture network at a small scale. The first task in studying the flow characteristics of the fracture system in this study was to choose the data for fracture properties used in DFN model so that the results of the small scale study could be used to infer the properties of the entire region.

The results of the analysis in Chapters IV and VI suggest that the fracture spacing and fracture length are affected by several geological factors. Fracture length, for example, is greater in tight folds than in open folds and the fractures are more through going in the NS than in the EW directions. Field observation shows that a number of EW fractures terminate at NS fractures. Field observation also suggests that half of the fractures in both sets terminate at bedding planes. Combining the results of the statistical analysis with the field observations, I identified the following important parameters for their effects on the flow characteristics of the fracture system in this study.

- Fracture length: to investigate the isotropy causing by the two fracture sets with different size and the effect of folding on the system conductivity.
- Fracture filling (cementation): the effect of fracture filling can be regarded as changing the fracture transmissivity (if the fractures are partially filled) or as reducing the fracture density (if the fractures are completely filled).
- Fracture termination: the fracture termination reduces the probability of cutting through more than one fractures and, hence, affects the flow conductance.

Specifically, I modeled the fracture system as consisting of two fracture sets: EW and NS striking. As a base case, the fracture spacing and fracture height for each set were taken from the combined dataset of the whole region and the fracture length were taken from the data for tight folds. I investigated the effect of having smaller fracture length on the system conductivity by using the data for open folds in the sensitivity study. Fracture aperture, being an important parameter of the fractures, will not be directly included into this study because of the related uncertainties discussed in Chapter II. Instead, I will indirectly investigate the effect of aperture on the fracture system conductivity by running cases where different fracture transmissivities are assigned to each fracture set. The effect of the fraction of fractures that are completely filled in each fracture set is taken to be the same as reducing the fracture density. I used fracture

height from the lumped dataset. The variation of the fracture height was not studied since we are mainly interested in flow conductance in the horizontal direction.

Since the data are lumped from different locations of the field, I did not discuss the selection of the statistical distribution to represent these data. Instead, I studied the effect of different distributions on the system flow conductance.

VII.2. Fracture Properties in DFN

A summary of the statistical parameters for fracture spacing, fracture height and length is given in Table 7.1. The histograms of the fracture height and length for these two sets are shown in Figure 7.1. The histograms show that fracture properties of the lumped dataset are skewed to the left. A portion of fractures grouped on the right side of the histogram, e.g. for fracture height, may represent the fact that fracture data are lumped from different locations with different bed thickness.

Table 7.1 – Summary of fracture spacing, height, and length for use in FracMan.

	Spacing, m		Height, m		Length, m			
					Tight folds		Open folds	
Fracture set	EW	NS	EW	NS	EW	NS	EW	NS
Average	0.26	0.28	0.92	1.16	0.83	1.63	0.45	0.51
Standard deviation	0.45	0.37	0.87	1.25	0.73	2.13	0.42	0.47

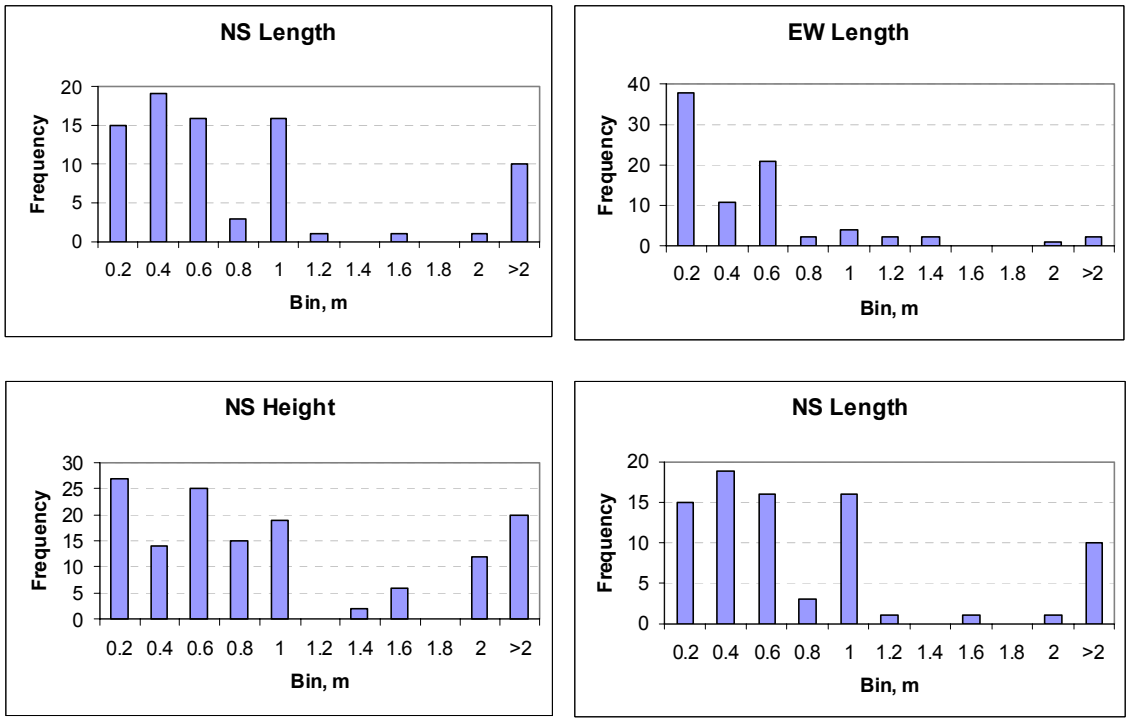

Figure 7.1 – Histograms of fracture height and fracture length for the combined dataset.

The L-moment plots (Hosking and Wallis, 1997) for spacing, height and length of these datasets are shown in Figure 7.2. On this figure, the plotting positions for our data are scattered around the line for the lognormal distribution. The plotting position for the NS fracture height and the NS fracture length in open folds is closed to the position for the exponential distribution. Karpov (2001) argued that different distributions can represent the fracture data. Lognormal and exponential distributions are often chosen to represent the fracture properties (Table 2.1, Chapter II). I chose the lognormal distribution to represent our fracture properties in FracMan. To investigate how different distributions may affect the modeled conductivity, I compare the results obtained from the exponential and lognormal distributions for fracture length of one of our cases.

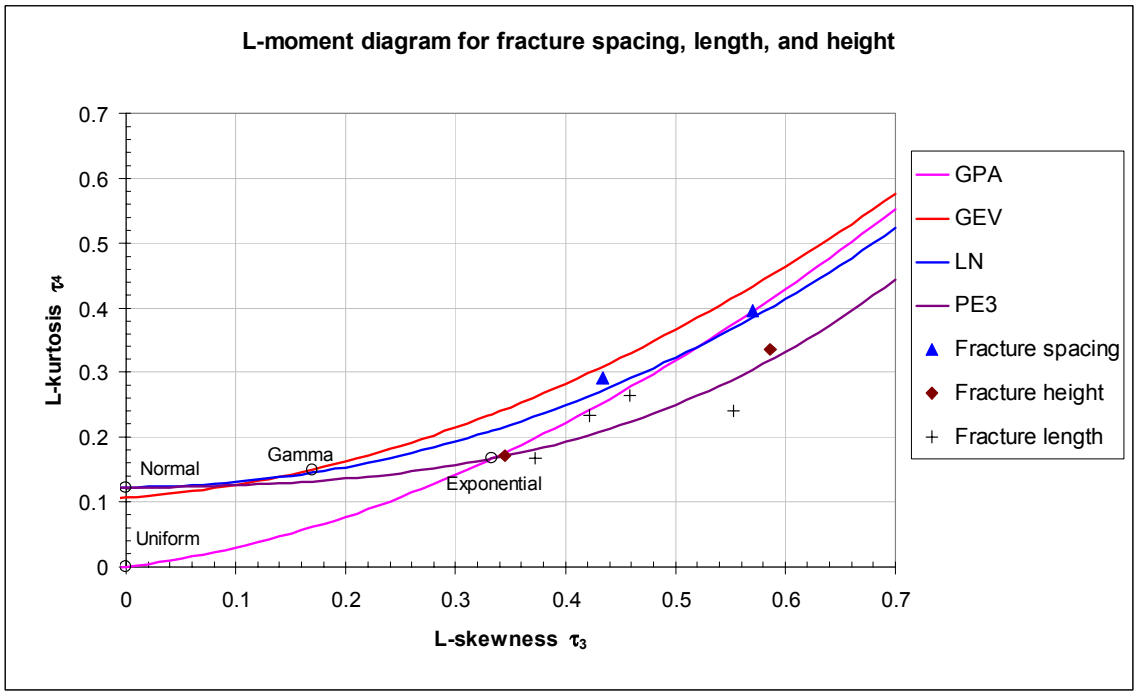

Figure 7.2 – L-moment plot for fracture spacing, height, and length used in FracMan.

With regard to the fracture orientation, the frequencies of fracture strike for both orientations are scattered around the mean values with large standard deviations (Figure 7.3). It is worth noting that, in using DFN, I model the fracture system in a small volume of rock (in the order of 10 m) which represents one sample location. The fracture orientation for both sets in the simulation is chosen as a bivariate distribution with the mean calculated from lumped data, and the standard deviation is the average value from all sampled locations. The fracture orientation data are given in Table 7.2.

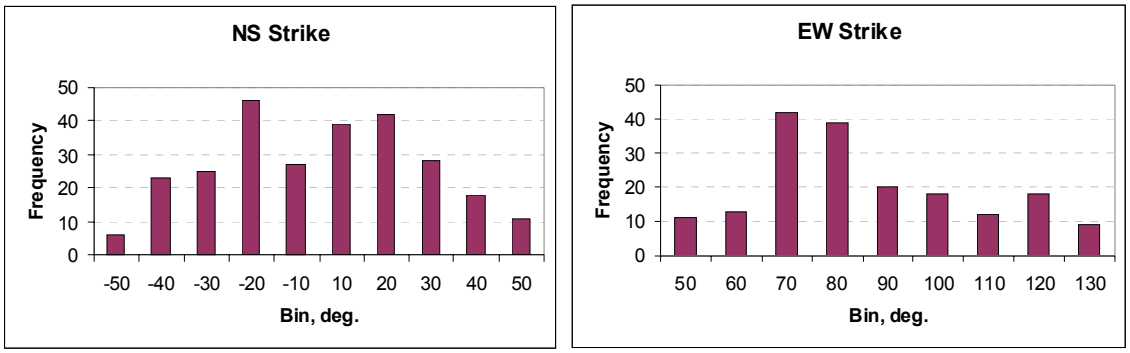

Figure 7.3 – Histogram of fracture strike for EW and NS sets.

Table 7.2 – Fracture orientation data for use in FracMan.

	Strike		Dip	
	Mean, deg.	Standard deviation, deg.	Mean, deg.	Standard deviation, deg.
EW fracture set	85	8.2	68.0	6.6
NS fracture set	0	7.7	72.4	6.4

VII.3. DFN Analysis

The conductivity of the fracture system in FracMan is calculated using the Pathway Analysis module. This module examines the occurrence of hydraulically continuous pathways between different locations within the simulated fracture network. It searches through all fractures to identify possible pathways and their properties.

Pathway Analysis requires the definition of the initiation and destination points for pathways, and the minimum property of the fractures in a network before they can be considered a pathway. In FracMan, the minimum cutoff is defined in terms of the pathway conductance C_p:

$C_p = \min \{T_{fi} W_{fi}\}$, $i=1,n_f$;

where T_f and W_f are the transmissivity and width perpendicular to flow of the i^{th} fracture and n_f is the number of fractures in the network.

The Pathway Analysis output parameters include:

1. Number of pathways;
2. Number of fractures in the pathway;
3. The conductance of the pathway, m^3/s;
4. Area of fractures in the pathway, m^2.

Two fracture sets representing NS and EW fractures are generated using FracMan within the rock region having dimension of 10x10x6m (Figure 7.4, left). The dimension of the rock region is chosen based on the limited number of fracture that this version of FracMan can handle. Given the fracture intensity in this study, adding 2 m to each side of this rock region would cause the program to be unstable. The horizontal measurement of the simulated rock region is about 6 times the average fracture length in NS direction and 12 times the average fracture length in EW direction (Table 7.1).

The input parameters of the model are as follows:

1. Poisson Rectangle geometric model. The choice of the fracture shape in the simulation is arbitrary. Without any specific data about the fracture shape and for simplicity, I assumed parallelogram shaped fractures. The fracture location is generated according to the Poisson process and the resulting fracture spacing will follow the exponential distribution.
2. "Surface Points" Generation Mode. With this mode, fracture location is not restricted to the condition that it should not cross the face of the simulated region. This mode was selected to eliminate the edge effect.
3. Strike and dip model (bivariate normal) with specified means and standard deviations.

4. Fracture height. Lognormal distribution with specified mean and standard deviation.

5. Fracture length. Lognormal distribution with specified mean and standard deviation. In the sensitivity study, an exponential model will be used to evaluate the effect of using a different distribution on the results.

6. Fracture termination. Termination percentage, a probability that a fracture will terminate at an intersection with a pre-existing fractures. Zero termination in base case. In a sensitivity study, 50% of EW fractures will terminate against NS fractures.

7. Fracture intensity. Area of fractures per unit volume (P_{32}) is chosen. Other options were "number of fractures (P_{31})" and "fracture volume per volume (P_{33})". P_{31} is scale-dependent. P_{33} depends on the fracture aperture and therefore cannot be assessed adequately in this study. P_{32} is aperture independent and can be used, once assigned, for a variety of sizes and shapes of the generation region. The value of P_{32} for each set is determined using an iterative procedure. During fracture generation, the fracture density for each set is sampled along 10 scan lines perpendicular to the mean orientation of this set. The fracture intensity is iteratively adjusted until the average spacing along those scan lines matches the value in the field.

8. Constant fracture aperture and transmissivity. In a sensitivity study, I will vary transmissivity for each fracture set.

Table 7.3 list the cases used in the study to assess the effects of fracture termination, length, and filling on the system conductivity.

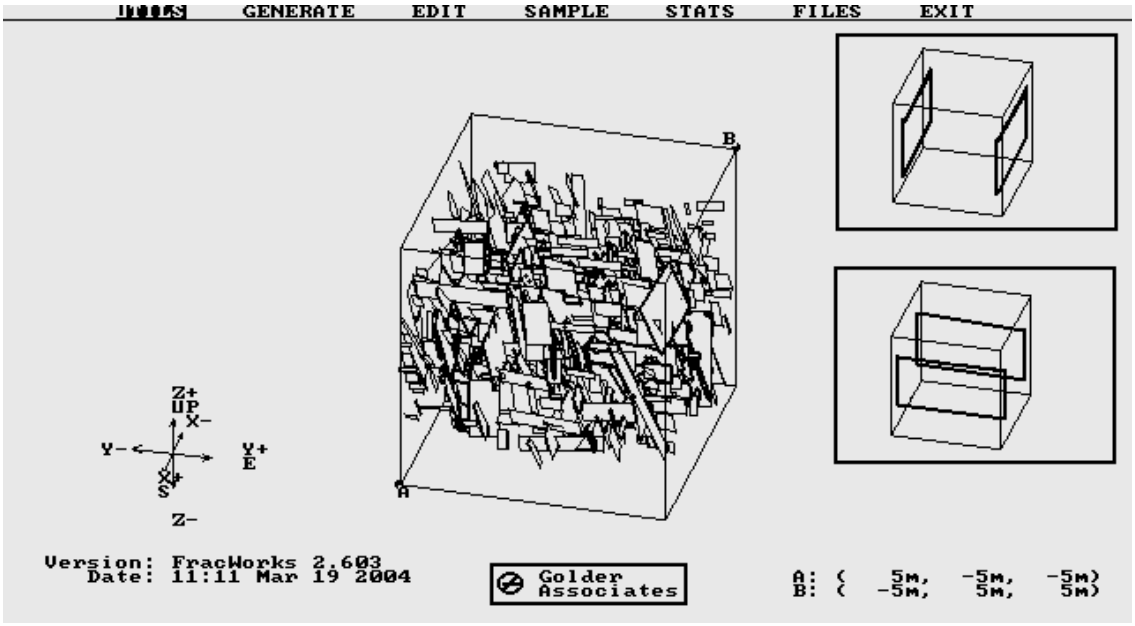

Figure 7.4 – Example of the fracture system in FracMan and the sampling planes.

For all cases, the fracture conductance was evaluated for two directions (north/south and east/ west) between two vertical planes placed perpendicular to the mean strike of each fracture set and 8 m apart from each other (Figure 7.4, right). For each set of parameters, I ran 10 different realizations of the fracture network. I chose planes instead of wellbores for assessing the flow conductance, because for this scale of simulation (10 m), the planes may better represent the picture about the direction of flow than the wellbores. A similar approach was used for studying the anisotropy of the fracture system (e.g., Cacas et al., 1990, Herbert and Lanyon, 1992).

Table 7.3 – DFN simulation cases.

	Cases	Description
Length in tight folds	Base case	Fracture length from tight fold, fracture spacing and height from lumped data, equal transmissivity in both sets.
	Transmissivity variation, cases T1, T2, T3, T4, T5	Varying fracture transmissivity in EW and NS sets
	Spacing variation, cases S1 to S7.	Varying fracture spacing in EW and NS sets
	EW termination, case E1	50% of EW fractures terminate at intersection with NS fractures
	Different statistical distribution, case D1	Use exponential distribution for fracture length
Length in open folds	Case L0	Fracture length from open folds
	Spacing variation, case L1	Varying fracture transmissivity in EW and NS sets
	EW termination, case L2	50% of EW fractures terminate at intersection with NS fractures

VII.3.1. Anisotropy

This case represents the case of strong degree of anisotropy with regard to two EW and NS orientations. The fracture length is taken from the data for tight folds. The average fracture length of the NS set is double the average length of the EW set. Fracture spacing and fracture height are taken from lumped datasets and are very similar for both sets (Table 7.1). Fracture transmissivity is constant and equal 0.001 m^2/s for all fractures.

The conductance between source and sink trace planes was evaluated 10 times with different realizations of fracture sets in the model. The comparison of the fracture network conductance for the two directions is shown in Figure 7.5. With the given configuration and parameters, the average conductance in the NS direction is almost 4 times larger than in the EW direction.

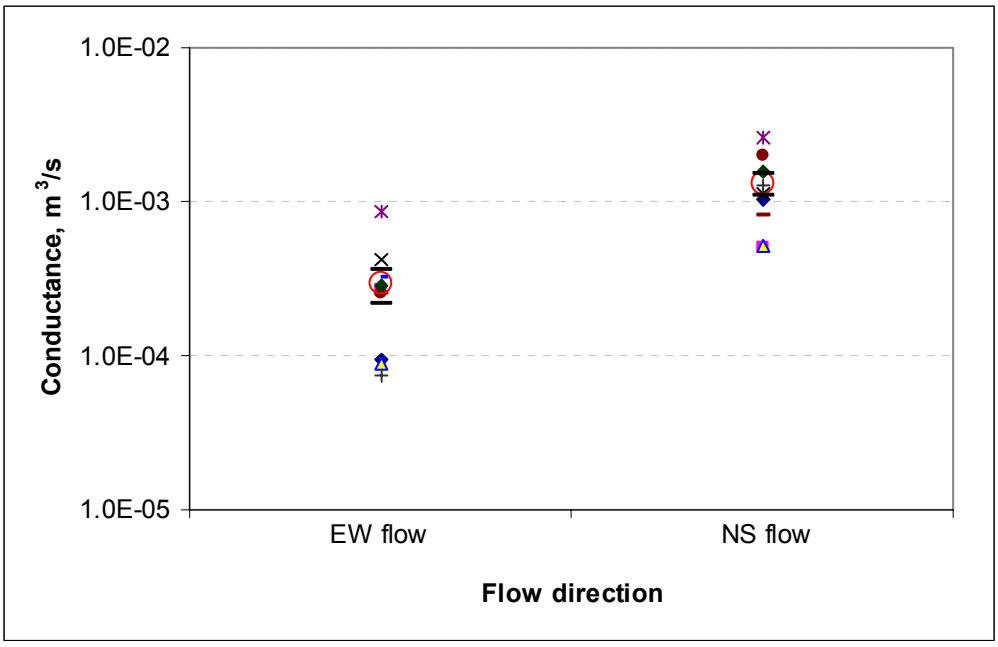

Figure 7.5 – Flow conductance in EW and NS directions. Given the same fracture spacing, fracture length causes the conductance anisotropy.

VII.3.2. Effects of Fracture Transmissivity

In this section, I change the transmissivity for each fracture set to investigate the effect on system conductance and anisotropy. Five cases were run.

- Case T1 and T2: the transmissivity of the EW fractures was increased by, correspondingly, 10 and 100 from the "base" case. NS fracture transmissivity was kept at the "base" case level and, therefore, 1 and 2 orders of magnitude lower than the EW set transmissivity.
- Cases T3 and T4: NS fracture transmissivity was increased by 10 and 100 time from the "base" case value for NS set.
- Case T5: the transmissivity correlates with the fracture area according to the following equation: $\log(T_i) = 1.0e^{-4}\log(S_i)$, where T_i is the transmissivity of fracture i, S_i is the area of fracture i.

Figure 7.6 shows the conductance in EW and NS directions for the cases T1 and T2 along with the base case conductance. The plot shows that the average conductance and its standard error are almost linearly proportional to the transmissivity in the case of constant transmissivity of each fracture set. Increasing the transmissivity in the EW direction slightly affects the average flow conductance in the NS direction. In particular, a 2 order transmissivity increase in the EW direction increases the average conductance in the NS direction by 2.5 times.

Similar behavior is observed for cases T3 and T4 (Figure 7.7). The conductance in the NS direction and its standard error linearly increase with the transmissivity of the NS set. However, a transmissivity increase in the NS direction does not affect the EW conductance.

When the transmissivity is entered as a function of the fracture area, the average conductance in the NS direction is almost 16 times greater than the average conductance in the EW direction.

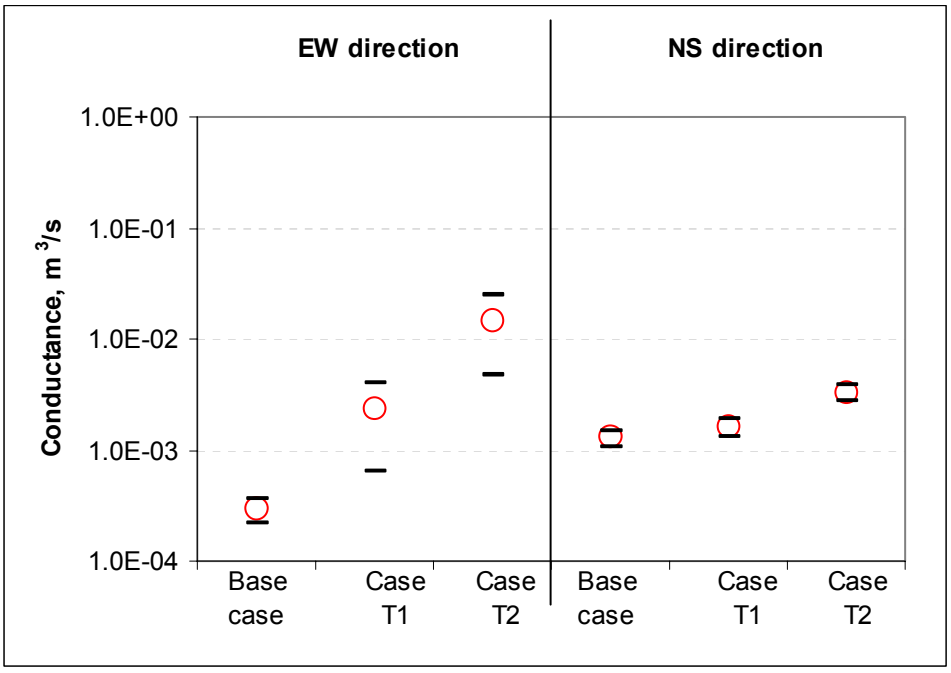

Figure 7.6 – Effect of increasing transmissivity in EW set on the flow conductance.

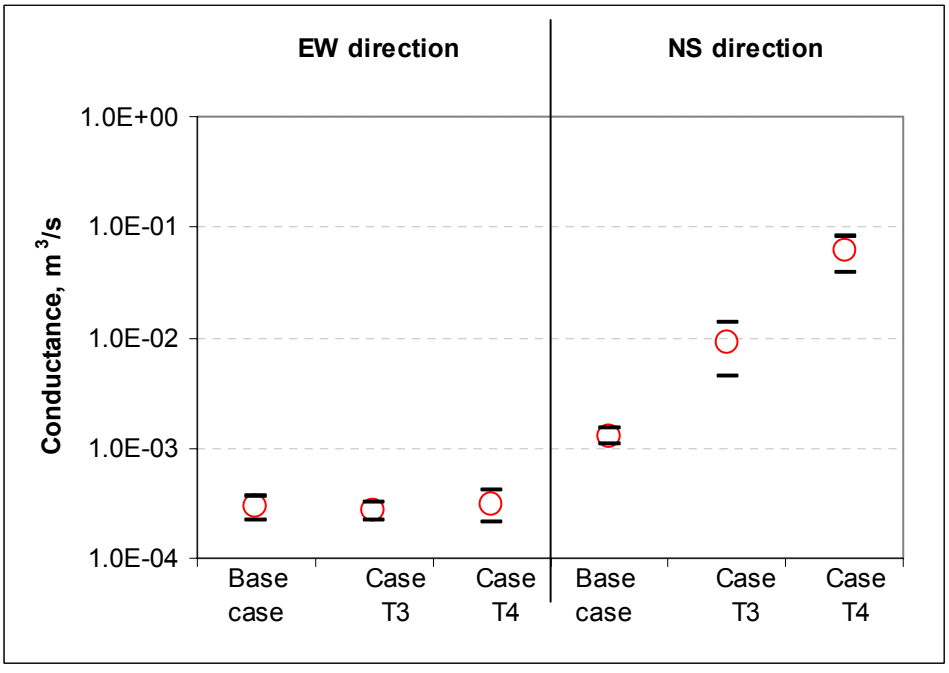

Figure 7.7 – Effect of increasing transmissivity in NS set on the flow conductance.

VII.3.3. Fracture Spacing

In reality, not all fractures conduct fluid due to the cementation and the stress field. Therefore, the model based on all observed fractures may overestimate the fracture density that participates in conducting fluid. I investigated the effect of filling on the fracture conductivity by reducing the fracture intensity when generating fracture sets. This means that a fraction of fractures is completely filled with the cementation. The effect of the partial fill of fractures is studied by changing the fracture transmissivity.

Figure 7.8 shows the flow conductance in the EW and NS directions when the fracture density of the EW set decreases by 50%, 75%, and 85% (cases S1, S2, and S3). The results suggest that the filling of EW fractures has a small effect on NS conductance. At 50% and 75% reduction of the fracture density in EW direction, the average conductance in EW direction decreases 50% and 80%, whereas the NS conductance does not change significantly (2% and 9%). At the reduction of 85% of fracture density in EW direction, 6 out of 10 realizations show zero conductance in EW direction. At this value of EW fracture density, the average NS conductance decreases 17%.

The general observation for these cases is that changing the fracture density of the set with smaller length does not affect the flow conductance in the orthogonal direction.

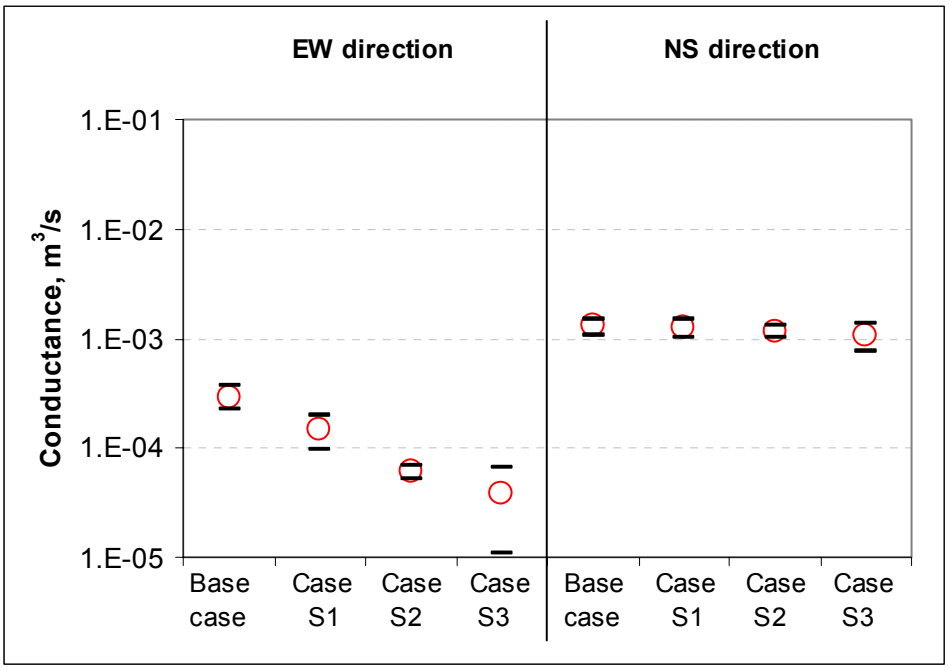

Figure 7.8 – Effect of decreasing fracture density of EW set on the flow conductance.

The NS fractures, in contrast to the EW fractures, have a strong effect on the conductance in the EW direction. Figure 7.9 shows the flow conductance in the EW and NS directions when the fracture density of NS set decreases by 50%, 75%, and 85% (cases S4, S5, and S6). At 50% and 75% reductions of the NS fracture density, the average conductance in NS direction decreases 38% and 79%, respectively, while the average EW conductance decreases 49% and 66%. At a reduction of 85% of the NS fracture density, 1 out of 10 realizations show zero conductance in each direction. That is, the system is at the percolation threshold.

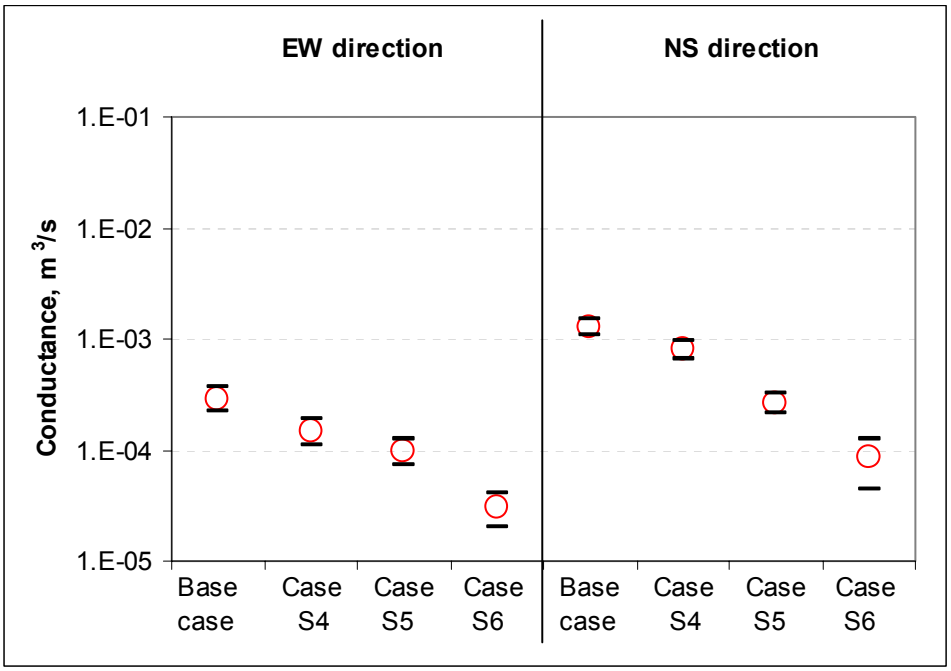

Figure 7.9 – Effect of decreasing fracture density of NS set on the flow conductance.

If the fracture density decreases simultaneously in both directions, the flow conductance decreases at a higher rate. In the case S7 where the fracture density in both directions reduces by 75% from base level, the average flow conductance in the EW direction decreases 22 times and the average flow conductance in the NS direction decreases 9 times, compared to the base case. The EW conductance is zero in 5 out of 10 realizations, and the NS conductance is zero in 1 realization.

VII.3.4. Fracture Termination

In case E1, 50% of the EW fractures terminate at the intersection with the NS fractures. The pathway analysis shows that the average flow conductance in the EW direction drops by 53% while the average flow conductance in the NS direction is almost unchanged. For the fractures used in the base case, the average fracture length of the

EW set is 0.83 m, or almost 3 times greater than the average fracture spacing in the NS direction. This implies that a number of the EW fractures may cut through 2 or more fractures in the NS set. In the termination case, however, 50% of the EW fractures terminate at the fractures that they intersect. Thus, the number of through-going fractures decreases. Following this line of argument, the effect of termination on the system conductance is expected to be a function of the relationship between the fracture length and fracture spacing of the other set.

VII.3.5. Effect of Different Statistical Distributions for Fracture Length

I evaluated the flow conductance when using different statistical distributions for fracture length. The exponential distribution for fracture length is used for comparison with the results obtained with the lognormal distribution. Except for the exponential distribution for the fracture length, all parameters are the same as in the base case, which uses the lognormal distribution for fracture length. The comparison of the results shows that the average flow conductance in the EW direction is 19% lower than that in the base case. The average flow conductance in the NS direction drops 26%.

Figure 7.10 shows the cumulative distribution functions (CDFs) of the exponential and the lognormal distributions having the characteristics used in the simulation for EW and NS fracture length. Figure 7.11 is the expanded version for fracture lengths in the NS set, with the value of fracture length ranging from 4 to 16. This plot suggests that about 2% of the generated fractures using the lognormal distribution will have length greater than 8 m, while this number for the exponential distribution is 0.5%. In other words, the probability that some fractures may cut through the whole rock region is 4 times higher for the lognormal case than the exponential case. Thus one may argue that the simulated rock region should be extended to reduce the possibility that one fracture may go across the entire region. On the other hand, if the flow conductance is strongly affected by the existence of a small number of large

fractures, which could be the case here, using another distribution may give still different results.

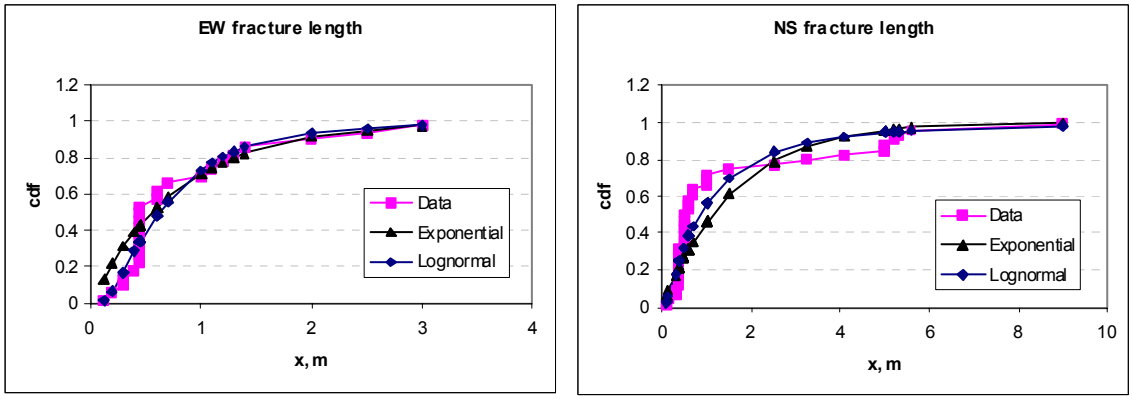

Figure 7.10 – Lognormal and exponential distribution for fracture length in EW and NS sets.

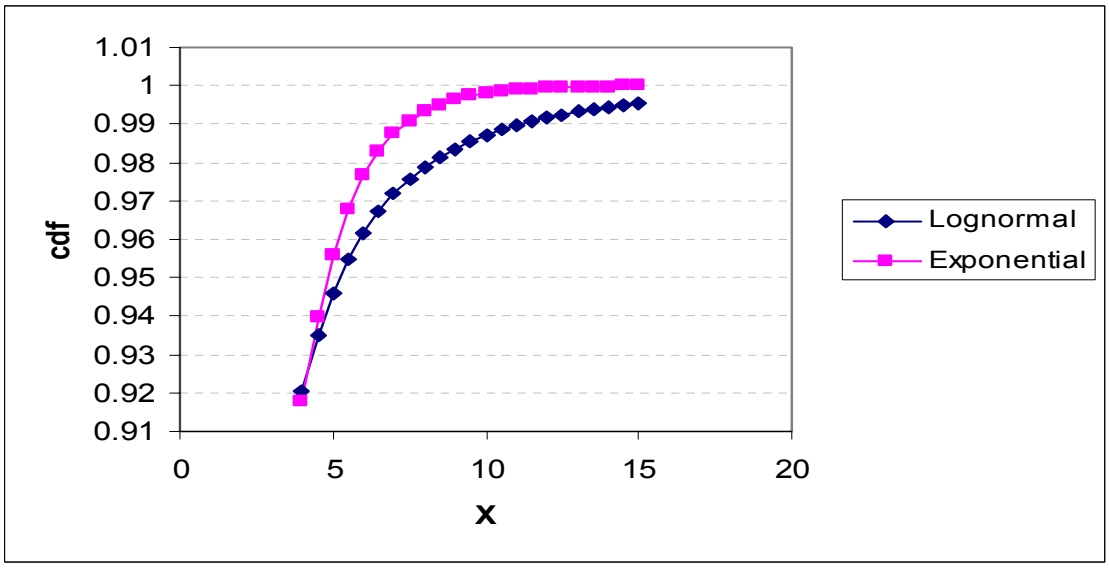

Figure 7.11 – Comparison of the lognormal and exponential distribution in representing NS fracture length. The plot is shown for fracture length in the interval from 4 to 16 m.

VII.3.6. Effect of Fracture Length

In this case, the parameters for the fracture length distribution are taken from the dataset representing open folds (Table 7.1). Since the mean and standard deviation of the two sets are similar, we expect that the system is isotropic. The simulation results show that the average flow conductance in the NS direction is about 1.4 times higher than in the EW direction. Compared to the base case, where the fracture length is taken from tight folds, the average conductance in the NS direction decreases 10 times and the average conductance in the EW direction decreases 3 times. Except for the fracture length, all other parameters of the model and of the fractures are the same as in the base case.

For these fracture data, two cases are run to investigate the relationship between the fracture spacing and fracture termination and fracture length. Case L1 is run with 50% of EW fractures terminating against the NS fractures. Case L2 is run with reducing the fracture density by half for both fracture sets.

The results of case 1 show that the change in average flow conductance is small (13% and 7% for EW and NS, respectively). This suggests that the effects of fracture termination on flow conductance depend on the fracture length entered in FracMan. If the fracture length is large compared to the fracture spacing of the other set, the termination has a strong effect on the flow conductance; if the fracture length is small, the effect of termination is also small.

The relationship between fracture spacing and fracture length is demonstrated in case 2. By decreasing the fracture density by half, 3 out of 10 realizations have zero conductance in each direction. The average flow conductance decreases by 4.2 and 3.6 times, respectively for the EW and NS directions.

VII.3.7. Discussions

Table 7.4 summarizes the results of the flow conductance analysis for all cases.

Table 7.4 – Summary of the flow conductance analysis.

	Average flow conductance, m^3/s		Degree of isotropy	Fraction from base case	
	EW	NS		EW	NS
Base case with fracture length from tight folds	2.93E-04	1.29E-03	4.4	1.00	1.00
10 fold increase of transmissivity in NS set	2.67E-04	8.93E-03	33.4	0.91	6.92
100 fold increase of transmissivity in NS set	3.09E-04	6.02E-02	194.5	1.05	46.62
10 fold increase of transmissivity in EW set	2.38E-03	1.60E-03	0.7	8.10	1.24
100 fold increase of transmissivity in EW set	1.47E-02	3.32E-03	0.2	49.95	2.57
Transmissivity correlates with size	4.43E-05	6.86E-04	15.5	0.15	0.53
50% decrease fracture density of EW set	1.46E-04	1.27E-03	8.7	0.50	0.98
75% decrease fracture density of EW set	5.98E-05	1.17E-03	19.6	0.20	0.91
85% decrease fracture density of EW set	3.87E-05	1.07E-03	27.6	0.13	0.83
50% decrease fracture density of NS set	1.51E-04	8.05E-04	5.3	0.51	0.62
75% decrease fracture density of NS set	9.94E-05	2.68E-04	2.7	0.34	0.21
85% decrease fracture density of NS set	3.12E-05	8.60E-05	2.8	0.11	0.07
75% decrease fracture density in both sets	1.31E-05	1.46E-04	11.2	0.04	0.11
50% EW termination	1.38E-04	1.31E-03	9.5	0.47	1.02
Exponential distribution for fracture length	2.38E-04	9.60E-04	4.0	0.81	0.74
Cases with fracture length from open folds	8.40E-05	1.23E-04	1.5	0.29	0.1
50% EW termination	7.31E-05	1.14E-04	1.6	0.25	0.09
50% decrease fracture density in both sets	2.05E-05	3.41E-05	1.7	0.07	0.03

In summary, the study of the flow conductance of the fracture network suggests the following:

- Given two fracture sets with similar spacing characteristics, significant anisotropy can be observed because of the difference in fracture size. With constant fracture transmissivity in both fracture sets, the average flow conductance in the NS direction can be as high as 4 times that in the EW direction. A higher degree of isotropy will result if the fracture transmissivity is correlated with fracture size.
- The set with the greater length plays an important role not only for flow along its principle direction but also in the orthogonal direction. The reduction of the fracture density of this set causes the reduction of the flow conductance in both directions.
- The termination of the EW set upon the fractures in the NS set may significantly reduce the flow conductance in the EW direction, depending on the size of EW fractures. In the case of small fracture length, the change in flow conductance is small.
- The use of different statistical distributions to describe fracture data may have an effect on the simulated flow conductance. Small differences in the sensitive region (for example, in the region of large fracture size in our case) can lead to big differences in the predicted flow conductance.

One of the major concerns in simulating the fracture system is the size of the rock region within which the fracture network is generated. Obviously, if the size of the simulated region is small, there is a possibility that a number of fractures can cut through that region and thus affect the value of the flow conductance. I have shown that the lognormal distribution for one of our fracture length datasets may produce up to 2% of fractures that have lengths greater than 8 m. Assuming that the rock region is large enough if the average flow conductance does not change with the distance between sample planes, we can assess the representative rock volume issue by examining the

flow conductance between planes of different separation distances. A detailed discussion of the representative elementary volume is given in Bear (1993).

Figure 7.12 shows the flow conductance in the EW and the NS directions as a function of the separation distance between sample planes. This plot shows that the average flow conductance in both directions significantly drops as the separation distance increases from 2 to 4 m. The average flow conductance in the EW direction stabilizes at the separation distance of 8 m, while the average flow conductance in the NS direction is still decreasing at this separation distance. This result suggests that the size of the simulated region should be increased in the NS direction to ensure that the average flow conductance will not change with distance. The pathway analysis module of this version of FracMan, however, limits the number of fractures and interconnections in the model. Removing small fractures from the model after they have been generated may help to increase the size of the model. But this may introduce uncertainty into the results, since we do not know the value of the fracture size below which we can remove fractures without affecting the flow conductance of the system.

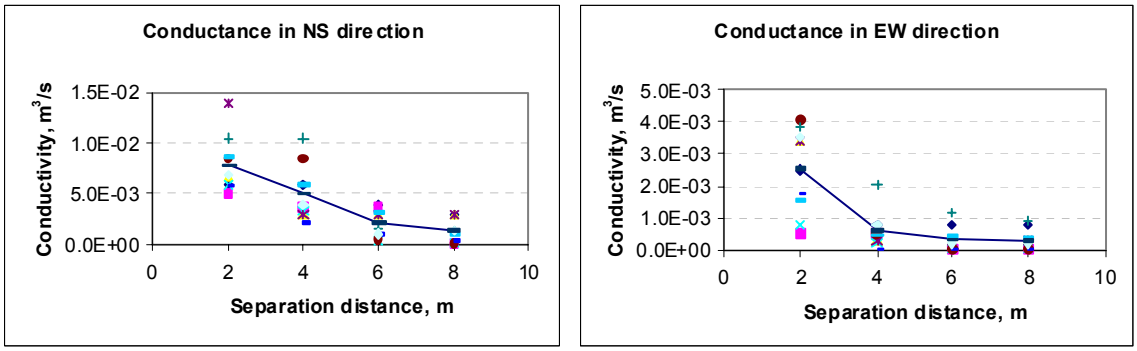

Figure 7.12 – Flow conductance in EW and NS directions as a function of the separation distance between sample planes.

Another concern is the number of realizations of the fracture network for flow conductance calculations. Due to the large number of cases investigated in this study, only 10 realizations were run for each case. This small number of realizations may give only general trends of the effects of different parameters on the flow conductance of the system, considering the wide range of conductance variation (Figure 7.5). More simulation runs are needed for assessing the flow conductance of a particular combination of the fracture properties and model parameters.

In presenting the results of the flow assessment, I used the average flow conductance from different realizations. In cases where the system is near the percolation threshold, this may be misleading. For example, in near percolation threshold cases (e.g., a case with a 75% reduction of fracture density in both directions), a large number of realizations show zero conductance while the average value is different from zero. The average also tends to be affected by extreme values (Jensen et al., 1997), thus the median of the prediction can be an alternative statistic for representing the flow conductance. The mode of the simulated flow conductance, being the most probable value of a distribution, may be a better estimator of the flow conductance calculated from DFNs. However, the mode may require a large number of network realizations and may not be well suited for a sensitivity analysis such as the one in this study.

A similar study was done by Karpov (2001) for the fracture data in the undeformed section of the Lisburne Group. In his study, the fracture length was assumed to be equal to the fracture height, estimated from photos of the exposed faces. This resulted into a weakly anisotropic system. Combining Karpov's and my results, it appears that the fracture density and length determine the system connectivity whereas the fracture length and transmissibility determines the system permeability anisotropy. The information of the fracture length distribution, especially for the large fractures, is essential in modeling the fracture system. For the fracture system in the Lisburne Group, folding appears to be the major factor in controlling the permeability anisotropy of the reservoir.

The effect of folding on the system anisotropy is also evidenced in the subsurface Lisburne Group. In the subsurface Lisburne reservoir, two major fracture orientations were observed: north-northwest and east-northeast striking. The east-northeast striking set is more common, but is frequently more mineralized and trends normal to the maximum compressive stress. The north-northwest striking set is less frequent but more open (Missman and Jameson, 1991; Hanks et al., 1997). The permeability test on full diameter samples which contain fractures indicates an average value of 1.5 to 3 for the maximum to minimum permeability ratio (Belfield, 1988).

The results of an interference test indicate that the preferential direction of the permeability is in the north-south direction with the maximum to minimum permeability ratio of 1.63 (Sampson and Marcou, 1988). This value agrees with the result of the core analysis and with our DFN analysis of the fracture data in open folds. Comparison between the DFN analysis of outcrop fracture data and analysis of the subsurface data suggest that folding plays an important role in determining the degree of the permeability anisotropy.

VII.3.8. Implications for Other Fracture Systems

The results of the flow conductance assessment have the following implications on the data collection and reservoir simulation of other fracture systems.

- Fracture termination and percentage of fracture fill appear to be important parameters and can significantly change the system connectivity and fluid flow behavior. The percentage of fracture fill can be the reduction in fracture transmissivity and/or the reduction of the fraction of open fractures. Both fracture termination and the percentage of fracture fill are determined by the relative age of fractures. Thus, the partition of the fractures into sets and the quantitative data on fracture termination percentage and filling are essential.
- Along with the fracture density, fracture length is an important parameter in modeling the fracture system. Often, the fracture length is assessed as it

correlates to the fracture height. At the scale such as in this study, a large fraction of fractures terminates at bedding planes, therefore, assuming fracture height-fracture length correlation may be misleading.

- In a large-scale reservoir simulation, the horizontal dimensions of the simulation block are often significantly greater than the vertical dimension. The relationship between the flow conductance and the separation distance (Figure 7.12) suggests that the vertical permeability (corresponding to the vertical dimension of the simulation block) may be significantly greater than the horizontal permeability (corresponds to the horizontal dimension of the simulation block). This observation is important in assigning values for permeability in a large scale reservoir simulation. Stable permeability for the simulation block requires that the block size to be much larger than the average fracture length (in horizontal direction) or height (in vertical direction). In cases where the vertical dimension of the simulation is less than or comparable with the average fracture height, the vertical permeability could be much higher than the horizontal permeability.

CHAPTER VIII

SUMMARY, CONCLUSIONS, AND FURTHER WORK

VIII.1. Summary

I investigated the effects of geological parameters on the distribution of fracture spacing, fracture height and length in detachment folds exposed in northeastern Brooks Range, Alaska, using fracture data from Lisburne Group outcrops. Fracture data were collected earlier by geologists at the University of Alaska. Two analysis methods were employed in this study: conventional statistical analysis of fracture spacing, fracture height and length; and neural network analysis of fracture spacing as a function of folding, bed thickness, structural position on folds, lithology, and stratigraphic position.

In using conventional statistical analysis, I grouped fracture data into groups representing two categories of fold tightness and bed thickness with the main purpose of increasing the statistical significance of the analysis.

I performed an analysis using neural networks to identify the relationships among variables, focusing on the issues related to the sparseness of available data. I examined the application of a model selection method for neural networks and the prediction variability analysis on known function before applying these tools to fracture spacing data. The application of neural networks allowed studying the effects of geological parameters on fracture spacing distribution, without having to assume independence of data from different combinations of geological parameters as was the case of using conventional statistical analysis.

I analyzed flow conductance in the fracture system using discrete fracture networks. A fracture system with the fracture properties representing our data was built. The effects of fracture length, fracture spacing and fracture termination pattern on the flow conductance of the system and on the system isotropy were studied. The results of

this analysis show the significance of different fracture properties in determining the flow conductance and the system anisotropy.

VIII.2. Conclusions

A review of the results of this research leads to following conclusions.

1. In the environment as encountered in exposed folds in northeastern Brooks Range, Alaska, the fracture properties distribution is a complex function of geological factors. Simple statistical analysis may give only the combined effects of different geological factors on fracture properties distribution, considering the limited number of fracture data available for this study.
2. Neural networks provide a useful alternative to conventional statistical analysis. The use of neural networks, however, is affected by a number of aspects. Only careful examination for each application will help to extract helpful information from available data. For the case of limited data, using multiple realizations of the leave-one-out cross validation helped to uniquely choose the optimal network configuration and assess the network prediction variability. The trade off of this approach is the increased computational cost and additional effort in coding of the neural network.
3. For limited data case, the linear activation function at the output layer of neural networks gives less biased prediction than sigmoidal and Gaussian functions.
4. The results of neural network analysis on fracture spacing data suggest that, overall, the stratigraphic position plays the most important role in average fracture spacing distribution, followed by the lithology and bed thickness. The degree of folding and the structural position are the least influential parameters on average fracture spacing. However, the effect of structural position is closely related to the fracture orientation. On the fold limbs, the

average fracture spacing in the EW orientation, parallel to fold axis, is systematically larger than in the NS direction. In the hinge, the average fracture spacing of EW fractures is systematically smaller than the average spacing of NS fractures.

5. Bed thickness has weak effect on fracture spacing. This is in agreement with the observation in un-deformed section of Lisburne Group (Hanks et al., 1997).

6. It may be that the fracture system has reached its saturation state and folding mostly affects fracture length. This conclusion has important implications for the assessment of the fracture system anisotropy and its flow characteristics since, in many cases, only fracture density catches the engineers' attention. Fracture height, which is often used to infer fracture length, may not accurately represent the true fracture length in layered formations since a large portion of fractures terminate at bedding planes.

7. The combination of fracture spacing, fracture length and field observation suggests that the fracture development may have been caused by different geological events, one of which is closely related to folding and one of which is not. However, I did not have enough information to classify our fractures according to separate events. Judging from change of the average fracture length with folding, the NS fractures appear to be more related to the folding.

8. The study of flow conductance of the fracture system shows that, given the same fracture spacing, differences in fracture length may introduce a significant anisotropy in the system. The fracture set with greater length plays an important role, not only for flow along its principle direction, but also in the orthogonal direction.

9. Overall, the fracture system in this study appears to be well connected at the scale of the study. However, if the fracture density is reduced by half in both directions and the fracture length is taken from available data for open folds,

a number of model realizations show zero conductance. It appears that the fracture density and the fracture size determine the system connectivity whereas the fracture length and transmissivity determine the system permeability anisotropy.

10. The fracture termination does have an effect on flow conductance. The magnitude of this effect depends on the fracture length. In cases of small fracture length with regard to fracture spacing, the effect of fracture termination in flow conductance can be negligible.

11. The system conductance strongly depends on the separation distance between source and sink planes. The flow conductance between two closely placed planes may be significantly greater than between two planes placed far from each other. This observation is very important in assigning the values for permeability in a large-scale reservoir simulation.

12. The choice of the statistical distribution has effect on the result of the flow conductance calculation. Even a small difference between the distributions in the region of large fracture length may cause a big difference in simulated results.

VIII.3. Recommendations and Further Work

I identified the following areas for further developments and investigation.

1. Convert the neural network program, which has been written in Visual Basic in Excel, into a separate program and develop an interface that allows easy use for network training and interpretation of the results.

2. Incorporate different training methods to improve the neural network training. The LOO cross validation method requires multiple network training and increases computational cost. A fast training algorithm will help to reduce the network training time.

3. Apply flow simulations to the discrete fracture network. Flow conductance analysis is easy and fast to calculate. It does not give the equivalent permeability of the system, a measurement that is used in a large scale continuum simulation. In applying the DFN to problems such as upscaling permeability for continuum simulation, flow simulation allows calculation of the equivalent permeability of the system.

REFERENCES CITED

Aguilera, R., 1995, Naturally Fractured Reservoirs: Pennwell Publishing Co., Tulsa, OK, 521 p.

Amari, S. I., N. Murata, K. R. Muller, M. Finke, and H. H. Yang, 1997, Asymptotic statistical theory of overtraining and cross validation: IEEE Transactions on Neural Networks, v. 8, p. 985-996.

Ash, T., 1989, Dynamic node creation in backpropagation neural networks: Connection Science, v. 1, p. 365-375.

Atkinson, P. K., and W. K. Wallace, 2003, Competent unit thickness variation in detachment folds in the northeastern Brooks Range, Alaska: Geometric analysis and a conceptual model: Journal of Structural Geology, v. 25, no. 10, p. 1751-1771.

Bai, T., and D. D. Pollard, 2000, Fracture spacing in layered rocks: A new explanation based on the stress transition: Journal of Structural Geology, v. 22, no. 1, p. 43-57.

Barton, C. A., and M. D. Zoback, 1992, Self-similar distribution and properties of macroscopic fractures at depth in crystalline rocks in the Cajon Pass scientific drill hole: Journal of Geophysical Research, v. 97, p. 5181-5200.

Bear, J., 1993, Modeling flow and contaminant transport in fractured rocks, *in* J. Bear, C. F. Tsang, and G. de Marsily, eds., Flow and Contaminant Transport in Fractured Rock: Academic Press, San Diego, CA, p. 1-35.

Belfield W. C., 1988, Characterization of a naturally fractured carbonate reservoir: Lisburne Field, Prudhoe Bay, Alaska: Society of Petroleum Engineers Annual Technical Conference and Exhibition, Houston, SPE Paper 18174.

Billaux, D., J. P. Chiles, K. Hestir and J. Long, 1989, Three-dimensional statistical modeling of a fracture rock mass – An example from the Fanay-Augeres mine: International Journal of Rock Mechanics and Mining Sciences, v. 26, p. 281-299.

Bishop, C. M., 1995, Neural Networks for Pattern Recognition: Clarendon Press, Oxford, 482 p.

Bowden, G. J., H. R. Maier, and G. C. Dandy, 2002, Optimal division of data for neural network models in water resources applications: Water Resource Research, v. 38, no. 2, p. 1-11.

Box, G. E. P., and Jenkins, G. M., 1976, Time Series Analysis: Forecasting and Control, Holden-Day, San Francisco, CA, 575 p.

Brinton, J., 2002, Natural fracturing in carbonate rocks as a function of lithology and structural position in a detachment fold: Examples from the northeastern Brooks Range, Alaska: M.S. thesis, University of Alaska, Fairbanks, AK, 126 p.

Cacas, M. C., E. Ledoux, G. de Marsely, B. Tillie, A. Barbreau, E. Durand, B. Feuga and P. Peaudecerf, 1990, Modeling fracture flow with a stochastic discrete fracture network: Calibration and validation 1: The flow model: Water Resources Research, v. 26, no. 3, p. 479-489.

Chauvin, Y., 1990, Dynamic behavior of constrained back-propagation networks, *in* D. S. Touretzky, ed., Advances in Neural Information Processing System 2: Morgan Kaufmann Publishers, San Mateo, CA, p. 642-649.

Chiles, J. P., and G. de Marsily, 1993, Stochastic models of fracture systems and their use in flow and transport modeling, *in* J. Bear, C. F. Tsang, and G. de Marsily, eds., Flow and Contaminant Transport in Fractured Rock: Academic Press, San Diego, CA, p. 169-231.

Chryssolouris, G., M. Lee, and A. Ramsey, 1996, Confidence interval prediction for neural network models: IEEE Transactions on Neural Networks, v. 7, p. 229-232.

Cosgrove, J. W., and M. S. Ameen, 2000, A comparison of the geometry, spatial organization and fracture patterns associated with forced folds and buckle folds, *in* J. W. Cosgrove and M. S. Ameen, eds., Forced folds and fractures: Geological Society of London, Special Publications, London, p. 7-21.

Dershowitz, W. S., and H. H. Einstein, 1988, Characterizing rock joint geometry with joint system models: Rock Mechanics and Rock Engineering, v. 21, p. 21-51.

De Villiers, J., and E. Barnard, 1993, Backpropagation neural nets with one and two hidden layers: Neural Networks, v. 4, no. 2, p. 136-141.

Doe, T., 1997, The problem of fracture flow: Water Environment and Technology, v. 9, p. 63-79.

Dunham, R. J., 1962, Classification of carbonate rocks according to depositional texture, *in* W. E. Ham, ed., Classification of carbonate rocks: Memoirs of the American Association of Petroleum Geologists 1, p. 108-121.

Dverstorp, B, and J. Anderson, 1989, Application of discrete fracture network concept with field data: Possibilities of model calibration and validation: Water Resource Research, v. 25, no. 4, p. 540-550.

Efron, B., 1993, An Introduction to the Bootstrap: Chapman and Hall, New York, 436 p.

Epard, J. L., and R. H. Jr. Groshong, 1995. Kinematics model of detachment folding including limb rotation, fixed hinges and layer-parallel strain: Tectonophysics, v. 247, p. 85-103.

Fausett, L., 1994, Fundamentals of Neural Networks Architectures, Algorithms, and Applications: Prentice Hall, Englewood Cliffs, NJ, 430 p.

Garson, G. D., 1991, Interpreting neural network connection weights: Artif. Intelligent Expert, v. 6, p. 47-51.

Garson, G. D., 1998, Neural networks: An Introductory Guide for Social Scientists: Sage Publications, Thousand Oaks, CA, 194 p.

Goh, A. T. C., 1995, Back propagation neural networks for complex systems: Artif. Intelligence in Engineering, v. 9, p. 143-151.

Guo, G., S. A. George, and R. P. Lindsey, 1999, Statistical analysis of surface lineaments and fractures for characterizing naturally fractured reservoirs, *in* R. Schatzinger and J. Jordan, eds., Reservoir characterization – Recent advances: AAPG Memoirs 71, p. 221-250

Hagan, M. T., and M. Menhaj, 1994, Training feedforward networks with the Marquardt algorithm: IEEE Transactions on Neural Networks, v. 5, p. 989-993.

Hanks, C. L., J. Lorenz, L. Teufel, and A. P. Krumhardt, 1997, Lithologic and structural controls on natural fracture distribution and behavior within the Lisburne Group, northeastern Brooks Range and north slope subsurface, Alaska: AAPG Bulletin, v. 81, no. 10, p. 1700-1720.

Hanks, C. L., J. Brinton, and J. Lorenz, 2000, Fracturing in the Lisburne Group as a function of carbonate lithology, mechanical stratigraphy and position in detachment folds, *in* The influence of fold and fracture development on reservoir behavior of the Lisburne Group of northern Alaska, first annual report: U.S. Department of Energy Contract DE-AC26-98BC15102, p. E1-E52.

Harris, J., G. Taylor, and J. Walper, 1960, Relation of deformational structures in sedimentary rocks to regional and local structure: AAPG Bulletin, v. 44, no. 12, p. 1853-1873.

Helgelson, D. E., and A. Aydin, 1991, Characteristics of joint propagation across layer interface in sedimentary rocks: Journal of Structural Geology, v. 13, no. 8, p. 897-911.

Henning, P. H., J. E. Olson, and L. B. Thompson, 2000, Combining outcrop data and three-dimensional structural models to characterize fractured reservoirs: An example from Wyoming: AAPG Bulletin, v. 84, no. 6, p. 830-849.

Herbert, A. W., and G. W. Lanyon, 1992, Discrete fracture network modeling of flow and transport within a fracture zone at Stripa, *in* L. R. Myer, N. G. W. Cook, R. E. Goodman, and C. F. Tsang, eds., Fractures and Jointed Rock Masses: Balkema Publishers, Rotterdam, Netherlands, p. 603-610.

Hirose, Y., K. Yamashita, and S. Hijiya, 1991, Back-propagation algorithm which varies the number of hidden units: Neural Networks, v. 4, no. 1, p. 61-66.

Homza, T. X., and W. K. Wallace, 1997, Detachment folds with fixed hinges and variable detachment depth, northeastern Brooks Range, Alaska: Journal of Structural Geology, v. 19, no. 3, p. 337-354.

Hornik, K., M. Stinchcombe, and H. White, 1990, Multilayer feed forward neural networks are universal approximations: Neural Networks, v. 3, no. 4, p. 359-366.

Hosking, J. R. M., and J. R. Wallis, 1997, Regional Frequency Analysis: Cambridge University Press, Cambridge, 224 p.

Huang, Q., and J. Angelier, 1989, Fracture spacing and its relation to bed thickness: Geological Magazine, v. 126, p. 355-362.

Huang, Z., J. Shimeld, M. Williamson, and J. Katsube, 1996, Permeability prediction with artificial neural network modeling in the venture gas field offshore eastern Canada: Geophysics, v. 61, p. 422-428.

Hwang, J. T. G., and A. A. Ding, 1997, Prediction intervals for artificial neural networks: Journal of the American Statistical Association, v. 92, p. 748-757.

Jacobs, R., 1988, Increase rates of convergence through learning rate adaptation: Neural Networks, v. 1, no. 4, p. 295-307.

Jamison, W. R., 1997, Quantitative evaluation of fractures on Monshood anticline, a detachment fold in the foothills of western Canada: AAPG Bulletin, v. 81, no. 7, p. 1110-1132.

Jensen, L. J., L. W. Lake, P. W. M. Corbett, and D. J. Goggin, 1997, Statistics for Petroleum Engineers and Geoscientists: Prentice Hall, Englewood Cliffs, NJ, 390 p.

Ji, S., and K. Saruwatari, 1998, A revised model for the relationship between joint spacing and layer thickness: Journal of Structural Geology, v. 20, no. 11, p. 1495-1508.

Kalell, R., M. Cottrell, and V. Vigneron, 2002, Bootstrap for neural model selection: Neorocomputing, v. 48, p. 175-183.

Karpov, V. A, 2001, Lisburne formation fracture characterization and flow modeling: M.S. thesis, Texas A&M University, College Station, TX, 113 p.

Ladeira, F. L., and N. J. Price, 1981, Relationship between fracture spacing and bed thickness: Journal of Structural Geology, v. 3, no. 2, p. 179-183.

LeCun, Y., J. S. Denker, and S. A. Solla, 1990, Optimal brain damage, *in* D. S. Touretzky, ed., Advances in Neural Information Processing System 2: Morgan Kaufmann Publishers, San Mateo, CA, p. 598-602.

Lek, S., M. Delacoste, P. Baran, I. Dimopoulous, J. Lauga, S. Aulagnier, 1996, Application of neural networks to modeling nonlinear relationship in ecology: Ecol. Modeling, v. 120, p. 65-73.

Leonard, J., and M. A. Kramer, 1990, Improvement of the backpropagation algorithm for training neural network: Computer Chem. Engineering, v. 14, p. 337-341.

Lewis, P. A. W., and E. J. Orav, 1989, Simulation Methodology for Statisticians, Operations Analysts, and Engineers, v. 1: Wadsworth Inc., Pacific Grove, CA, 534 p.

Lisle, R. J., 1994, Detection of zones of abnormal strains in structures using gausian curvature analysis: AAPG Bulletin, v. 78, no. 12, p. 1811-1819.

Lisle, R. J., 2000, Predicting patterns of strain from three-dimensional fold geometries: neutral surface folds and forced folds, *in* J. W. Cosgrove and M. S. Ameen, eds., Forced folds and fractures: Geological Society of London, Special Publications, London, p. 213-221.

Long, J. C. S., J. S. Remer, C. R. Wilson, and P. A. Witherspoon, 1982, Porous media equivalents for networks of discontinuous fractures: Water Resources Research, v. 18, no. 5, p. 645-658.

Maier, H. R., and G. C. Dandy, 1998, Understanding the behavior and optimizing the performance of back-propagation neural networks: An empirical study: Environmental Modeling and Software, v. 13, p. 179-191.

Mathab, A., S. Xu, P. Grasso, and F. S. Kendorski, 1995, Use of alternative distributions for characterizing joint extent and spacing, *in* L. R. Myer, N. G. W. Cook, R. E. Goodman, and C. F. Tsang, eds., Fractured and Jointed Rock Masses: Balkema Publishers, Rotterdam, Netherlands, p. 47-59.

McQuillan, H., 1973, Small-scale fracture density in Asmari formation of southwest Iran and its relation to bed thickness and structural setting: AAPG Bulletin, v. 57, no. 12, p. 2367-2385.

Missman, R. A., and J. Jameson, 1991, An evolving description of a fractured carbonate reservoir: the Lisburne field, Prudhoe Bay, Alaska, *in* R. Sneider, W. Massell, R. Mathis, D. Loren, and P. Wichmann, eds., The integration of geology, geophysics, petrophysics, and petroleum engineering in reservoir delineation, description, and management: AAPG-SPE-SPWLA Archie Conference, Houston, TX, p. 204-224.

Montroll, E. W. and M. F. Schlesinger, 1983, Maximum entropy formalism, fractals, and 1/f noise: A tale of tails: Journal of Statistical Physics, v. 32, p. 209-230.

Moody, J. E., and J. Utans, 1992, Principle architecture selection for neural networks, *in* J. E. Moody, S. J. Hanson, and R. P. Lippmann, eds., Advances in Neural Information Processing System 4: Morgan Kaufmann Publishers, San Mateo, CA, p. 683-690.

Moore, T. E., W. K. Wallace, K. J. Bird, S. M. Karl, C. G. Mull, and J. T. Dillon, 1994. Chapter 3: Geology of northern Alaska, *in* G. Plafker and H. C. Berg, eds.: The geology of Alaska: The geology of North America, vol. Gi: Geological Society of America, Boulder, CO, p. 49-140.

Murray, G. H., 1968, Quantitative fracture study – Spanish pool, North Dakota: AAPG Bulletin, v. 52, no. 1, p. 57-65.

Narr, W., and J. Suppe, 1991, Joint spacing in sedimentary rocks: Journal of Structural Geology, v. 13, no. 10, p. 1037-1048.

Neave, H. R., and P. L. Worthington, 1988, Distribution Free Tests: Unwin Hyman Ltd., London, 430 p.

Nelson, R. A., 2001, Geologic Analysis of Naturally Fractured Reservoirs: Gulf Publishing Co., Houston, TX, 232 p.

Ouenes, A., A. Zellou, P. M. Basinski, and C. F. Head, 1998, Practical use of neural networks in tight gas fractured reservoirs: Application to the San Juan Basin: Society of Petroleum Engineers Rocky Mountain Regional/Low Permeability Reservoirs Symposium and Exhibition, Denver, SPE Paper 39965.

Ouenes, A., and L. J. Hartley, 2000, Integrated fractured reservoir modeling using both discrete and continuum approaches: Society of Petroleum Engineers Annual Technical Conference and Exhibition, Dallas, SPE Paper 62939.

Ozesmi, S. L., and U. Ozesmi, 1999, An artificial neural network approach to spatial habitat modeling with interspecific interaction: Ecological Modeling, v. 116, p. 15-31.

Poblet, J., and K. McClay, 1996. Geometry and kinematics of single-layer detachment folds: AAPG Bulletin, v. 80, no. 7, p. 1085-1109.

Pollard, D. D., and P. Segall, 1987, Theoretical displacements and stress near fractures in rocks: with applications to faults, joints, veins, dikes and solution surfaces, *in* B. K. Atkinson, ed.: Fracture Mechanics of Rock: Academic Press, London, p. 277-349.

Price, N. J., and J. W. Cosgrove, 1990, Analysis of Geological Structures: Cambridge University Press, Cambridge, 502 p.

Ramsey, J. G., and M. I. Huber, 1987. Folds and Fractures, The Techniques of Modern Structural Geology, vol. 2: Academic Press, London, 307 p.

Ripley, B. D., 1996, Pattern Recognition and Neural Networks: Cambridge University Press, Cambridge, 416 p.

Rivals, I., and L. Personnaz, 2000, Construction of confidence intervals for neural networks based on least squares estimation: Neural Networks, v. 13, no. 4, p. 463-484.

Rives, T., M. Razak, J. P. Petti, and K. D. Rawnsley, 1992, Joint spacing: Analog and numerical simulations: Journal of Structural Geology, v. 14, no. 8, p. 925-937.

Rogers, S. J., J. H. Fang, C. L. Karr, and D. A. Stanley, 1992, Determination of lithology from well logs using a neural network: AAPG Bulletin, v. 76, no. 5, p. 731-739.

Rouleau, A., and J. E. Gale, 1985, Statistical characterization of the fracture system in the Stripa Granite, Sweden: International Journal of Rock Mechanics and Mining Sciences and Geomechanics Abstracts, v. 22, p. 353-367.

Rumelhart, D. E., and J. L. McClelland, 1986, Parallel Distributed Processing: Explorations in the Microstructure of Cognition, vol. 1: MIT Press, Cambridge, MA, 576 p.

Sahimi, M., 1995, Flow and Transport in Porous Media and Fractured Rock: VCH Publishers, Weinheim, Germany, 482 p.

Sampson, L. E, and J. A. Marcou, 1988, Interference test in a fractured carbonate: A Lisburne case history: Society of Petroleum Engineers Annual Technical Conference and Exhibition, Houston, SPE Paper 18138.

Siegel, A. F., and C. J. Morgan, 1996, Statistics and Data Analysis – An Introduction: John Wiley and Son, New York, 635 p.

Silva, F. M., and L. B. Almeida, 1991, Speeding up back propagation: Advance Neural Computers, v. 4, p. 67-69.

Smith, L., and F. W. Schwartz, 1993, Solute transport through fracture networks, *in* J. Bear, C. F. Tsang, and G. de Marsily, eds., Flow and Contaminant Transport in Fractured Rock: Academic Press, San Diego, CA, p. 129-168.

Stearns, D. W., 1967, Certain aspects of fracture in naturally deformed rocks, *in* R. E. Riecker, ed., NSF advanced science seminar in rock mechanics: Air Force Cambridge Research Lab. Report, Bedford, MA, p. 97-118.

Stearns, D. W., and M. Friedman, 1972, Reservoirs in fractured rock: AAPG Memoir, v. 16, p. 82-100.

Twomey, J. M., and A. E. Smith, 1998, Bias and variance of validation methods for function approximation neural networks under condition of sparse data: IEEE Transactions on Systems, Man, and Cybernetics – Part C: Applications and Reviews, v. 28, p. 417-430.

Xue, G., A. Datta-Gupta, P. Valko, and T. Blassingame, 1997, Optimal transformations for multiple regression: Application to permeability estimation to permeability estimation from well logs: SPEFE, v. 7, p. 85-92.

Wallace, W. K., and C. L. Hanks, 1990, Structural provinces of the northeastern Brooks Range, arctic national wildlife refuge, Alaska, AAPG Bulletin, v. 74, no. 7, p. 1100-1118.

Wasserman, P. D., 1993, Advanced Methods in Neural Computing: Van Nostrand Reinhold, New York, 255 p.

Wessels, L., and E. Barnard, 1992, Avoiding false local minima by proper initialization of connections: IEEE Transactions on Neural Networks, v. 3, p. 899-905.

Whalen, M. T., 2000, Baseline stratigraphy of the Lisburne Group, *in* The influence of fold and fracture development on reservoir behavior of the Lisburne Group of northern Alaska, first annual report: U.S. Department of Energy Contract DE-AC26-98BC15102, p. B1-B14.

Wu, H., and D. D. Pollard, 1995, An experimental study of the relationship between joint spacing and layer thickness: Journal of Structural Geology, v. 17, no. 6, p. 887-905.

Zapranis, A., and A-P. Refenes, 1999, Principles of Neural Model Identification, Selection and Adequacy: Springer-Verlag, London, 190 p.

VITA

Name: Thang Dinh Bui

Address: PetroVietnam
22 Ngo Quyen, Ha Noi, Viet Nam
email: thangbui04@yahoo.com

Education: Texas A&M University, College Station, TX, USA
Ph.D., Petroleum Engineering, (August 2004)
M.S., Petroleum Engineering (May 1998)

Moscow Institute of Oil and Gas, Moscow, Russia
B.S., Petroleum Engineering (June 1991)

Affiliations: Society of Petroleum Engineers (SPE)

Honors: First place in the Master Division of the 1998 Gulf Coast Region Student Paper Contest, Corpus Christi, TX.

Experience: Summers 2002, 2003: Engineering Intern – Schlumberger WCP, Houston, Texas.

1995 – 1999: Reservoir Engineer, PetroVietnam, Ha Noi, Viet Nam.

1992 – 1995: Production Engineer, VietSovPetro, Vung Tau, Viet Nam.

Publication: Had published 4 professional papers since 1998.